EVANESCENT WAVE SPECTROSCOPY USING MULTIMODE OPTICAL FIBRES

BY

JOSEPH ANTHONY MURPHY

A THESIS PRESENTED

TO

DUBLIN CITY UNIVERSITY

FOR THE DEGREE OF M.Sc.

AUGUST 1990

PHYSICS DEPARTMENT,

DUBLIN CITY UNIVERSITY,

IRELAND.

ACKNOWLEDGEMENTS

A project of this nature cannot be brought to completion without the help of many people, and I would like to thank all who have helped me in any way.

The author wishes to express sincere thanks for the hours of dedication, untiring encouragement and extending all possible help offered by my supervisors Dr. Brian MacCraith and Dr. Vincent Ruddy, of the Optical Sensors Group, Dublin City University.

To the Physics technicans, Alan, Al, Joe, John, Susan and Mike for their co-operation and assistance while I have been at the University. To Tommy (Mechanical Engineering) for his endless efforts and advice.

To the Physics Department, Trinity College, Dublin for the use of their scanning electron microscope.

To Joan (British Gas plc) for the excellent work on the diagrams and Mr. D. Pinchbeck for his advice.

Finally, but certainly not in order of importance, I would like to thank my parents for their continued support and understanding and to Orla for her encouragement and patience during the course of this study.

DEDICATION

This thesis would not be possible without the support and encouragement from my parents and the love, understanding and patience of Orla "Pud".

ABSTRACT

The use of multimode optical fibre as an intrinsic chemical sensor, with application in on-line analysis in the process industry, is described. The technique of attenuated total reflection spectroscopy is applied to the unclad section of the fibre which is in contact with the chemical being detected. A model based on selective mode propagation is developed to relate the evanescent absorption coefficient of the fibre probe to the bulk absorption coefficient of the absorbing species.

An experimental system was constructed to verify the theoretical model. Evanescent wave absorption in an aqueous dye solution was performed using multimode fused silica fibre which was unclad at the sensing region. In order to produce modes close to cutoff in the sensing region, tunnelling modes were launched into the clad lead-in fibre.

The measured evanescent absorbance of the dye solution was found to vary linearly with the exposed core length and to exhibit a square root dependence on concentration. The former effect is predicted from theory while the latter is attributed to adsorption on the core surface which obeys a Debye-Hückel-type concentration dependence. In adddition, a concentration enhancement of two orders of magnitude was observed due to this adsorption.

Because the adsorption process is of an irreversible nature, the potential for evanescent wave spectroscopy on fused silica fibre is severly limited for ionic solutions. The effect may be exploited, however, in disposable probes to give increased sensitivity due to the enhanced surface concentrations.

TABLE OF CONTENTS

CHAPTER 1

INTRODUCTION

1.1 Historical Introduction.

The field of fibre optics is based on the guidance of light by multiple reflections along channels formed from glass or plastic. The reflection process is that of total internal reflection (TIR) at a dielectric interface, and the first recorded observation of this principle was by Tyndall (1) in 1854.

It was not until the early twentieth century that a practical application of this phenomenon was proposed. In 1927, Baird (2) in the UK, and Hansel (3) in the USA applied for patents for image-transferring devices using fibres of silica.

However, since uncoated fibres were used, the efficiency was low and applications were few. It was not until 1954 that Van Heel (4) announced the invention of the cladded dielectric waveguide. The major milestone in fibre optics, however, came in 1966 when Kao and Hockham (5), working from STL in Harlow, England, published a paper demonstrating that light may be guided with low loss in thin, flexible glass fibre guides. Over two decades later, the industry has become established and lightwave communications has become one of the most important cornerstones of the telecommunications industry.

1.2 Optical Fibre Sensors.

The future of the optical fibre as a practical communications channel is now firmly established, particularly for long distance communications. However, there is a great deal of interest in the design and development of optical fibre sensors for scientific and industrial applications for the measurement of parameters such as displacement, acceleration, strain, pressure, flow rate, fluid level, temperature, current, magnetic field and chemical composition (6).

An optical sensor may be defined as a device in which an optical signal is modulated in response to a measurand field, such that the measurand may be recovered from the modulated signal. This may mean modulation in intensity, frequency, phase, colour, polarisation (or any combination of these properties) of the guided light.

Optical fibre sensors may be generally classified as extrinsic or intrinsic and each of these categories may be subdivided further into coherent and incoherent devices.

Extrinsic sensors merely use the fibre as a light-guiding medium to transport light to and from more conventional optical sensors which, in response to an external parameter, modify the coupling between the input and output fibre(s). They may, however, be affected by small environmental changes in cable properties unless particular care is taken in their design. Intrinsic sensors, in

contrast, rely on the optical fibre itself as the sensing element.

A very wide range of optical fibre sensors based on both coherent and incoherent optical techniques are currently undergoing development. Incoherent devices are based on multimode fibres in which the coherence of the guided beam is not maintained and the beam is rapidly depolarized; phase and polarization information is hence lost. In consequence, measurand induced modulation is primarily restricted to intensity changes. A detailed discussion of these sensors is given by Jones (7).

The availability of monomode optical fibres, in which beam coherence is maintained, has allowed the development of phase modulation sensors. In general, these exhibit much greater sensitivity and versatility than the intensity modulated devices; since the phase is recovered interferometrically, they are generally termed interferometric (8).

Many of the initial engineering applications of optical sensors rely on their inherent advantages over the more conventional electrically based sensors:

(i) Freedom from Electromagnetic Interference (EMI)

(ii) Intrinsic safety in hazardous environments

(iii) Passive operation

(iv) High electrical isolation

(v) Geometric versatility

The main thrust of this project is the application of optical fibres to chemical sensing.

1.3 Remote Spectroscopy.

Recently there has been considerable interest in the use of Remote Fibre Spectroscopy (RFS) and a number of schemes have been devised for probing hostile or otherwise inaccessible environments by using optical fibres to link a centralized spectrometer and excitation source to a remote location (9,10,11,12). Systems combining spectroscopic techniques with fibre optics can yield quantitative measurements of composition and other fluid properties. Moreover, the approach permits use of multiple probes, not necessarily all sensitive to the same variable, to provide multiple on-stream measurements, nearly in real time.

David et al (13) have reported the use of colour-changing reagents coated on glass rods acting as optical wave-guide sensors. Lubbers and Opitz presented their "Optrode" (optical + electrode) concept (14): an optical transducer at the distal end of an optical fibre provides chemical specificity in an RFS environment. The transducer in this case consists of chemical reagents whose optical properties (absorbance or fluorescence) respond to a particular analyte.

An alternative to the Optrode approach is to use the optical fibres as "light pipes" to obtain spectroscopic information from a remote cell (15). The simplicity of this

technique is demonstrated in a series of papers by Inaba et al (16,17,18,19,20). A remote detection system for methane, propane and other explosive gases was demonstrated over a 2-km silica optical fibre link.

A similar system has been used to monitor ammonia using mid-infrared absorption. This is the first reported use of mid-infrared transmitting fibres for spectroscopic monitoring (21).

The main disadvantage of the Optrode and "light pipe" techniques is that a structure (either optical or chemical) be fixed to the fibre end for RFS applications. An alternative approach is to use the fibre itself as an in-situ spectroscopic sensor. This technique relies on the interaction of the evanescent wave, that is established at each point of total internal reflection within the waveguide, with the surrounding medium.

1.4 Evanescent Wave Spectroscopy.

An all fibre remote spectroscopic sensor overcomes many of the disadvantages of the two approaches outlined in section 1.3. It is potentially more reliable and sensitive and is particularly attractive for distributed sensing.

Evanescent wave sensing is a generalization of total internal reflection spectroscopy, with the guided wave continuously probing the optical properties of an external medium. The totally reflected light beam generates a non-propagating evanescent wave. This evanescent wave

penetrates the surrounding medium to a depth of the order of one wavelength and decays exponentially with distance in the lower index region. If the wavelength of the guided light falls within an absorption band of the external medium, then evanescent wave absorption will occur. The amount of absorption will depend on the concentration of the species to be measured. Attenuation of the evanescent tail in the cladding region causes a reduction in the guided wave power in the core which, when detected, permits the analyte concentration to be quantified.

Evanescent wave measurements have been reported in "attenuated total internal reflection" cells (22) and Fourier transform infrared (FTIR) spectrometers (23). Total internal reflection devices have relied primarily on evanescent interaction by prism coupling to fluids. Fibre optic evanescent wave absorption cells have been demonstrated by Simhony et al.(24) using IR fibre and by Tanaka et al.(25) using silica fibre.

This work describes the characteristics of evanescent wave spectroscopy of absorbing dyes using multimode silica optical fibres.

CHAPTER 2

THEORETICAL BACKGROUND.

2.1 Introduction.

When a light beam is incident on the interface between two transparent media, travelling from the medium of higher refractive index ($n_1 > n_2$), total internal reflection (TIR) occurs (26) when the angle of reflection Θ is larger than the critical angle Θ_c.

$$\Theta_c = \sin^{-1}(n_2 / n_1) \qquad (1)$$

Closely related to this phenomenon is the existence of an electromagnetic wave form which is generated in the optically rarer medium near to the reflecting surface. This evanescent wave penetrates the lower refractive index medium and can interact optically with compounds close to or at the surface.

It was Fahrenfort (27) and Harrick (28) who used TIR as a spectroscopic tool and developed what is today known as Internal Reflection Spectroscopy (IRS). IRS according to Harrick (29) is the technique of recording the optical spectrum of a sample material that is in contact with an optically denser but transparent medium; the wavelength dependence of the reflectivity of this interface is measured by introducing light into the denser medium, as shown in figure 1.

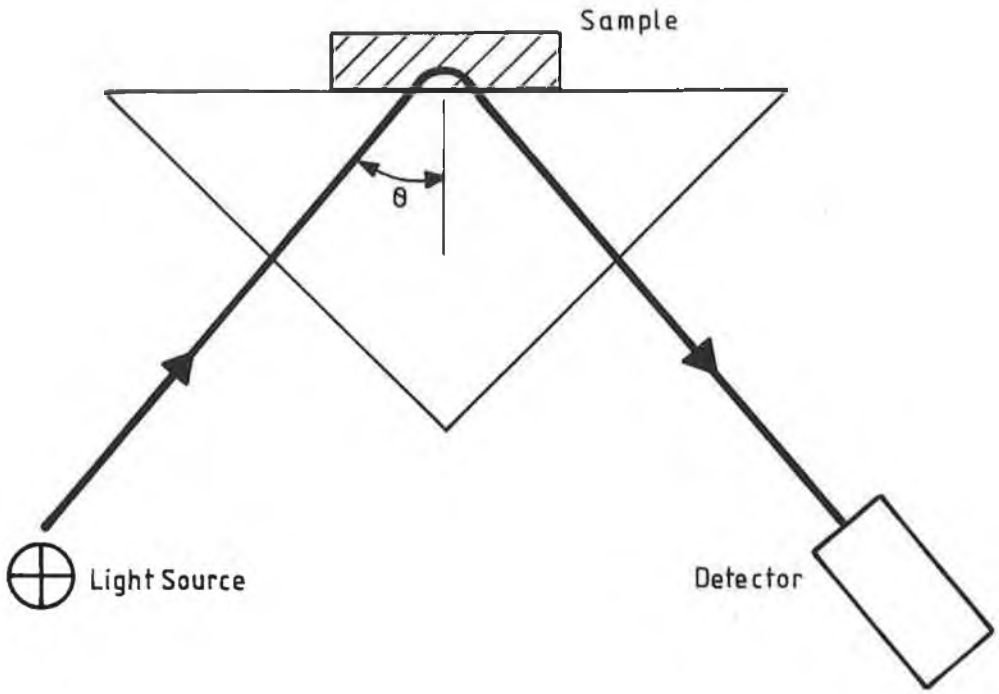

Fig.1 : Internal Reflection Spectroscopy
The Sample Material Absorbs Energy via
Interaction with the Evanescent Wave

2.2 Internal Reflection Spectroscopy.

Although geometric optics provides the condition for total internal reflection to occur, it offers no explanation of the phenomenon or any information about the energy distribution at reflection. To gain further insight in to this phenomenon, the results of electromagnetic theory must be applied to the case. The following discussion, detailed in Appendix A, is partially based on the treatment outlined by Hecht and Zajac (26).

Suppose that the incident monochromatic light wave is plane polarized so that it has the form

$$E_i = E_{oi} \exp [i (\tilde{k}_i.r - \omega_i t)] \qquad (2)$$

The reflected and transmitted waves can be written as

$$E_r = E_{or} \exp [i (\tilde{k}_r.r - \omega_r t)] \qquad (3)$$

$$E_t = E_{ot} \exp [i (\tilde{k}_t.r - \omega_t t)] \qquad (4)$$

It is shown in appendix A that when TIR occurs

$$|E_{or}| = |E_{oi}| \quad (\text{for } \Theta_i > \Theta_c) \qquad (5)$$

Since $|E_{or}| = |E_{oi}|$, all the energy in the wave is reflected, which implies that $|E_{ot}| = 0$.

Therefore, although the transmitted wave does exist, it cannot, on average, carry energy across the interface.

However, in order to satisfy the boundary conditions, there must be a disturbance in the second medium and this is shown to be

$$E_t = E_{ot}\, e^{-\delta z_e i(k_t x \sin\Theta_i/n_{ti} - \omega t)} \qquad (6)$$

i.e. the disturbance in the less dense medium is periodic in x but exponentially decaying in the z direction. This is the evanescent wave. In the denser medium a stationary wave pattern is set up owing to the interference between the incident and reflected beams and in the less dense medium the amplitude falls off exponentially, although the amplitudes are equal at the interface.

The spatial rate of decay of the field in the second medium is determined by the attenuation constant δ. Related to this constant δ is a very important characteristic of the evanescent wave known as the **depth of penetration** (d_p). This is defined as the distance required for the electric field amplitude to fall to exp (-1) or 37% of its value at the surface and is given by

$$d_p = 1/\delta = \frac{(\lambda/n_1)}{2\pi\,[\sin^2\theta_1 - n_{t1}^2\,]^{1/2}} \qquad (7)$$

where n_{t1} is the ratio of the refractive indices of the incident and transmitting media. Illustrated in figure 2 is a standing-wave near a totally reflecting interface. The evanescent wave couples to the reflected wave, and therefore the properties of the reflected wave are determined by the environment just beyond the interface. Consequently, if the evanescent wave penetrates into an absorbing medium, the net effect is that some of the previously totally internally reflected energy is absorbed. The penetration depth divided by the wavelength λ_1 is

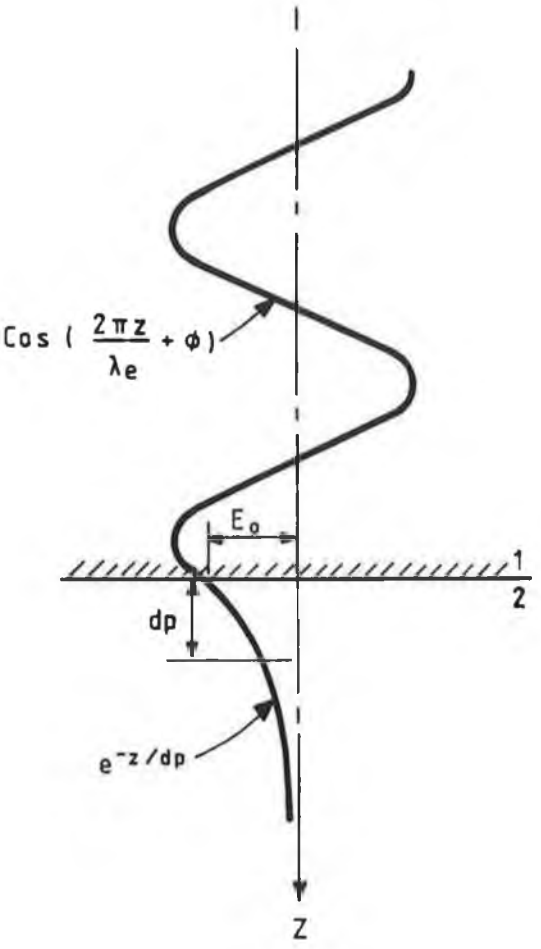

Fig.2 : Standing-Wave Amplitudes Established near a Totally Reflecting Interface
There is a Sinusoidal Dependence of the Electric Field Amplitude on the Distance from the Surface in the Denser Medium 1 and an Exponentially Decreasing Amplitude in the Rarer Medium 2 (29)

is plotted versus angle of incidence, in figure 3, for a number of interfaces (29). Harrick (29) points out that the penetration is about one-tenth the wavelength in the denser medium near grazing incidence ($\Theta \sim 90^{\circ}$) for high index materials, but becomes infinitely large as Θ approaches Θ_c. Carniglia et al (30) investigated the interaction at the microscopic level of evanescent waves with atomic dipoles and showed that the evanescent absorption is proportional to the transmitted intensity. This is shown in figure 4, which illustrates the molecular absorption probability, with angle of incidence Θ, for a molecule located in an evanescent field for different ratios of distance *a* of molecule from interface to wavelength. One can observe from this plot that the probability of an evanescent photon being absorbed by the surrounding medium increases dramatically as the angle of incidence approaches the critical angle and falls off with increasing angle at a rate depending on the distance of the molecule from the interface.

Equation (6) also shows that the penetration depth is larger with closer index matching (i.e as $n_t/n_i \longrightarrow 1$) and increases with increasing wavelength. Thus, by an appropriate choice of the refractive index n_i of the internal reflecting element (IRE), of the incident angle Θ and of the wavelength λ, one can select a d_p to promote optical interaction mainly with compounds close to or

NO	1	2	3	4	5	6	7	8	9	10	11	12	13	14	15	16
θ_c	10°	15°	20°	25°	30°	35°	40°	45°	50°	55°	60°	65°	70°	75°	80°	85°
n_{21}	.174	.259	.342	.423	.500	.574	.643	.707	.766	.819	.866	.906	.940	.966	.985	.996

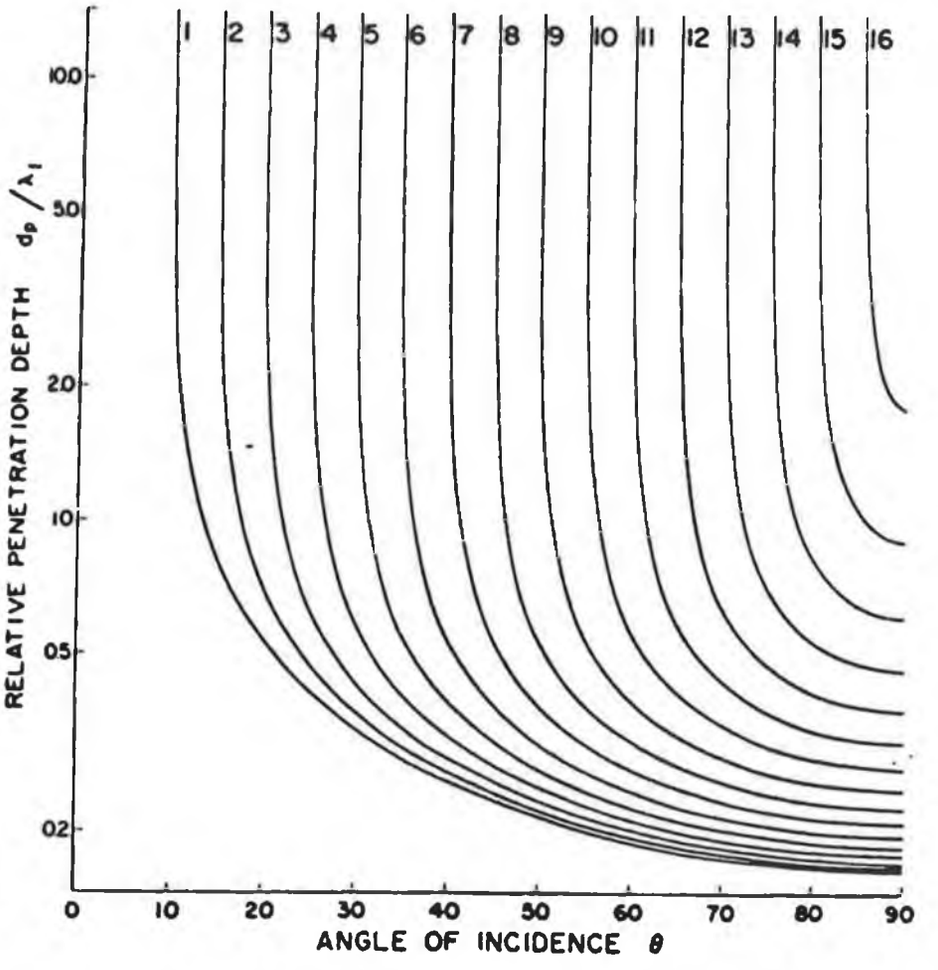

Fig.3 : Fractional Penetration Depth of Electromagnetic Field in Rarer Bulk Medium for Total Internal Reflection *vs* Angle of Incidence for a Number of Interfaces. The Penetration Depth is Infinitely Large at the Critical Angle (29)

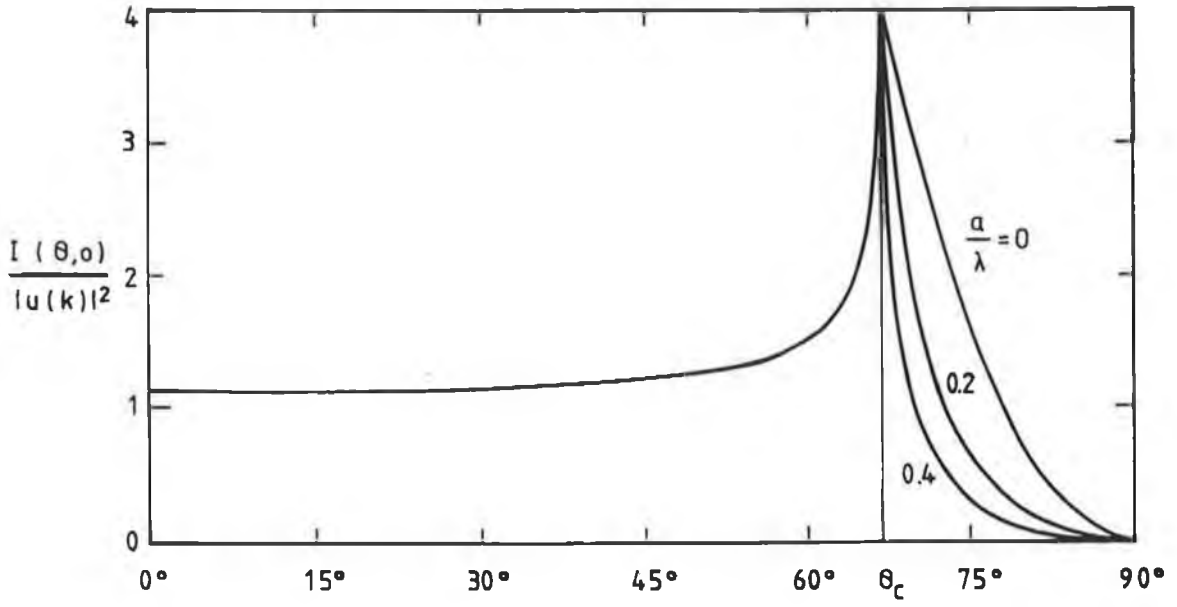

Fig.4 : The Molecular Absorption Probability, with Angle of Incidence θ, for a Molecule Located in an Evanescent Field, for Several Different Ratios of Distance a, of Molecule from Interface to Wavelength (30)

affixed at the interface and minimise interaction with bulk solution.

The depth of penetration is one of four factors which determine the attenuation caused by absorbing films in internal reflection. The other factors are the polarization dependent electric field intensity, the interaction area which increases with number of reflections N and matching of the refractive index of the two media.

Of the various factors which influence IRS, the most significant is the internal reflection element (IRE). The geometry of the IRE is a function of both the nature of the sample (usually a small quantity of liquid) and the IRS technique employed.

A large variety of IRE's have been developed (29), the simplest of which is the single reflection prism, shown in Fig.1.

The number of reflections (N) is a function of the length (L), the thickness of the waveguide (T) and angle of incidence (Θ) and is given by

$$N = (L/T)\cot\Theta \qquad (8)$$

The longer and thinner the waveguide, the larger is N and the more frequently the evanescent wave interacts with the surrounding medium. It is shown by Sutherland et al (31) that the reflection loss R after N reflections is:

$$R^N = 1 - N\alpha \qquad (9)$$

for small α, where α is the absorption coefficient.

A very promising multiple reflection element IRE is the optical fibre. Here light is introduced at angles exceeding the critical angle and propagates through the fibre by total internal reflection. Fibres are used as IRE's because of their small diameter and (potentially) unlimited length so that the effective number of reflections can be very large.

The remainder of this chapter is devoted to IRS using multimode optical fibre as the sensing element and the development of a model relating evanescent wave absorption in a liquid to the corresponding reduction of light intensity in the fibre.

2.3 Optical Fibre Considerations.

The picture of light propagation in optical fibres that has been used so far, that is of rays of light reflected back and forth from the core - cladding boundary and thereby travelling zig-zag fashion along the fibre, is adequate for most purposes. But light is an electromagnetic wave phenomenon and modes of guided wave propagation, rather than rays, provide a more comprehensive representation.

2.3.1 Optical Fibre Modes.

An optical fibre is a dielectric waveguide that operates at optical frequencies. The propagation of light along the waveguide can be described in terms of a set of propagating, electromagnetic field distributions called the modes of the waveguide. These guided modes are referred to

as the bound or trapped modes of the waveguide. Each guided mode is a pattern of electric and magnetic field lines that is repeated along the fibre at intervals equal to the operating wavelength. The most widely accepted waveguide structure is the single solid dielectric cylinder of radius *a* and index of refraction n_1 shown in figure 5. The cylinder is known as the core of the fibre. The core is surrounded by a solid dielectric cladding having a refractive index n_2 that is less than n_1. Variations in the material composition of the core give rise to the two commonly used fibre types, step-index and graded-index, as shown in figure 6. Both the step-index and the graded-index fibres can be further divided into single mode and multimode classes. As the name implies, a single mode fibre sustains only one mode of propagation, whereas multimode fibres may contain many hundreds of modes.

A mode traveling in the positive z-direction (that is along the fibre axis) has a time and z dependence given by (32)

$$e^{i(\omega t - \beta z)} \qquad (10)$$

The factor β is the z component of the wave propagation vector k whose magnitude is $2\Pi/\lambda$ (where λ is the free space wavelength) and is the main parameter of interest in describing fibre modes. For guided modes β can only assume certain discrete values, which are determined from the requirement that the mode field must satisfy Maxwell's equations and the electric and magnetic field boundary

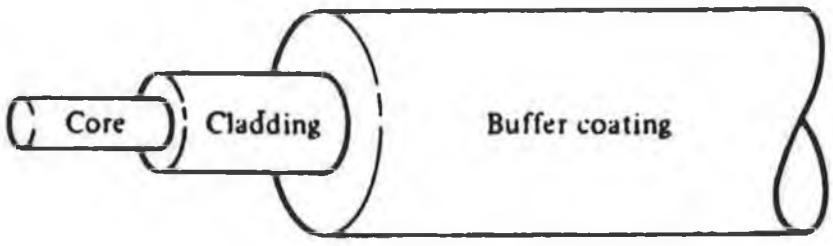

Fig.5 : Schematic of a Single Fibre Structure

A Circular Solid Core of Refractive Index n_1 is Surrounded by a Cladding having a Refractive Index $n_2 < n_1$. A Plastic Buffer Encapsulates the Fibre

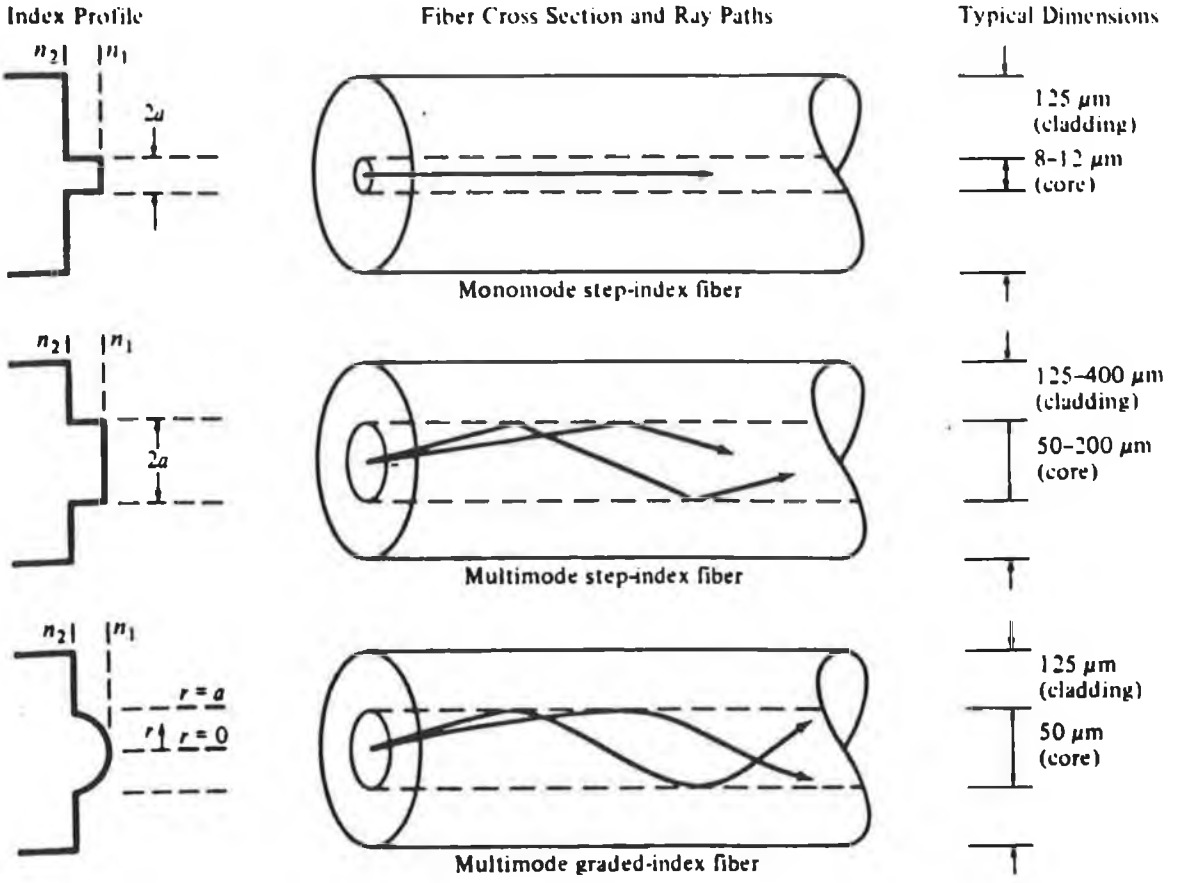

Fig.6 : Comparison of Single-Mode and Multimode Step-Index and Graded-Index Optical Fibres (32)

conditions at the core-cladding interface.

Figure 7 represents a cross-sectional view of an optical fibre cut along its axis. It shows the field patterns of several low order modes. The order of a mode is equal to the number of field maxima across the guide. The order of the mode is also related to the angle that the ray corresponding to this mode makes with the axis of a fibre; that is, the steeper the angle, the higher the order of the mode. The figure shows that the electric fields of the guided modes are not completely confined to the core (that is, they do not go to zero at the core-cladding boundary), but, instead, they extend partially into the cladding. The fields vary harmonically in the guided region of refractive index n_1 and decay exponentially outside of this region. For low order modes, the fields are tightly concentrated near the centre of the core with little penetration into the cladding region. On the other hand, for higher order modes the fields are distributed more toward the edges of the core and penetrate further into the cladding region.

Solving Maxwell's equations shows that, in addition to supporting a finite number of guided modes, the optical fibre waveguide has an infinite continuum of radiation modes that are not trapped in the core and guided by the fibre but are still solutions of the same boundary-value problem. The radiation field basically results from the optical power that is outside the fibre acceptance angle

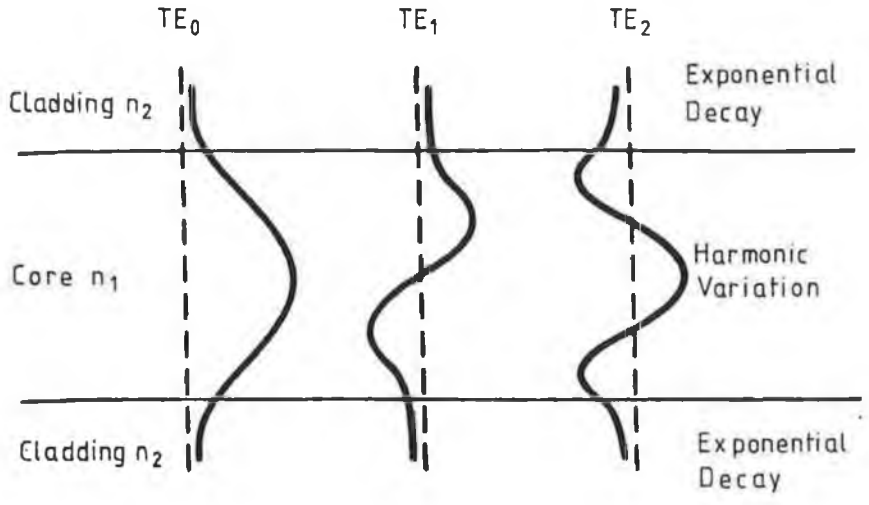

Fig.7 : Cross-Sectional View of an Optical Fibre Cut Along its Axis, Showing the Field Patterns of Several Low Order Modes

being refracted out of the core. Because of the finite radius of the cladding, some of this radiation gets trapped in the cladding, thereby causing cladding modes to appear. As the core and cladding modes propagate along the fibre, mode coupling occurs between the cladding modes and the higher order modes. This coupling occurs because the electric fields of the guided modes are not completely confined to the core but extend partially into the cladding. A diffusion of power back and forth between the core and cladding modes occurs, which generally results in a loss of power from the core modes.

In addition to bound and refracted modes, a third category of modes called tunneling modes (33,34,35) is present in optical fibres. These are called tunneling modes as they appear to tunnel a finite distance into the cladding. The modes are attenuated by continuously radiating their power from the core as they propagate. Refracted and tunneling modes are collectively known as leaky modes as both experience power loss.

It can be shown that a mode remains guided as long as β satisfies the condition

$$n_2 k_0 < \beta < n_1 k_0 \qquad (11)$$

where k_0 is the free space propagation constant = $2\pi/\lambda_0$ and λ_0 is the free space wavelength.

The boundary between truly guided modes and leaky modes is defined by the cutoff condition $\beta = n_2 k_0$. As soon as β

becomes smaller than $n_2 k_0$, power leaks out of the core into the cladding. Leaky modes can carry significant amounts of power in short fibres (36).

2.3.2 Total Number of Modes.

A mode is referred to as being cutoff when its field in the cladding ceases to be evanescent and is detached from the guide, that is, the field in the cladding does not go to zero. As stated in section 2.2, the rate of decay of the field in the cladding is determined by the value of the constant δ. For large values of δ, the field is tightly concentrated inside and close to the core. With decreasing values of δ, the field reaches farther out into the cladding. Finally, for $\delta = 0$, the field detaches itself from the guide. The frequency at which this happens is called the cutoff frequency. An important parameter connected with the cutoff condition is the normalized frequency V (also called the V-number) defined by

$$V = (2\pi a/\lambda)\ (n_1^2 - n_2^2)^{1/2} \qquad (12)$$

where n_1 and n_2 are core and cladding refractive indices respectively and a is the core radius. The modes that can exist in a waveguide as a function of V may be expressed in terms of a normalized propagation constant *b* defined by

$$b = \frac{(\beta/k)^2 - n_2^2}{n_1^2 - n_2^2} \qquad (13)$$

A plot of *b* as a function of V is shown in figure 8.

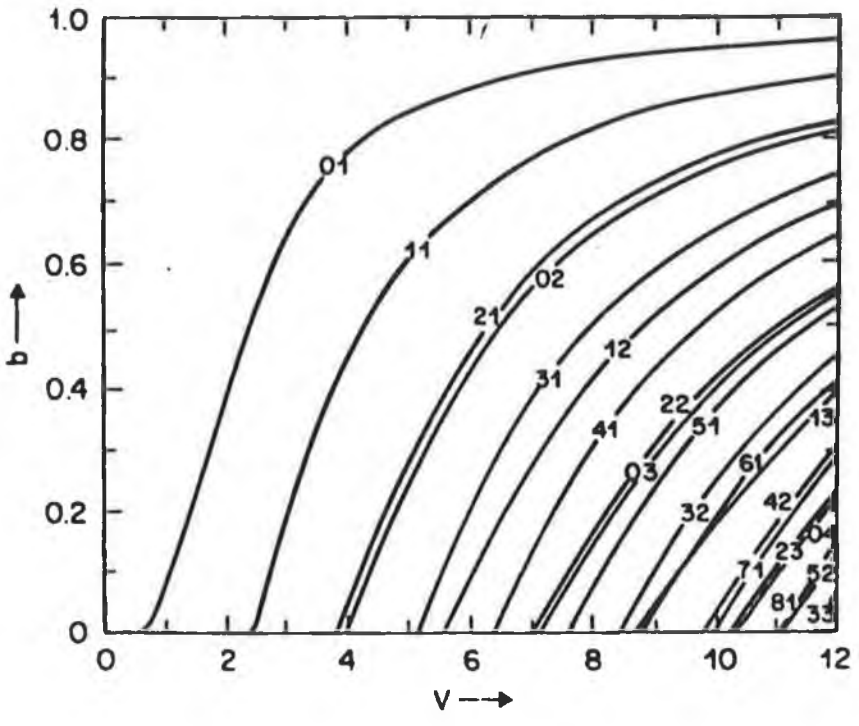

Fig. 8 : Normalized Propagation Constant as a Function of V
The Figure Shows that Each Mode can only Exist
for V-Values that Exceed a Certain Limiting Value Vc
This is Called the Cut Off Value (37)

This figure shows that each mode can exist only for values of V that exceed a certain limiting value. The modes are cut off when $\beta/k = n_2$.

The parameter V can also be related to the number of modes M in a multimode fibre when M is large (32). In appendix B it is shown that the total number of modes M which can be guided in a fibre is given by

$$M \sim V^2/2 \qquad (14)$$

2.3.3 Power Flow In The Cladding.

As is illustrated in figure 7, the electromagnetic field for a given mode does not go to zero at the core-cladding interface, but changes from an oscillating form in the core to an exponential decay in the cladding. The further a mode is from its cutoff frequency, the more concentrated its energy is in the core. The relative amounts of power flowing in the core and the cladding can be obtained by integrating the Poynting vector in the axial direction

$$S_z = 1/2\ Re(E \times H^*).e_z \qquad (15)$$

over the fibre cross section.

By assuming that there is a very small difference in the refractive indices of the core and cladding ($n_1 - n_2 << 1$ = weakly guided mode approximation), Gloge (38) has derived the fractional power flow in the cladding of a step-index fibre as a function of V, as illustrated in figure 9. In addition, far from cutoff, the average total power in the cladding has been derived for fibres in which many modes

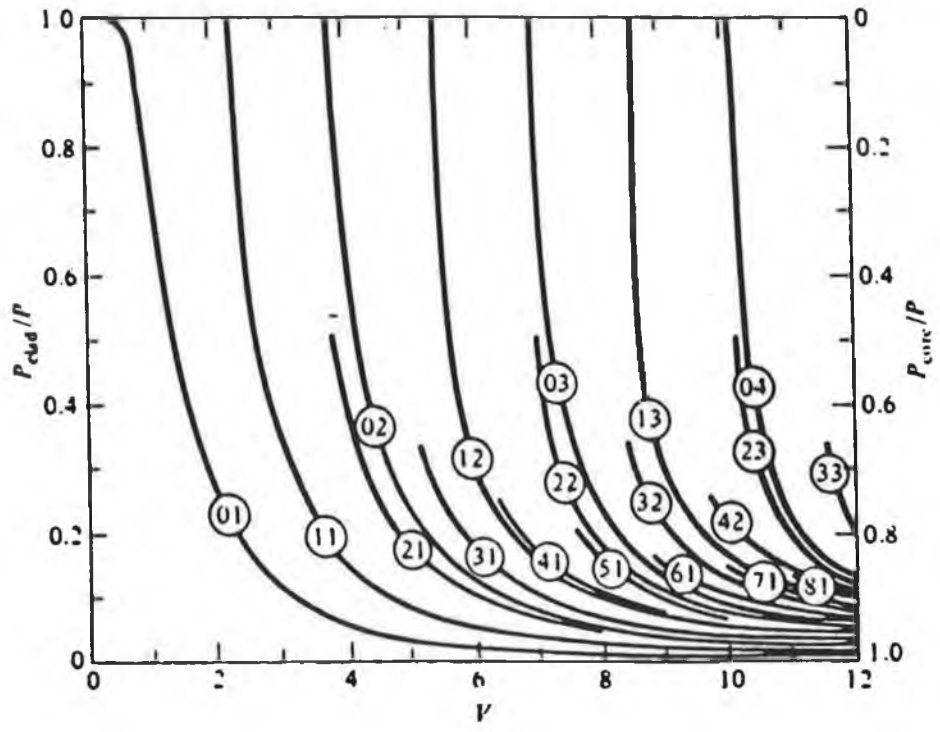

Fig.9 : Fractional Power Flow in the Cladding of a Step-Index Optical Fibre as a Function of V-Number (38)

can propagate. Because of this large number of modes, those few modes that are appreciably close to cutoff can be ignored to a reasonable approximation.

The derivation assumes an incoherent source, such as a tungsten filament lamp, which, in general, excites every fibre mode with the same amount of power. It is shown by Gloge (38) that the total average cladding power can be obtained from the expression

$$r = \frac{P_{clad}}{P_{tot}} = \frac{4}{3}\frac{\sqrt{2}}{V} \qquad (16)$$

where P_{clad} is the evanescent field intensity in the cladding and P_{tot} is the total light intensity in the core and cladding. The power flow in the cladding decreases as V increases.

For example, a 600 μm fibre of numerical aperture 0.4 operating at a wavelength of 500nm, has a V-number of 1508. From equation (16), approximately 0.125% of the power propagates in the cladding. For a typical single mode fibre of V-number 1 and same operating wavelength, about 70% of the total power flows in the cladding.

2.4 Evanescent Wave Spectroscopy Using Multimode Fibres.

If the cladding of a fibre is replaced locally by an absorbing fluid, characterised by a complex refractive index $n_{fluid} = n_2 - ik_2$, then the propagated power in the fibre is attenuated by evanescent absorption. The transmitted power is predicted to be (39)

$$P(L) = P(0)e^{-\gamma L} \qquad (17)$$

where L is the distance along the unclad length, $P(0)$ is the power transmitted in the absence of an absorbing species and γ is an evanescent absorption coefficient. The above equation (an equivalent Beer-Lambert relationship) takes into account the power distribution within the fibre. The evanescent absorption coefficient may be related to the bulk absorption coefficient α for two cases: (i) where all bound modes are launched and (ii) where selected modes only are launched.

(i) All Modes:

Tanaka et al (39) have shown that, using equation (16) and equation (17), the transmitted power becomes

$$P(L) = P(0)\ e^{-r\alpha L} \qquad (18)$$

Therefore, the evanescent absorbance $Log_{10}(P(0)/P(L))$ of an unclad fibre of length L surrounded by a fluid of bulk absorption coefficient α is given by

$$A_{ev} = \frac{\gamma L}{2.303} = \frac{r\alpha L}{2.303} \qquad (19)$$

This equation predicts that the evanescent absorbance in an

optical fibre **depends linearly** on both **exposed fibre length L** and **fluid concentration** and **inversely** on the **fibre V-number** from equation (16), for any fluid which obeys the Beer-Lambert law.

Analysis of the above discussion illustrates that by decreasing the V-number [= $2\pi a/\lambda \ (n_1^2 - n_2^2)^{1/2}$], r increases and more light becomes available for interaction with the surrounding fluid. Therefore, as the refractive index of the fluid n_2 approaches that of the core n_1 the light energy in the external medium increases.

(ii) Selected Modes:

This analysis is based upon the expression of Snyder and Love (36)

$$\gamma = NT \qquad (20)$$

where N is the number of reflections per unit length of fibre and T is the Fresnel transmission coefficient at the interface of a lossless core and and absorbing cladding.

In the case of meridional rays[a] in a weakly guiding waveguide ($n_1 \simeq n_2$) of normalized frequency parameter V, the relationship between the evanescent absorption coefficient γ and bulk absorption coefficient α for a lossy cladding is shown to be (Appendix C)

a) *Meridional Rays* are those which cross the fibre axis between reflections as distinct from skew rays which spiral around the fibre without crossing the axis.

$$\frac{\gamma}{\alpha} = \frac{1}{V}\left[\frac{\Theta_z}{\Theta_c'}\right]^2 \frac{1}{[1-(\Theta_z/\Theta_c')^2]^{1/2}} \qquad (21)$$

where Θ_z is the angle the ray makes with the core axis and Θ_c' is the complementary critical angle ($\cos^{-1} n_2/n_1$) as illustrated in figure 10. The result is accurate for all bound meridional rays whose direction is not close to the critical angle. However, this expression needs to be modified to cater for non-weakly guiding modes which occur when the cladding refractive index (in this case a water based liquid) of approximately 1.33 is not close to the core index of 1.46 for silica glass. Removing this condition, and allowing all values of $\Theta_z < \Theta_c'$ the value for T can be shown (appendix C) to be

$$T = \frac{\alpha \lambda n_2 \cos\Theta}{\pi (n_1^2 - n_2^2)\sqrt{\sin^2\Theta - (n_2/n_1)^2}} \qquad (22)$$

Using equation (20) and equation (22) the evanescent absorption coefficient then reduces to

$$\frac{\gamma}{\alpha} = \frac{\lambda n_2 \cos^2\Theta}{2\pi a \sin\Theta (n_1^2 - n_2^2)\sqrt{\sin^2\Theta - (n_2^2/n_1^2)}} \qquad (23)$$

where Θ is the angle between the ray and normal to the interface ($\Theta = \pi/2 - \Theta_z$) and Θ_c is the conventional critical angle for the two media ($\Theta_c = \sin^{-1} n_2/n_1$).

For fluids obeying the Beer-Lambert law the bulk absorption coefficient (α) is proportional to fluid concentration.

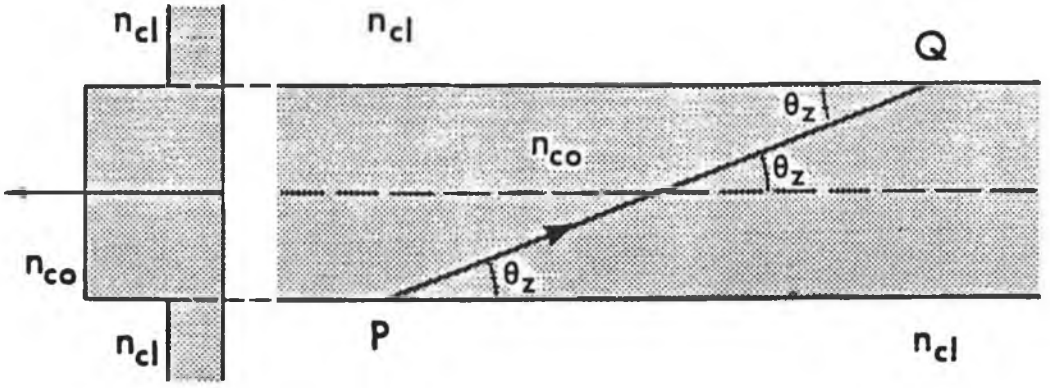

Propagation along a straight line between interfaces in the core of a step-profile planar waveguide.

Fig. 10 : The Incident Ray at Q is Totally Internally Reflected If $0 \leqslant \theta_z < \theta'_c$ (36)

From equation (23), therefore, the **evanescent absorption coefficient** is predicted to be **proportional** also to **concentration.**

A typical fibre used in this work has a 600μm core diameter and a numerical aperture (NA) of 0.4.

Since N.A. = 0.4 = $\sin\phi_{max} = (n_{co}^2 - n_{cl}^2)^{1/2}$ this yields a maximum launch angle $\phi_{max} = 23.6^\circ$ for bound meridional rays. This maximum launch angle gives rise to the critical angle Θ_c, at the core-cladding interface.

$$\Theta_c \text{ for clad fibre} = 90^\circ - \sin^{-1}(0.4/1.457)$$

$$\Theta_c = 74^\circ.$$

However, in the sensing region, where the removed cladding is replaced with an aqueous solution, whose refractive index $n_{cl} \simeq 1.33$, the local critical angle is given by

$$\Theta_c = \sin^{-1}(1.33/1.457)$$

$$\Theta_c = 66^\circ$$

Accordingly, it is not possible to launch <u>bound</u> modes in the clad fibre which will be incident at the core-fluid interface at angles closer than 8° to the critical angle.

As outlined in section 2.3.1, the fibre, by virtue of its cylindrical geometry, will sustain non-bound or tunneling modes which are launched at angles greater than the meridional numerical aperture permits. These modes can propagate for substantial distances with negligible attenuation (40) and some of them will satisfy the bound mode condition on reaching the sensing region. Low order

modes, which have little power in the cladding, can be blocked using an annular beam mask placed at the launch optics (41). Alternatively, higher order modes may be generated at the sensing region by tapering the fibre at this location (42) or by bending (15).

As in the case of all bound modes, equations (19) and (23) predict that evanescent absorption varies linearly with both unclad fibre sensing length and concentration for fluids obeying the Lambert-Beer law in bulk absorption.

The sensitivity per unit length of the fibre optical sensor can be determined from equation (18). When the sensor is a multimode optical fibre, the value of the evanescent wave ratio, r, is dependent on the excitation state of the propagation modes of the sensor, i.e. with electromagnetic energy distribution amongst the fibre modes. As a result of this, reproducibility of the sensitivity of the sensor will not necessarily be obtained.

2.5 Summary.

The theoretical model predicts the relationship between the evanescent absorption coefficient γ and bulk absorption coefficient α for two separate situations when using an optical fibre with part of its cladding removed.

When all bound modes are launched, equation (19) predicts that the evanescent absorbance depends linearly on both exposed fibre length L and fluid concentration and inversely on the fibre V-number, for any fluid that obeys

the Beer-Lambert law.

When selected modes only are launched, equation (23) which is corrected for non-weakly guiding modes, predicts the evanescent absorption coefficient to be linearly proportional to concentration.

CHAPTER 3

EXPERIMENTAL SYSTEM

3.1 Measurement System.

The experimental system is shown in figure 11 and consists of a light source, monochromator, sample chamber, electronics with data acquisition and a microcomputer.

Optical radiation is supplied by a quartz tungsten halogen source (12V, 50W) and focused onto an f/4 monochromator (PTR Optics, USA, Model MC1-02). A Hamamatsu photomultiplier (model R1546) tube monitors the light intensity from the terminated optical fibre. The analogue output from the detector can be used to obtain a chart recording and/or sent to a 12 bit analogue-digital converter. The digital output is then averaged and analysed by the BBC microcomputer.

The monochromator is a Fastie-Ebert design and consists of a spherical collimating/focusing mirror that directs parallel light onto a plane reflective holographic diffraction grating and converges a segment of the dispersed light on to the exit slits as shown in figure 12. Two diagonal mirrors fold the beam in to an in-line configuration. The full specification of the monochromator is given in appendix D.

The monochromator is stepper motor driven by a microprocessor based controller/driver. This unit contains a 200 byte internal memory and is programmable by any ASCII

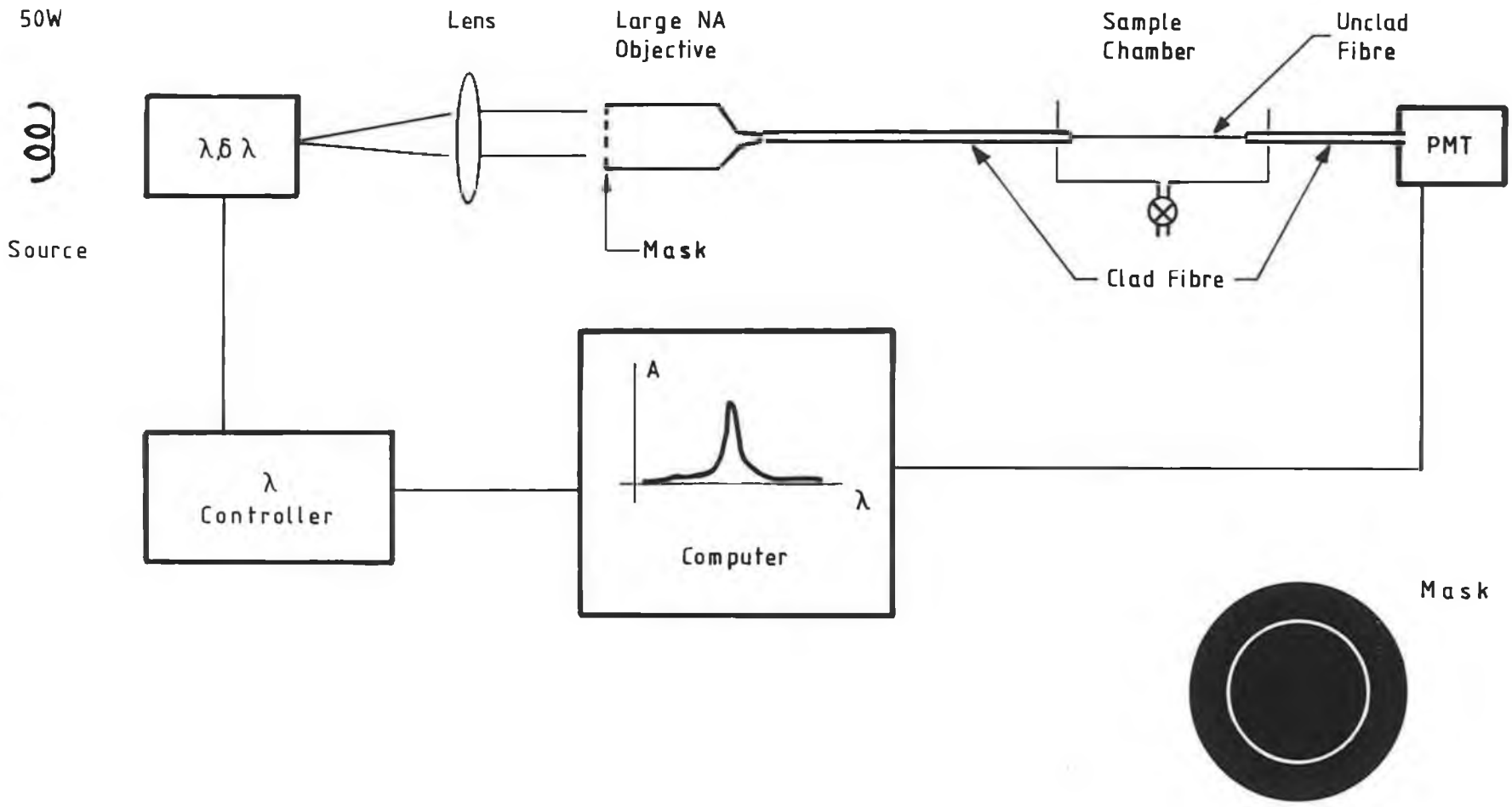

Fig. 11 : Schematic of Experimental System and Optical Mask

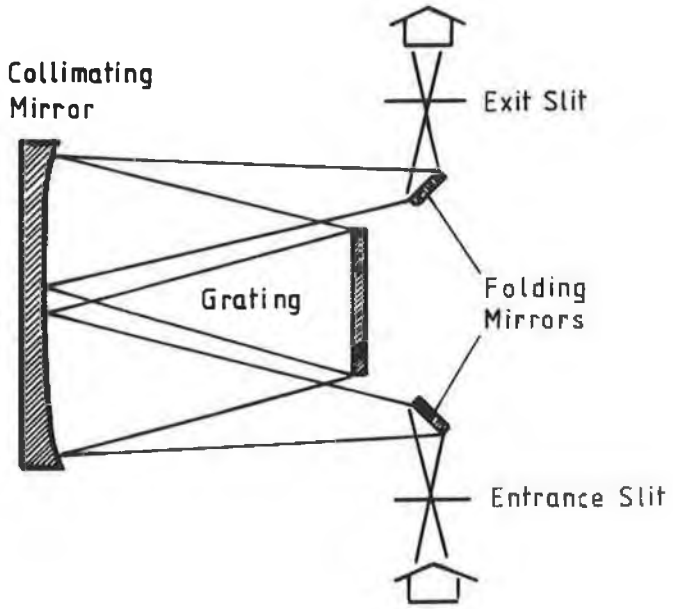

Fig. 12 : Schematic Diagram of the Fastie-Ebert Monochromator

keyboard or computer. Over 30 ASCII high level commands allow the user to program "move distance", "initial velocity", "ramp slope and length", "half or full step" operation together with a "search for zero order". In particular, a routine is stored within the unit to return the monochromator to zero order wavelength. Because the controller has such a small memory capacity, it was decided to interface it to the BBC microcomputer via the RS 232 port. In this way all the software was written in BASIC and stored on floppy disk.

A silicon photodetector or photomultiplier tube is mounted at the exit port of the sample chamber. The spectral response curves of these photodetectors are shown in figures 13 and 14, respectively. Although the spectral response of silicon is wider, a photomultiplier has a greater sensitivity in the visible region. It was therefore decided to use this detector for all experimental work.

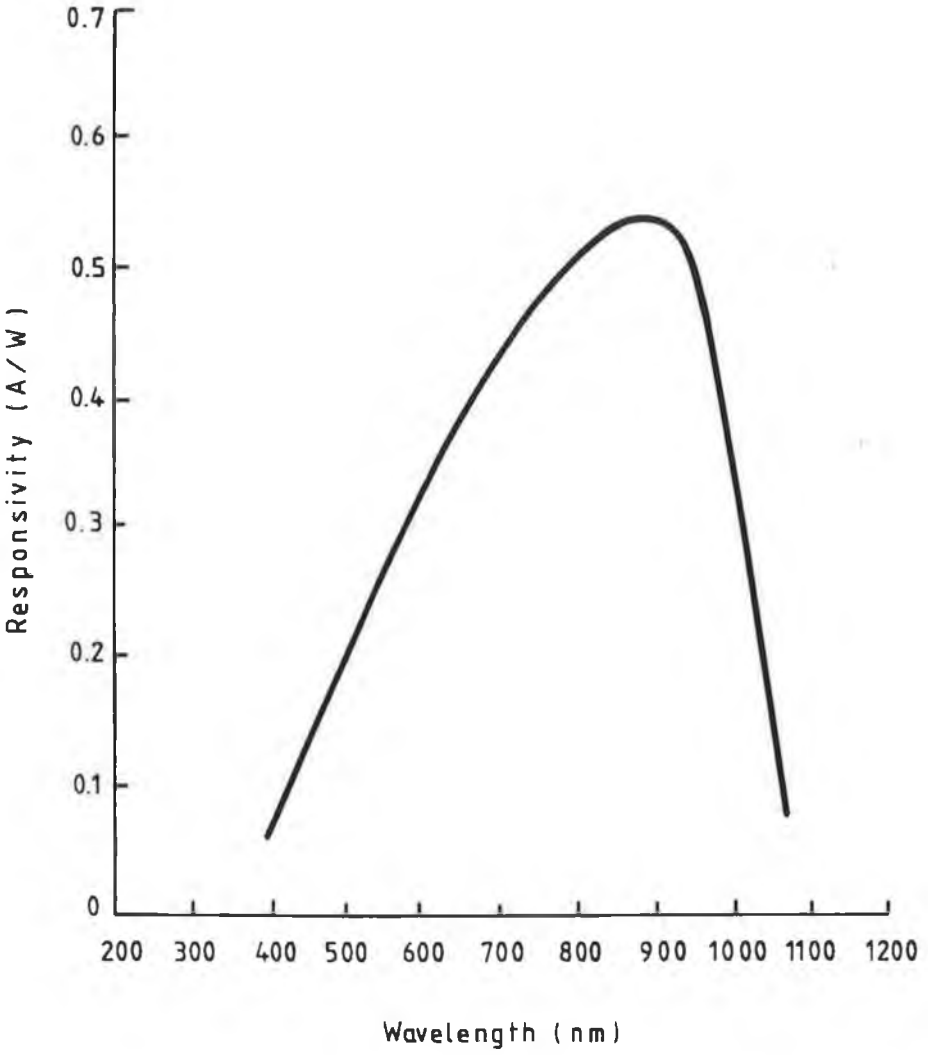

Fig.13 : Spectral Response of a Silicon Photodetector (43)

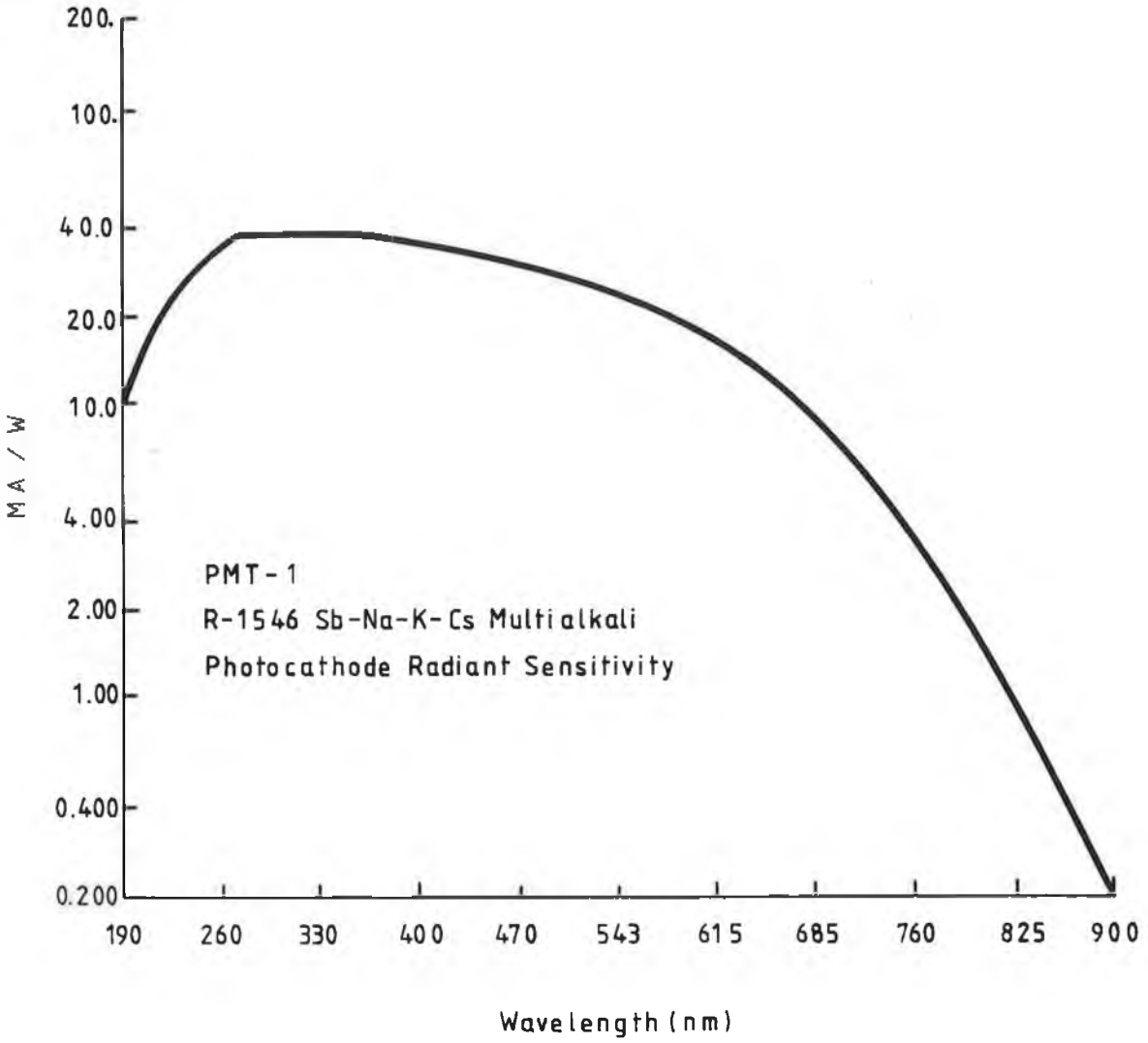

Fig.14 : Spectral Response of a Photomultiplier Tube(43)

3.2 Calibration and System Response.

The grating mount has an upper and lower limit switch to protect it from being damaged. The wavelength range is defined by the separation between these two limits. Calibration may be performed at any wavelength of interest provided a reference source is available at that wavelength. It was decided to calibrate at zero order for two reasons:

(i) as all wavelengths are transmitted through the monochromator, the output energy is large relative to the diffracted wavelength output and is easier to detect as a definite peak in output energy. Therefore, no special spectral sources are required.

(ii) the manufacturers (PTR Optics, USA) calibrate the diffracted wavelengths relative to zero order.

The calibration consisted of the determination of the low and high limits relative to zero order. Therefore, the location of zero order is always known and from this all other wavelengths are measured. A program was written to perform this procedure automatically and is listed in the software section.

The calibration was then checked using a Mercury arc lamp and the spectral output is shown in figure 15.

The system spectral response from 100nm to 800nm is shown in figure 16. This indicates the spectral range over which useful data can be obtained. In investigating the response

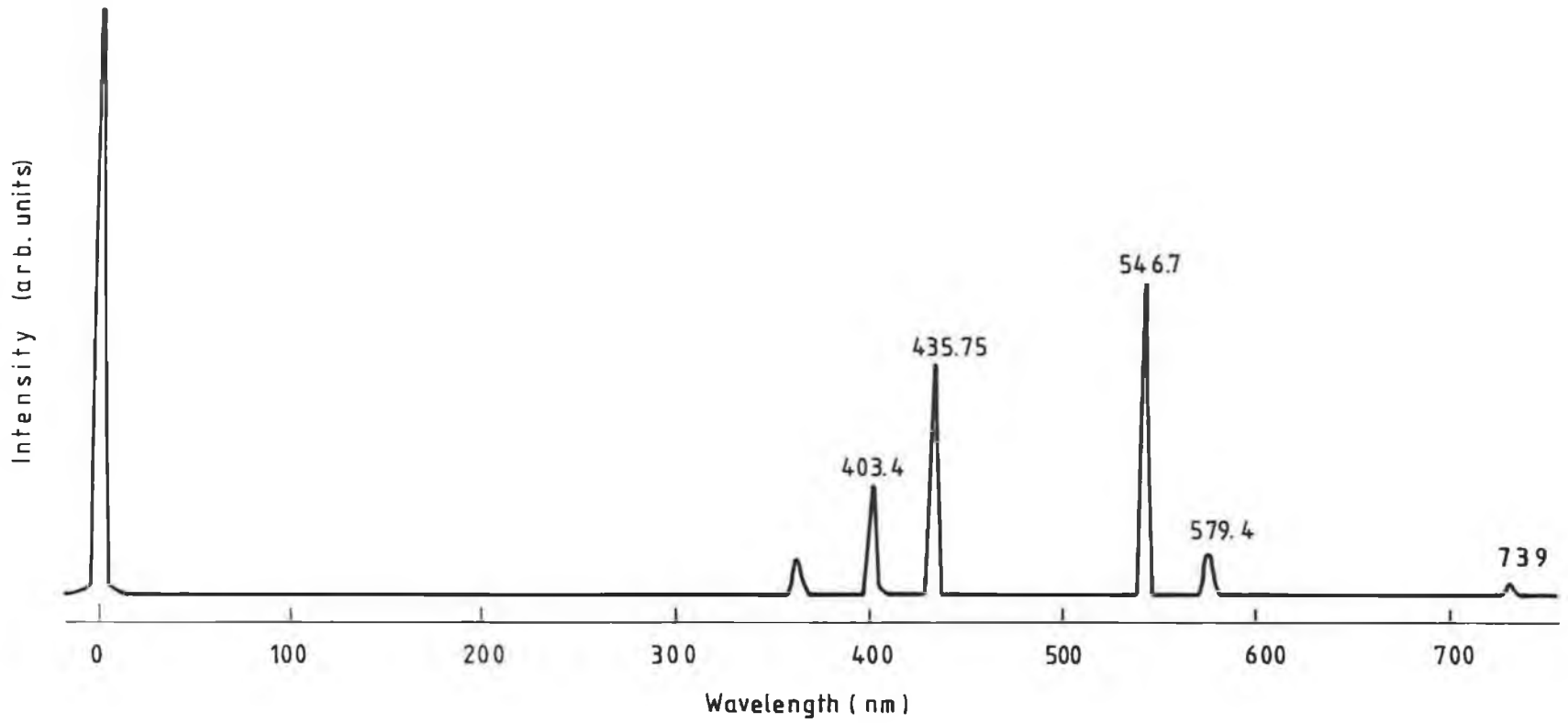

Fig. 15 : Calibration of System Using Mercury Arc Lamp

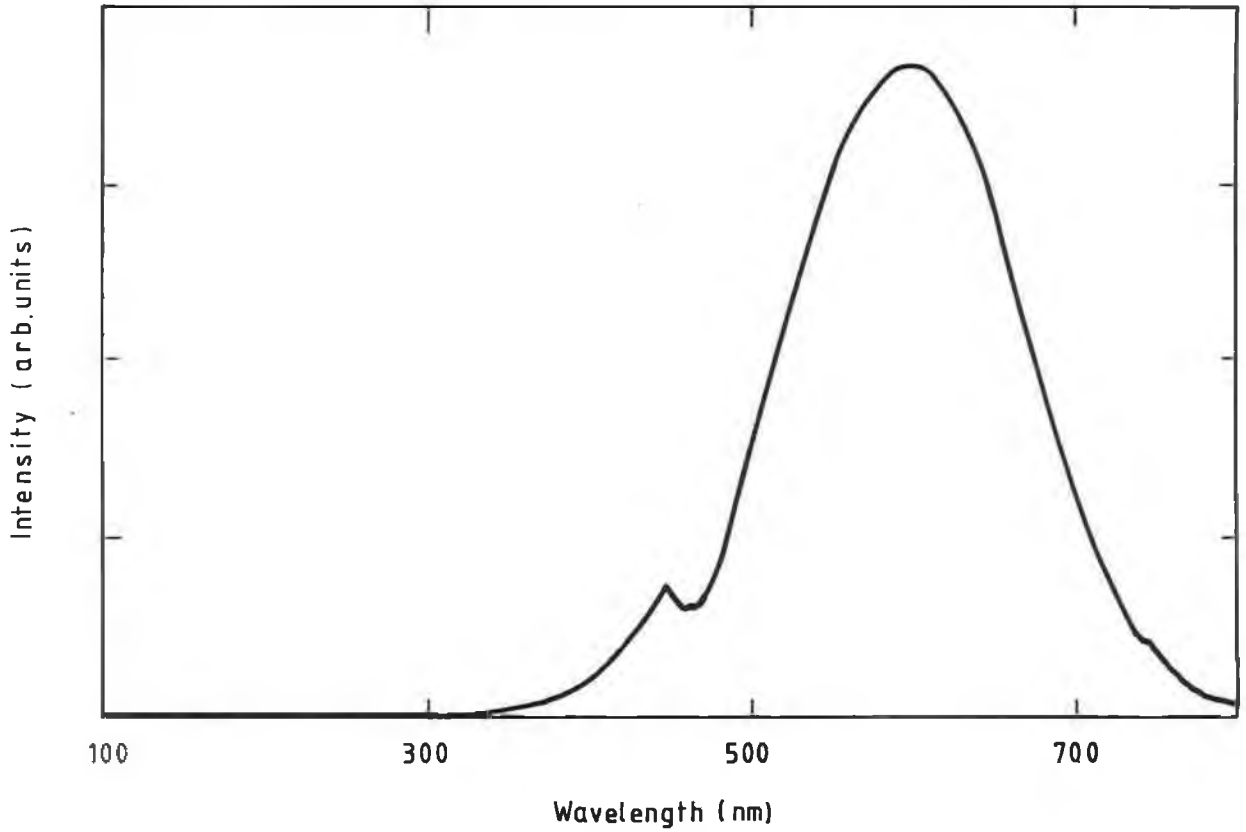

Fig. 16 : System Spectral Response

two problems were encountered which were of significant importance in the setting up of the experimental system. As seen in figure 16 there is a peculiar feature or "kink" at 460nm of full width half maximum 20nm. Having ruled out dirty optics, misalignments or other obvious reasons by a process of systematic elimination, it was discovered to be a grating anomaly. It is one of three major anomalies occurring in the $\underset{\sim}{E}$ polarization efficiency of the holographic grating used in this monochromator. The feature can be seen in the efficiency curve of the grating and relative throughput curve in figure 17 and figure 18, respectively. While these anomalies are undesirable they do not indicate a grating defect.

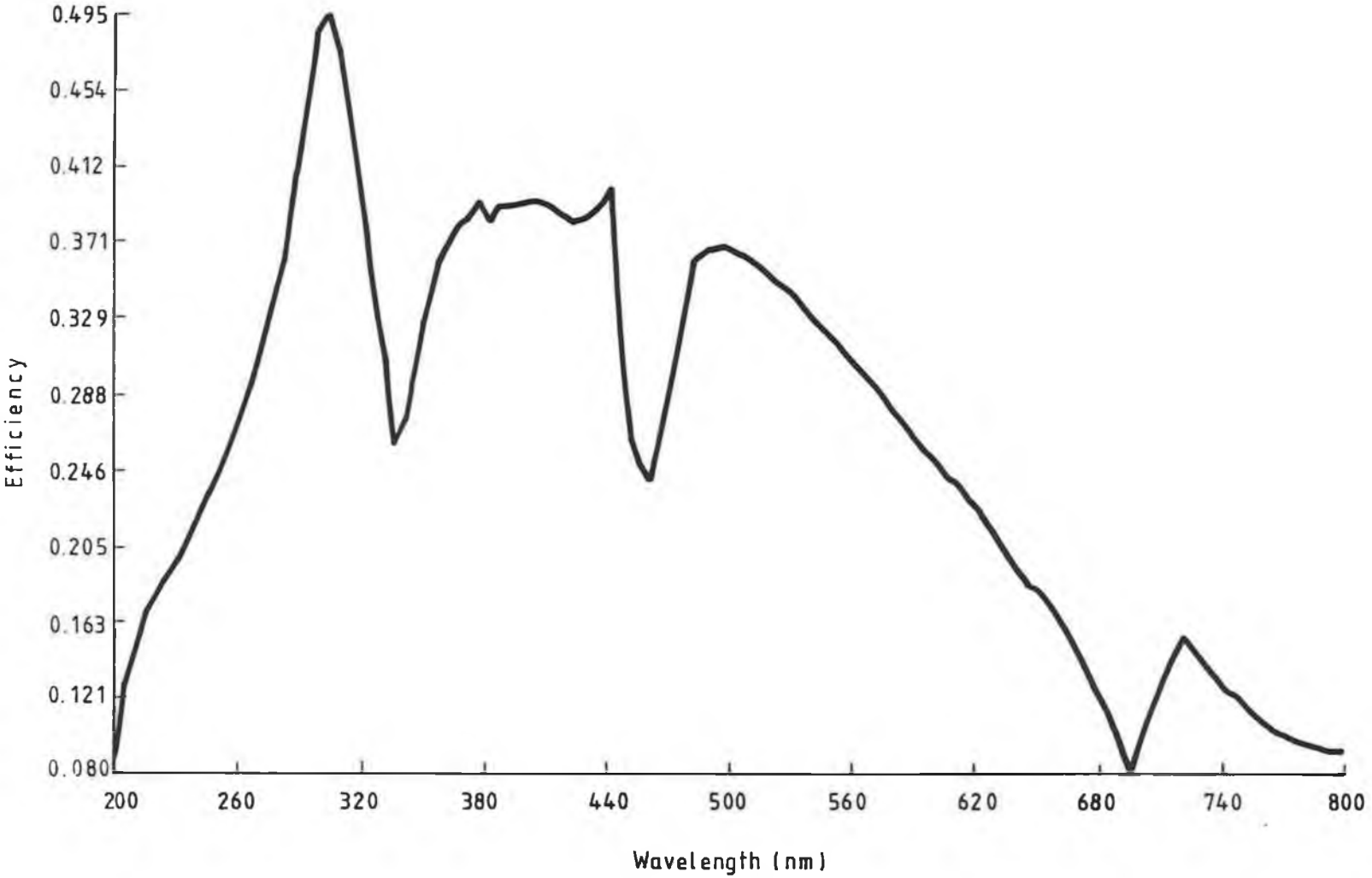

Fig. 17 : Efficiency Curve of the Holographic Grating as a Function of Wavelength (43)

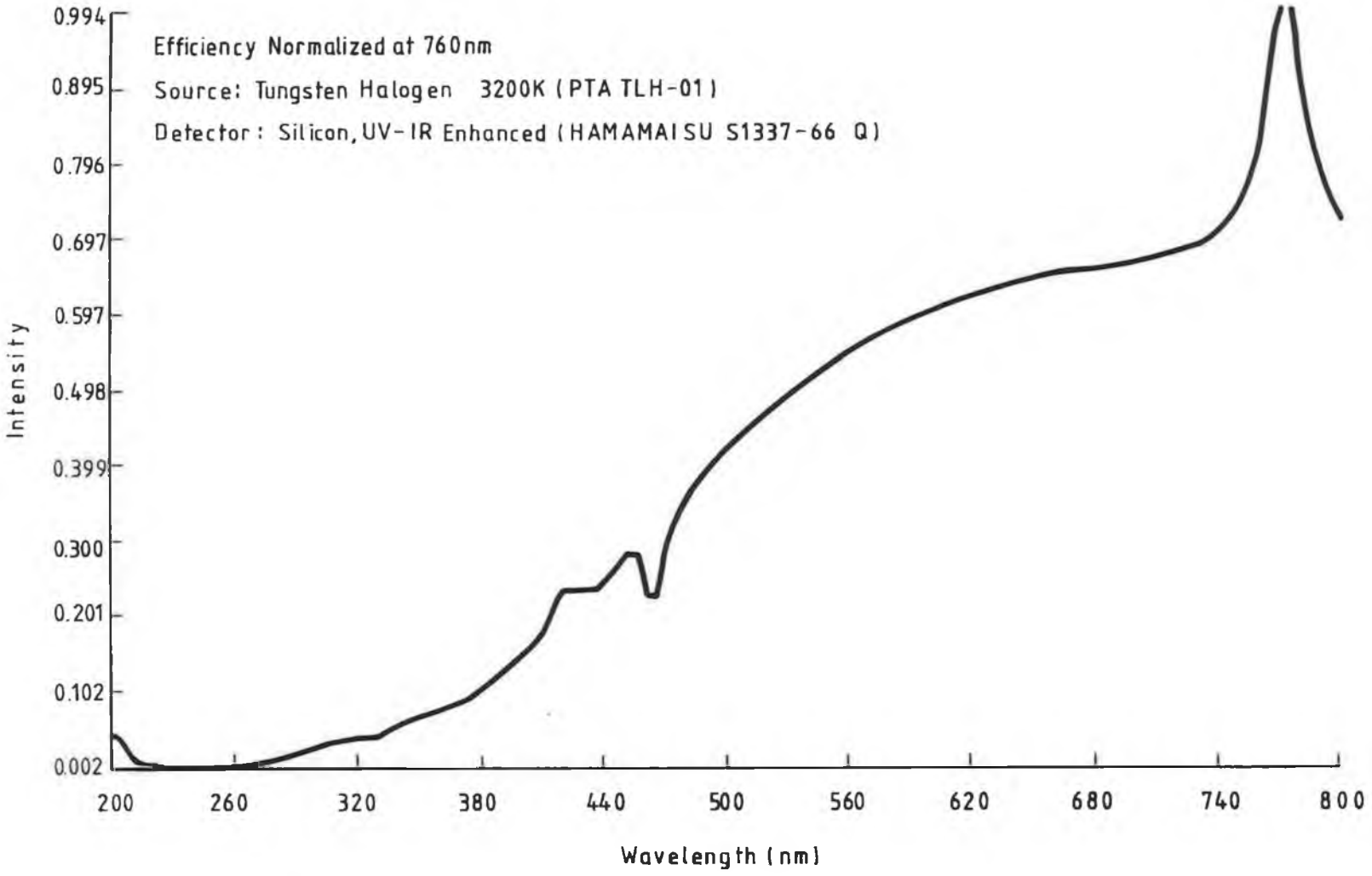

Fig. 18 : Relative Throughput Curve of the Monochromator (43)

3.3 Sensing Fibre and Preparation.

The optical fibre selected as the sensor in these experiments was plastic clad silica (PCS) fibre (TSL,UK). The core is made of high purity fused silica to allow low attenuation across a wide spectral range. As illustrated in figure 19, the attenuation of the fibre in the range 400nm to 700nm is less than 30 dB/km. The cladding is a silicone resin and surrounding this is a protective plastic Tefzel (ETFE) outer coating to provide mechanical protection. This multimode step index fibre was originally chosen because of the ease in which the cladding can be stripped from the core to provide the sensing element. Another advantage of this fibre is the high transmission characteristics in the near UV and visible range. The fibre is also readily available in either 200μm or 600μm core diameter, both of numerical aperture 0.4. This enables efficient coupling of light in to the fibre and also provides a large sensing volume to interact with the absorbing species. The specification for 200μm and 600μm fibres is outlined in appendix E.

The length of fibre used in the experimental set-up was approximately 1m. For efficient coupling of radiation into the fibre it is necessary that the end-faces are flat and perpendicular to the optical axis of the fibre. Several commercially available fibre cleaving tools provide smooth mirror-like end-faces for fibres of core diameter between

Guaranteed Values of Attenuation	
λμm	dB/km
0.50	30
0.60	20
0.70	14
0.85	12

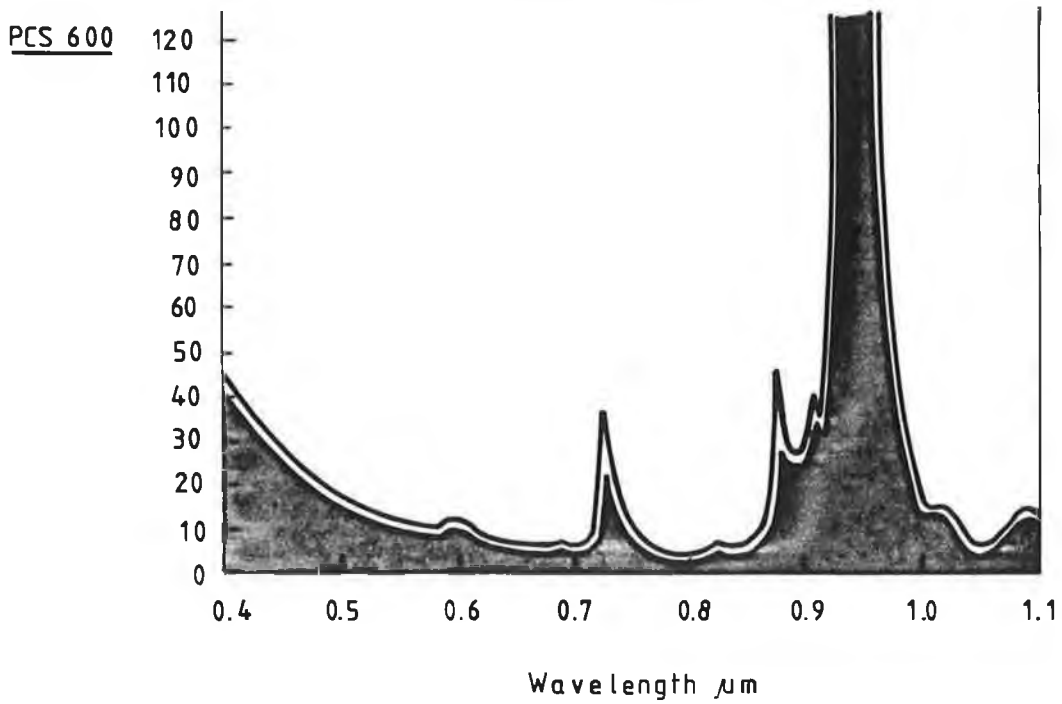

Fig.19 : Attenuation Curve of Plastic Clad Silica Core Optical Fibre (44)

3μm and 50μm and cladding diameter of 125μm. However, in view of the large core diameter of the fibre used here, there is no cleaving tool available that would produce a satisfactory quality endface. A polishing and lapping machine (Logitech Ltd,U.K.) is used to produce good quality end-faces (figure 20). The fibres are placed in a mild steel barrel and waxed in position, being slightly proud of the end. When the wax has solidified, the barrel is secured in a polishing jig and this is then placed on the polishing plate.

The polishing occurs first on the wax, then the fibres and finally on the base of the cylinder. Assuming the barrel is perpendicular to the plate, one is assured that the fibre end-face is perpendicular to its axis. It was observed that the more packed the barrel is with fibres, the more stable and secure they are. Otherwise, macro-cracks will develop a few mm from the endface. To obtain a satisfactory quality end-face, 9μm grit (Al_2O_3) is used at first. Thereafter, for greater quality, 3μm grit is used.

An important aspect in developing the in-line sensor was choosing an adequate procedure to obtain a clean core interaction region. First the Tefzel outer coating is removed using a mechanical stripping tool. Following this, the remaining cladding is removed by etching. Several different etchants were examined such as boiling chromic acid, sodium hydroxide in ethanol and a proprietary solvent.

Fig. 20 : A Polishing and Lapping Machine Used to Produce Good Quality End-Faces

Newby (45) subjected similar fibres to a combination of processes: hot chromic acid, autoclave, and radio frequency glow analysis. The cores were then examined by Xray photoelectron spectroscopy (XPS), and scanning electron microscopy (SEM). The reason XPS was used is that the core consists primarily of silicon and oxygen, while the cladding contains a high percentage of carbon atoms. Very high Si/C and O/C ratios indicate a cladding free surface. Although this technique was not available to us, Newby's results did indicate that chromic acid might be a suitable etchant.

The fibre was laid on a flat surface and the protective Tefzel coating removed from a central location using a scalpel, being careful not to scratch the core. It is important that all the cladding be removed since any particles on the surface would produce a scattering effect which would impair the surface sensitive qualities of the sensor. To ensure a clean sensor area, the stripped fibre was immersed in a container containing chromic acid at 85°C, for 40 minutes to remove the residual cladding. The sensor was then cleaned thoroughly in ethanol and finally wiped using an acetone soaked tissue.

This procedure was repeated for acid bath treatment durations of 10, 40, 70, and 100 minutes and SEM was used to determine the amount of residual cladding. Figure 21 shows a series of micrographs of 600μm fibre for 70 and

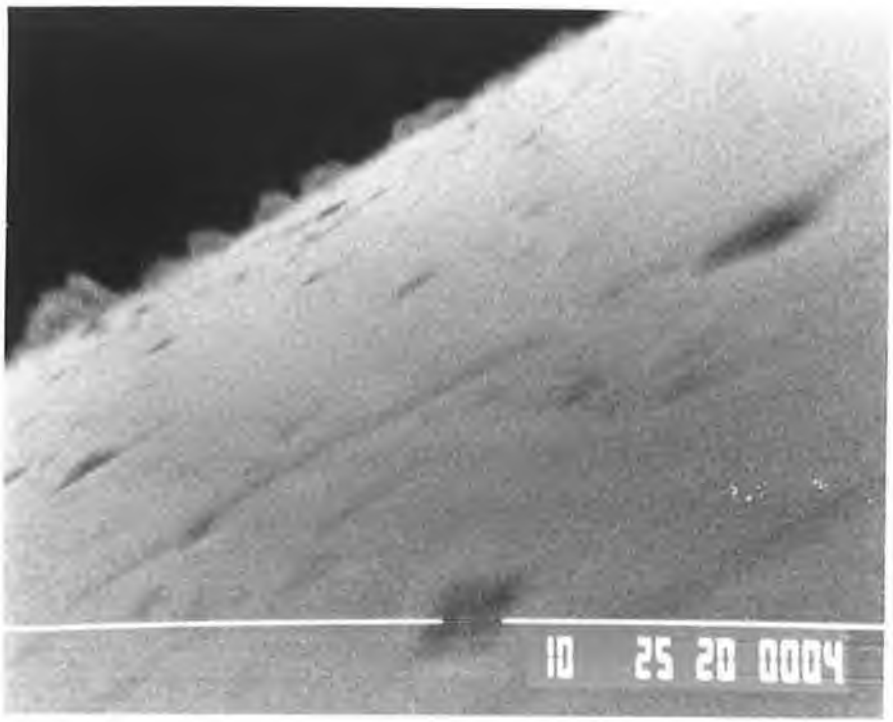

Fig.21 : Two Micrographs of 600μm Fibre for 70 and 100minute Treatments in Chromic Acid at 85°C

and 100 minute treatments in chromic acid at 85°C. As apparent from these photographs, there appears to be no reproducibility or improvement with treatment time in the quality of the fibre sample. In view of the unsatisfactory quality of the sensor surface and because of the hazards of the chemicals required this technique was not pursued.

The next technique consisted of placing the stripped fibre in a solution of sodium hydroxide in ethanol. However, the fibre had to be left in the bath for a period of between 12 and 14 hours. From the micrograph shown in figure 22 it is evident that an irregular contour of the surface is formed with this method and in no case was all the cladding removed.

The etching procedure adopted as a standard in this work used a solvent which was less hazardous than the previous two methods and removed the cladding relatively quickly. The proprietary solvent, Optical Fibre Stripper, (Lumer, France) developed to remove silicone coatings, was placed in the evanescent sample chamber with the fibre as shown in figure 23. Several short samples were prepared using a scalpel and placed in a Lumer solution for time durations of between 5 minutes and one hour. The etched fibre was then cleaned with ethanol followed by distilled water. Figure 24 illustrates SEM micrographs of samples for different etching times and it can be clearly seen that for etching times greater than 20 minutes, a clean glass

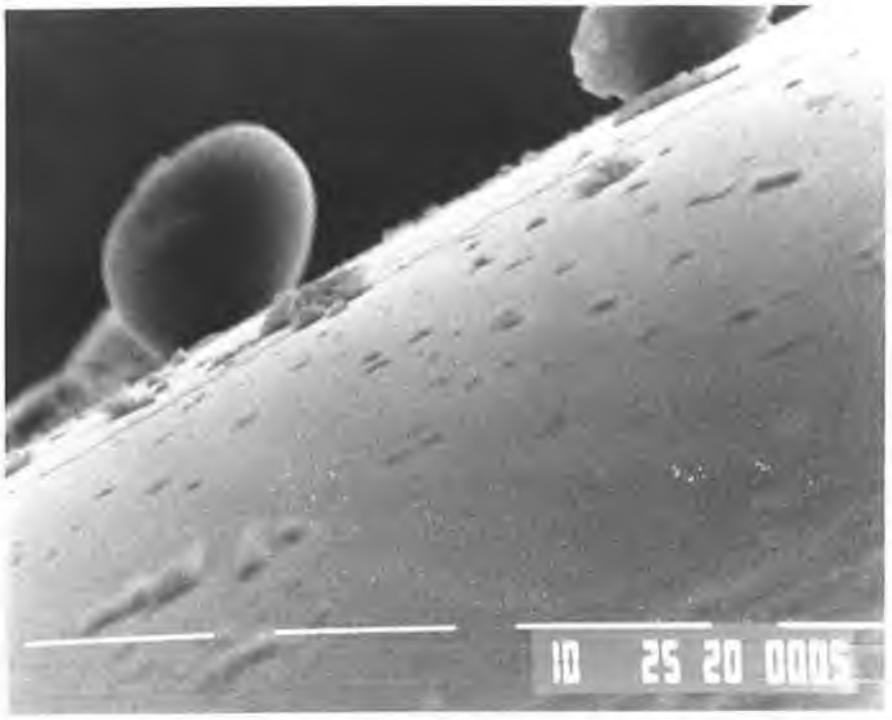

Fig. 22 : Micrograph of 600μm Fibre After Been Left in a Solution of Sodium Hydroxide in Ethanol for a Period of Between 12 and 14 hours

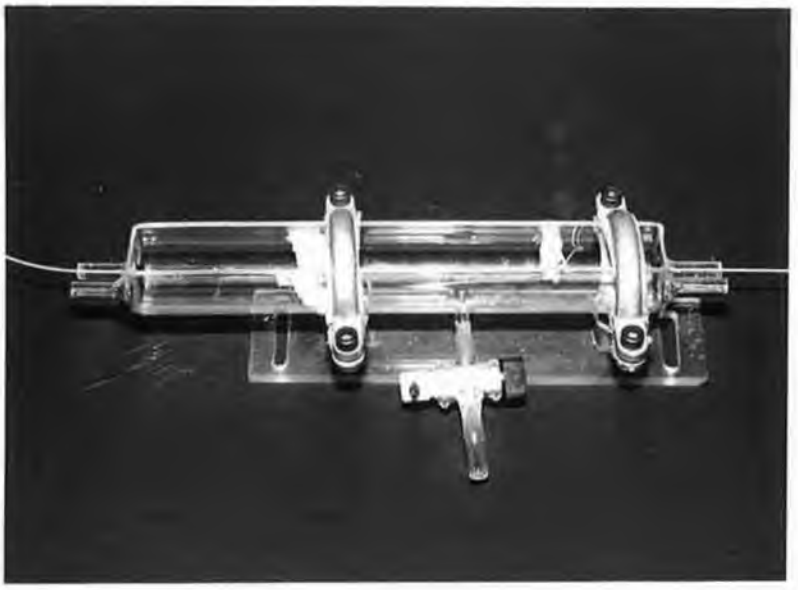

Fig. 23 : Evanescent Sample Chamber with Fibre In-Line

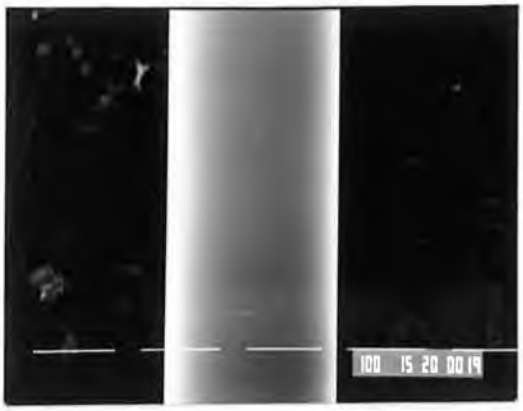

220μm PCS Fibre in
Etchant for 5mins

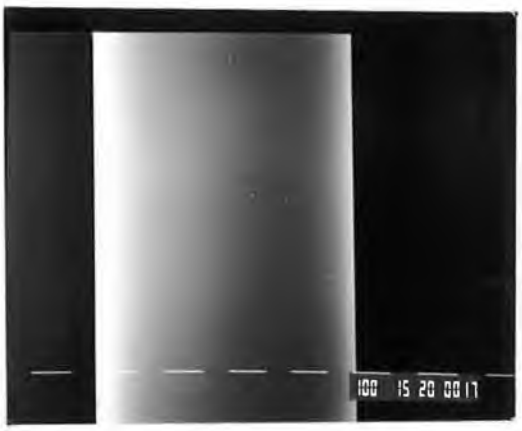

600 μm PCS Fibre in
Etchant for 30mins

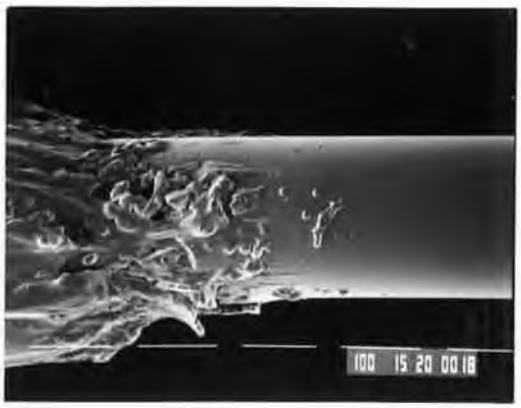

200μm PCS Fibre in
Etchant for 5mins
Showing Core/Cladding
Interface

Fig. 24 : Illustrates SEM Micrographs of Samples for Different Etching Times in Lumer Solution

surface with no visible residual particles is obtained.
A comparison of the above three methods shows that the Lumer etchant is the most suitable as it removes the residual cladding relatively easily, in the shortest possible time, and minimizes hazards in a laboratory.

3.4 Mask and Sample Chamber.

As illustrated in figure 11, the experimental set-up includes a cylindrical flow cell with the sensing fibre placed within it. The bare core is exposed to the sample solution along a maximum length of 22cm. The emerging beam from a 1mm diameter exit port of the monochromator is collimated by a 10 cm focal length lens and then launched into the fibre using a x40 microscope objective of numerical aperture 0.65. Assuming that the collimated beam completely fills the entrance plane of the microscope objective, the half angle of the exiting light is 40.5°, calculated from $NA = n_0 \sin\phi_{max}$, where n_0 is the refractive index of air, and ϕ_{max} is the maximum angle of emission. However, the fibre has a numerical aperture of 0.4 and an acceptance angle $\ominus$ of 23.5°,where $\ominus$ is the maximum angle between an incident ray and the fibre axis that will allow propagation by total internal reflection (neglecting skew rays that will not pass through the fibre axis). Therefore, by using high numerical aperture launch optics bound as well as non - bound modes will be populated.

Some of the light propagates in the cladding where it quickly decays away due to the high attenuation of the cladding.

However, as stated in section 2.4, some non-bound or tunnelling modes which are launched into the fibre at angles greater than the meridional numerical aperture permits are sustained. It is these modes that are used to enhance the evanescent absorption in this work. An annular mask was fabricated to launch high order modes and tunnelling modes only. The outer non transparent section of the mask prevented the launching of leaky refracting modes in the cladding.

An x-y micropositioner at the launch end was used to optimise the coupling between the source and optical fibre. The opposite end of the fibre was terminated in a modified SMA connector and was connected to the adapted mount at the entrance port of the photomultiplier.

As explained in chapter two, in order to enhance the sensitivity of an evanescent wave sensor, it is desirable to have the highest possible ratio of

$$\frac{P_{clad}}{P_{core}}$$

where the parameters are as defined in section 2.3.3.

Experimentally, this theory was investigated by placing various sized annular masks in the backplane of the microscope objective to preferentially excite the higher

order modes only. The mask shown in figure 11 was made by making a large scale drawing first and then photographically reducing to the appropriate size. It was then photocopied onto an acetate sheet and cut out using a scalpel. A series of masks were made of constant outer diameter and inner core ranging from 1.4 mm to 5.5 mm. A series of measurements of evanescent wave absorption with the various masks revealed the optimum mask size to be 4 mm. This was a compromise between the mask size that gave maximum evanescent wave absorption and maximum optical throughput of the system.

Figure 25 is a graph of evanescent wave absorption as a function of wavelength for different mask diameters. The absorbing fluid is Eosin:Tetrabromofluorescein with a peak absorption at 520nm. It can clearly be seen that the larger the inner mask diameter the greater the ratio of P_{clad}/P_{core}, a greater fraction of higher order modes were excited and therefore the greater the sensitivity.

It is important to note that the same Eosin concentration was used for all measurements and the sensing fibre was cleaned thoroughly after each measurement by flushing the cell with ethanol and wiping the bare core with an acetone soaked tissue followed by de-ionized water.

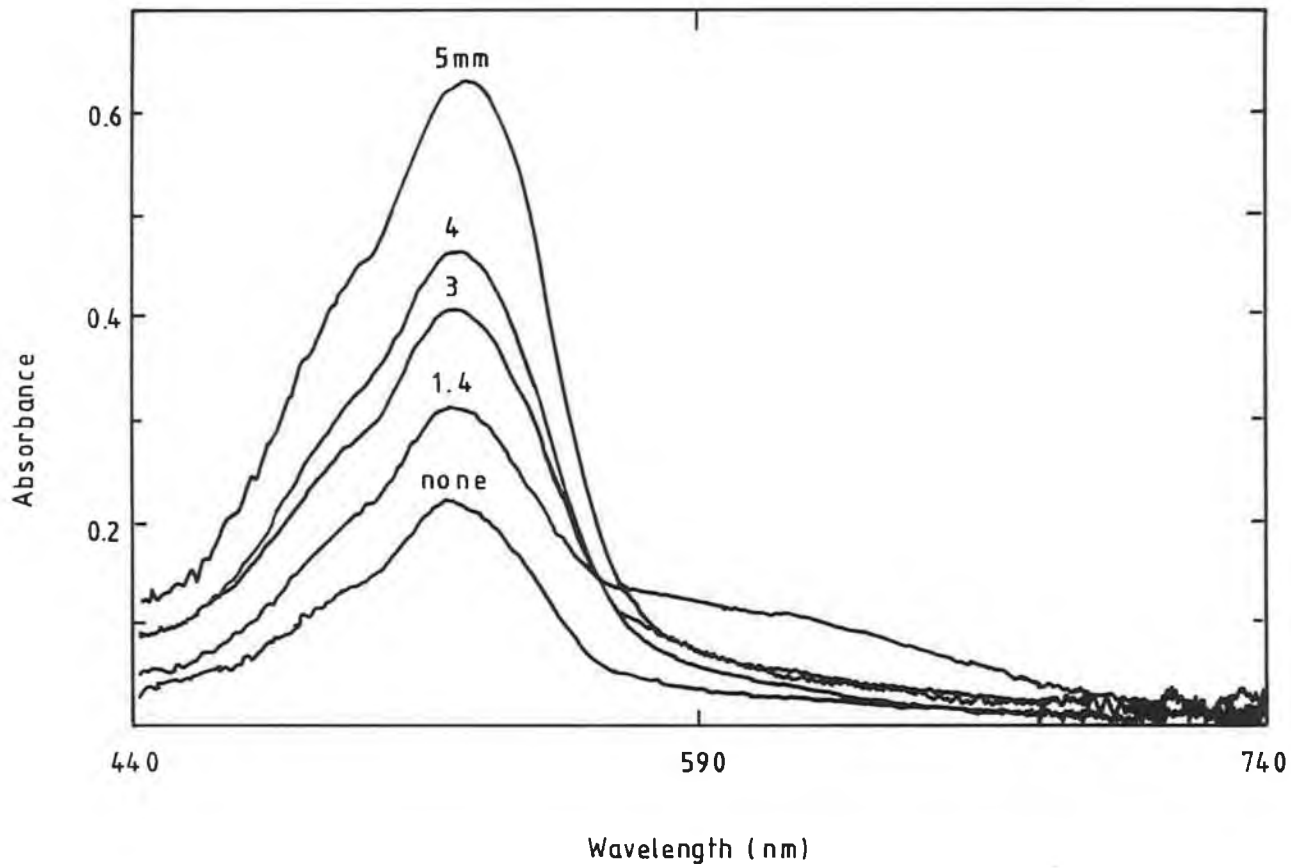

Fig. 25 : Evanescent Absorption as a Function of Wavelength for Different Inner Mask Diameters and Constant Outer Diameter The Absorber, Eosin: Tetrabromoflourescein, was of Constant Concentration for all Measurements

3.5 Electronics and Software Development.

3.5.1 Electronics.

A schematic diagram of the hardware electronics is shown in figure 26. A 12 bit analog to digital converter (ADC) and digital to analog converter (DAC) with built in power supply unit was made to interface the BBC microcomputer to the photomultiplier. This entailed signal conditioning, analog to digital conversion, and interfacing electronics to computer buses.

The ADC accepted any unipolar analog input in the range 0 to 10V. In order to use the full range of the ADC, a non-inverting variable gain amplifier of gain X1, X2, X5, and X10 was used to condition the signal before digitising. This amplifier also protects the ADC from high voltage inputs. The 351 operational amplifier from Motorola was also used to drive an analog meter which allowed monitoring of the signal strength.

The ADC chip used is a successive approximation type AD574A, obtained from Analog Devices. Using the above signal conditioning and sufficient signal averaging, an accuracy of 0.025% was obtained.

The electronics interface consisted of decoding the address lines and buffering of the data lines to the 1 MHz bus of the BBC microcomputer.

The power supply was filtered, well-regulated, and free from high frequency noise. Use of noisy supplies may cause

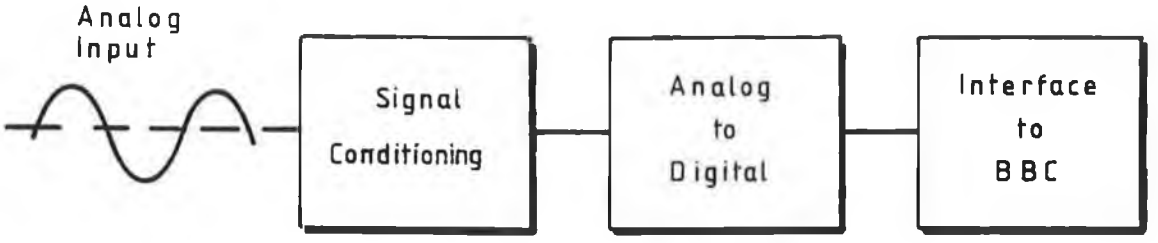

Fig.26 : Schematic Diagram of the Electronics Hardware

unstable output codes to be generated. Decoupling capacitors were placed on all the power supply lines and the signal lines were well screened.

The corresponding circuit diagrams of the above electronics are shown in appendix F.

3.5.2 Software Development.

The signal processing software was written in BASIC such that memory space was conserved at all times. The structure was as shown in figure 27 i.e. divided into three main sections; (i) acquisition, (ii) processing, (iii) analysis and display of data. The software is included in appendix G for reference.

(i) Data acquisition.

This program interfaces the BBC microcomputer with external peripherals via the ADC, thereby enabling the operator to control the stepping motor and sample the detector at specific time intervals over the desired wavelength range.

The monochromator is incremented by one nanometre and 60 data points are sampled, then averaged and the resulting value stored in an array. The process is repeated following the next increment.

The flow chart of the program is illustrated in figure 28.

FLOW CHART OF PROGRAM STRUCTURES

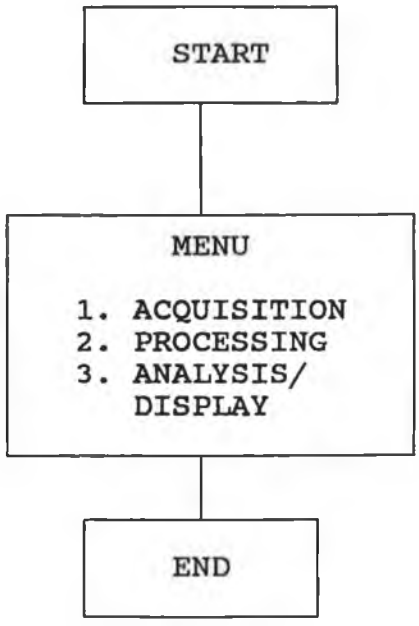

Figure 27: Flow Chart of Program Structure.

FLOW CHART OF DATA ACQUISITION

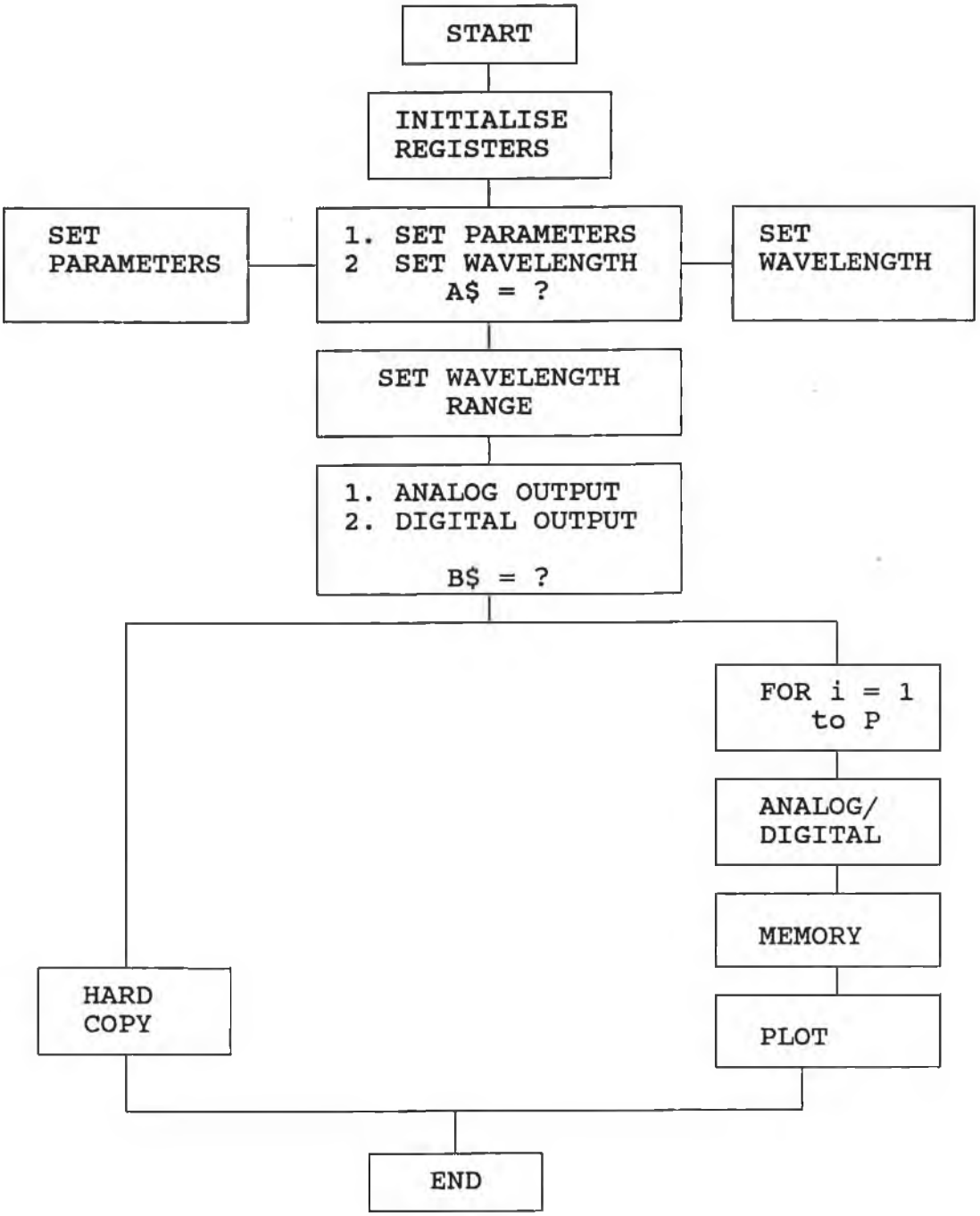

Figure 28: Flow chart of data acquisition.

(ii) Data processing.

This program corrects spectra by dividing the recorded spectra by the overall system spectral response in order to give a true transmission spectrum of the analyte. The true absorption spectrum is obtained by dividing spectrum A (in sample) by spectrum B (in water). It will also perform a moving point average to reduce noise content in the measurement of interest. This entails summing three points before and after each point and storing the result in memory.

The structure of the program is shown in figure 29.

(iii) Data analysis and display.

This program calculates the absorbance at a particular wavelength using Log_{10} $[I_0(\lambda)/I(\lambda)]$ where I_0 is the transmitted intensity of the sensor in water, and I is the transmitted intensity in the presence of Methylene Blue. The maximum absorbance for a particular wavelength is displayed and a plot of absorbance versus wavelength is then obtained on a plotter.

The structure of the program is shown in figure 30.

FLOW CHART OF DATA PROCESSING.

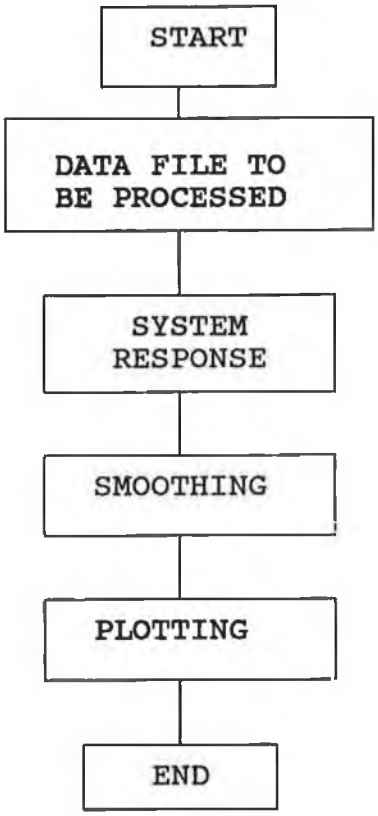

Figure 29: Flow chart of data processing routine.

FLOW CHART OF DATA ANALYSIS.

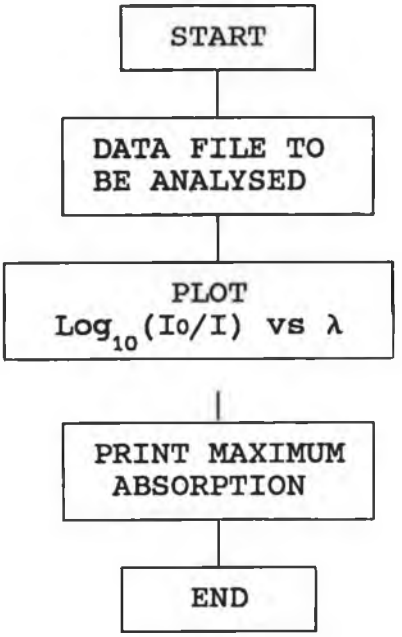

Figure 30: Flow chart of the data analysis program.

CHAPTER 4

RESULTS and ANALYSIS

4.1 Methodology.

In figure 11, the optical system used to launch tunneling modes in either 200μm or 600μm fibre of numerical aperture 0.4 is shown. Light from a 50W tungsten halogen source was dispersed in an f/4 monochromator which had a 1mm diameter exit aperture and the emerging beam was collimated and then focused by a 0.65 NA objective lens into the end-face of the clad fibre. The objective lens contained the annular beam mask to restrict the launched light into higher order modes and tunneling modes only, as described in section 3.4. The intensity profile emerging from the objective lens was consistent with a range of incident angles at the core-cladding interface of 70° to 72.5°; these angles being greater than the critical angle (= $\sin^{-1}(n_2/n_1)$) for a fused silica/water interface of 66°. As the variation in refractive index of the Methylene Blue was not greater than 1 part in 10^5 over the concentration range used, it was assumed that there was negligible change in the critical angle as a function of concentration.

At approximately the centre of the length of fibre used the cladding was removed by etching and then cleaned with ethanol as previously described in section 3.3.

In order to investigate the dependence of evanescent absorbance on absorber concentration, it was decided to use

a fluid whose bulk absorption varied linearly with concentration (i.e. obeyed the Beer-Lambert Law). The following fluids were examined for Beer-Lambert behaviour: Acid Yellow, Potassium Permanganate, Potassium Chromate, Phenol Red, Bromocresol Purple, Eosin:Tetrabromofluorescein and Methylene Blue.

The Methylene Blue, of molecular weight 319g, was the only fluid that obeyed the Beer-Lambert law, over a large range of concentrations.

A 1×10^{-3} molar solution was prepared by dissolving 0.319g of Methylene Blue in 1 litre of deionised water. This was used as the standard concentration and subsequent concentrations were obtained by appropriate dilutions, e.g. diluting 100mls in 900mls of deionised water was used to give a 1×10^{-4} molar solution. This procedure was repeated to produce solutions down to 1×10^{-9} molar concentration. A Hewlett Packard diode array spectrophotometer was used to measure bulk absorbance in the range 400nm to 800nm. A Methylene Blue absorbance spectrum, obtained with a 1×10^{-6} molar dye in a 1cm cuvette, is shown in figure 31. The spectrum shows a clear peak at 664nm corresponding to the monomer form of the molecule and a shoulder emerging at 595nm due to dimer formation. The absorbance values used throughout were based on the monomer peak at 664nm. The bulk absorbance as a function of concentration, for Methylene Blue, is shown in figure 32, from which the Beer

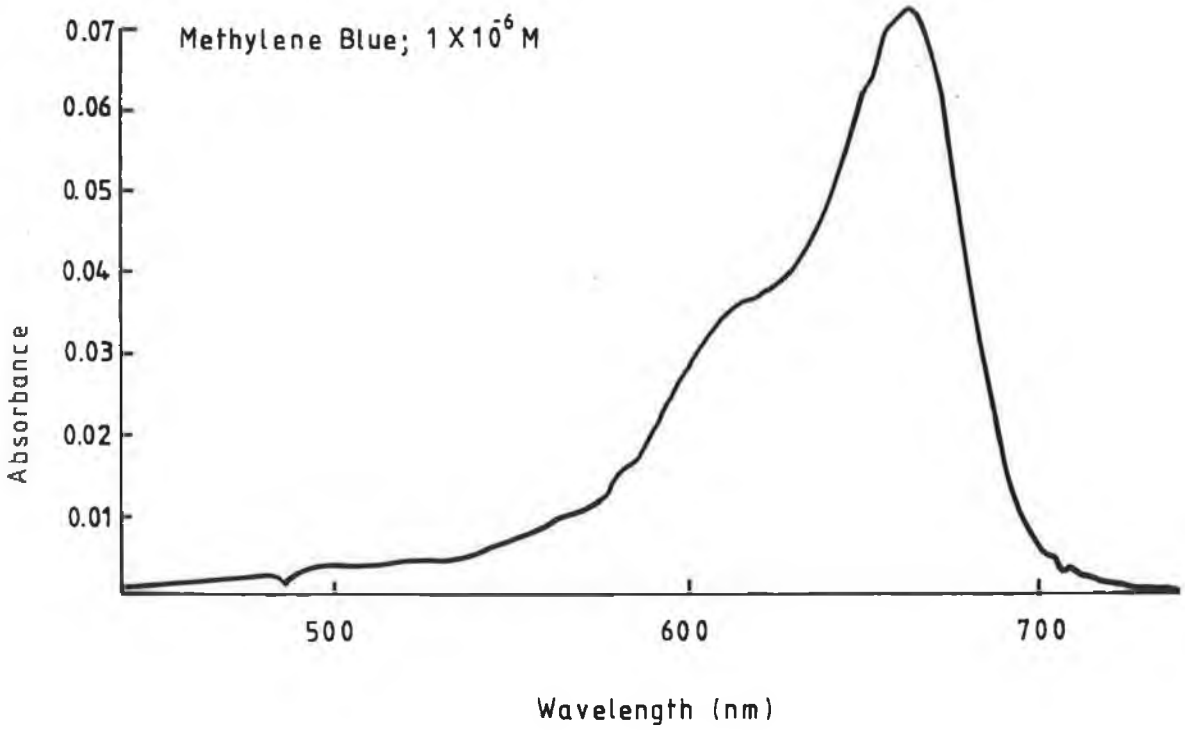

Fig. 31 : Methylene Blue Bulk Absorbance Spectrum, Obtained with a 1×10^{-6} Molar Dye in a 1cm Cuvette

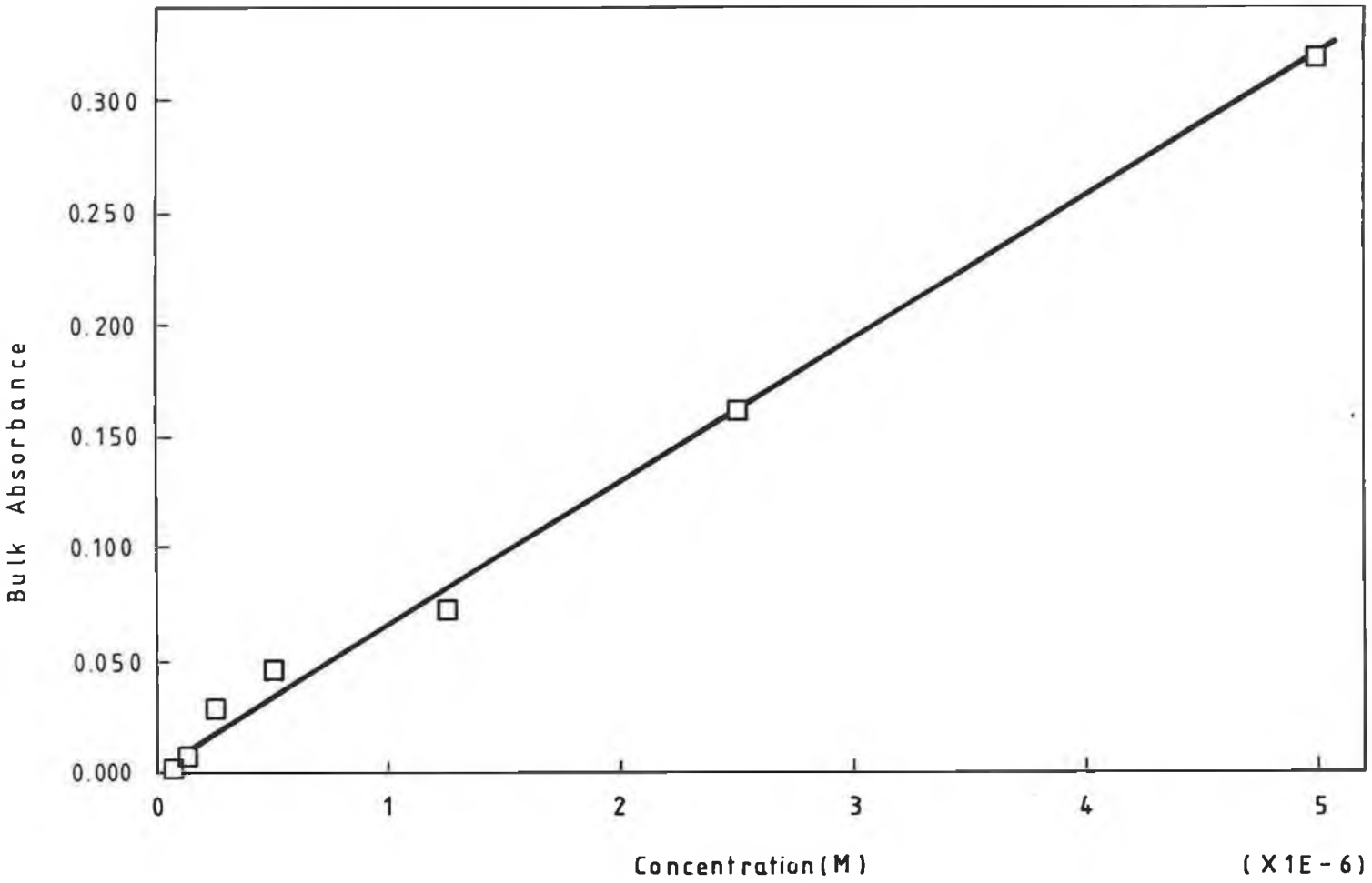

Fig. 32 : Bulk Absorbance as a Function of Concentration for Methylene Blue

from which the Beer-Lambert bnehaviour is shown.

Using the unclad fibre and the apparatus described in section 3.1, transmittance and absorbance values were obtained in the case of the same aqueous solutions of Methylene Blue by referencing each spectrum against the spectrum obtained with deionised water alone in the sample chamber. To minimise problems associated with surface contamination the sensor region was cleaned carefully (with ethanol) before a spectrum was recorded. A typical evanescent spectrum of 1 x 10^{-6} molar Methylene Blue solution is shown in figure 33. This spectrum is similar to the bulk absorbance spectrum in figure 31.

4.2 Results.

In order to characterise the evanescent wave sensor the following parameters were investigated:

(i) Evanescent absorbance vs length

(ii) Evanescent absorbance vs concentration

(iii) Evanescent absorbance vs fibre V - number

4.2.1 Evanescent Absorbance vs Sensing Length.

To measure the dependence of evanescent absorbance with unclad length (for a fixed dye concentration), a series of sensing lengths were prepared as discussed in section 3.3. 600μm PCS fibre was used in an aqueous solution of the absorbing dye Eosin at a concentration of 1 x 10^{-3} M. The dependence of the evanescent absorbance on sensor length is shown in figure 34.

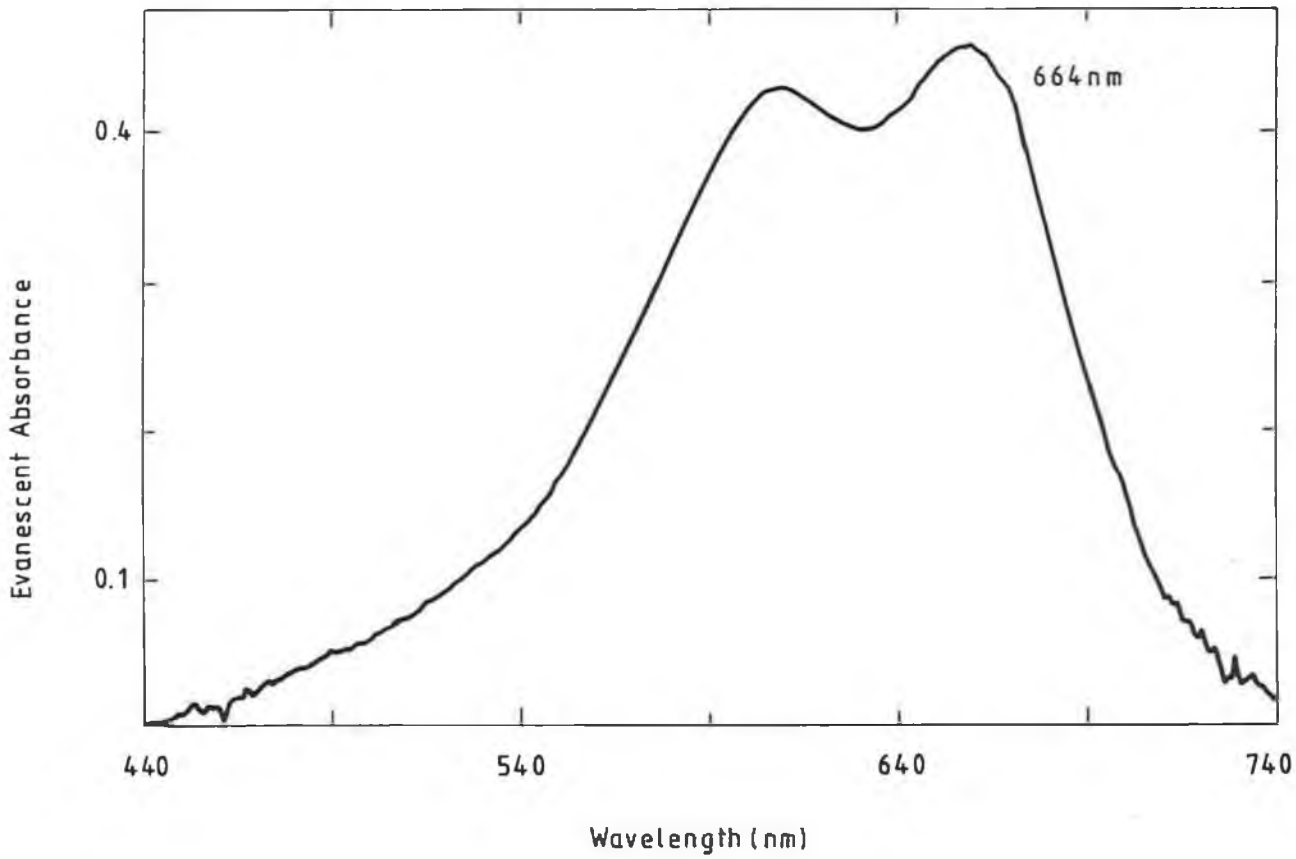

Fig.33 : Methylene Blue Evanescent Absorbance Spectrum, Obtained with a 1×10^{-6}M Solution

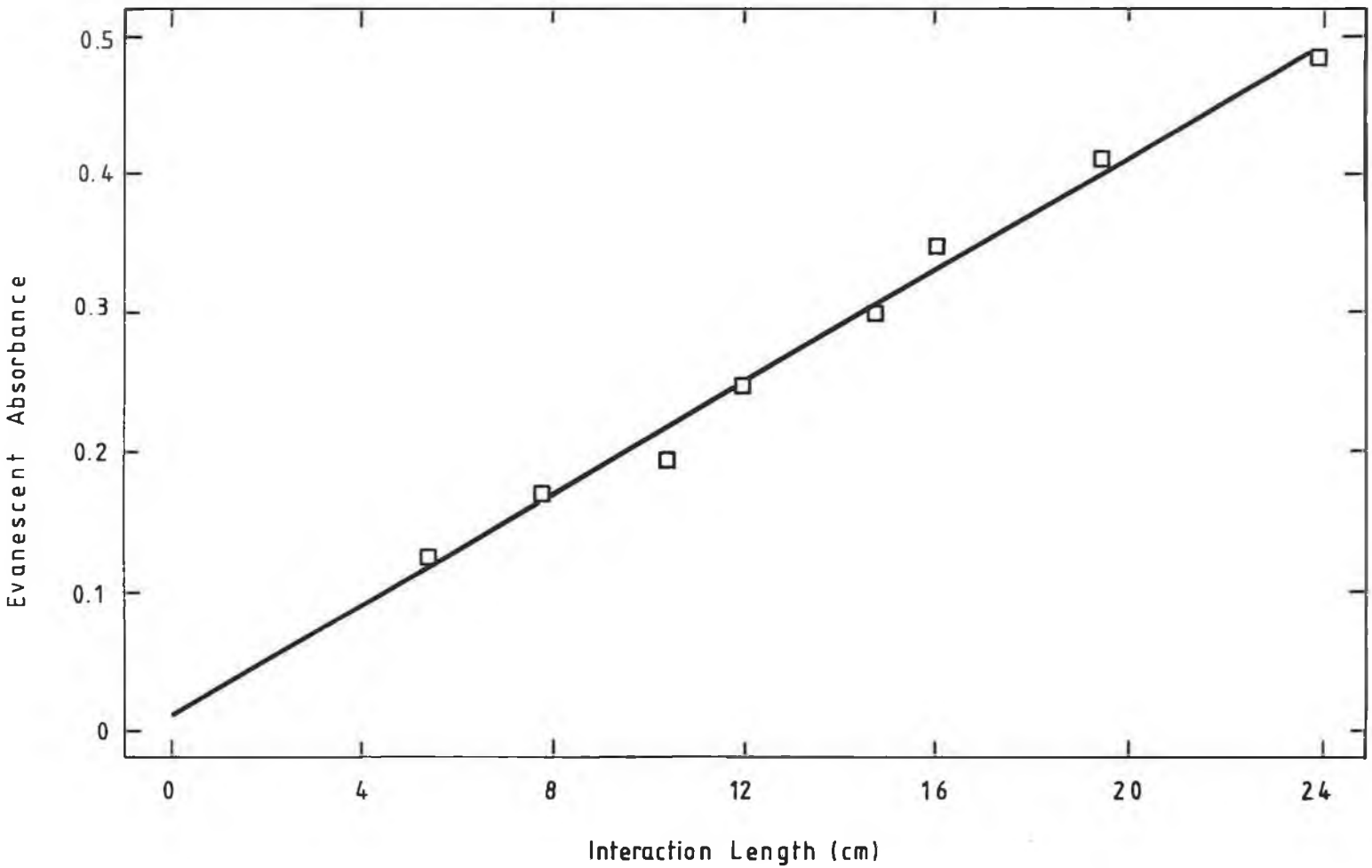

Fig. 34 : Variation of Evanescent Absorbance with Unclad Fibre Length for Absorber Eosin: Tetrabromofluorescein of Constant Concentration

The observed linear behaviour is consistent with the predicted functional forms of equations 18 and 19. From these equations the slope of the evanescent absorbance vs length plot is given by $r\alpha/2.303$ where r is the cladding power ratio and α is the absorption coefficient. Using the slope of this graph and the measured bulk absorbance, a cladding power ratio, r, of approximately 0.7% is obtained. This is considerably larger than the value of 0.1% reported by DeGrandpre and Burgess (15). However, the value of r for the mask used in our work (corresponding to a $\ominus$ range of 70^{o} - 72.5^{o}) can be calculated from an expression developed by Ruddy (46) to be 0.87%. Thus an enhanced absorbance which is mask dependent is observed.

4.2.2 Evanescent Absorbance vs Concentration.

Evanescent absorbance values at 664nm for a concentration range of 3×10^{-8}M - 5×10^{-6}M of aqueous Methylene Blue were measured using both PCS 200μm and 600μm fibres.

The interaction lengths were 22cm and 20.5cm, respectively. The results are shown in figure 35. The non-linear nature of the evanescent data is evident.

Using equation 23, the theoretical evanescent absorption coefficient values for 1×10^{-6}M aqueous Methylene Blue in contact with 600μm diameter core silica fibre can be calculated as a function of incident angle ($\ominus$) as shown in figure 36. The model uses n_1 = 1.457, n_2 = 1.335, λ = 664nm, a = 300μm. For the launch optics used in this work,

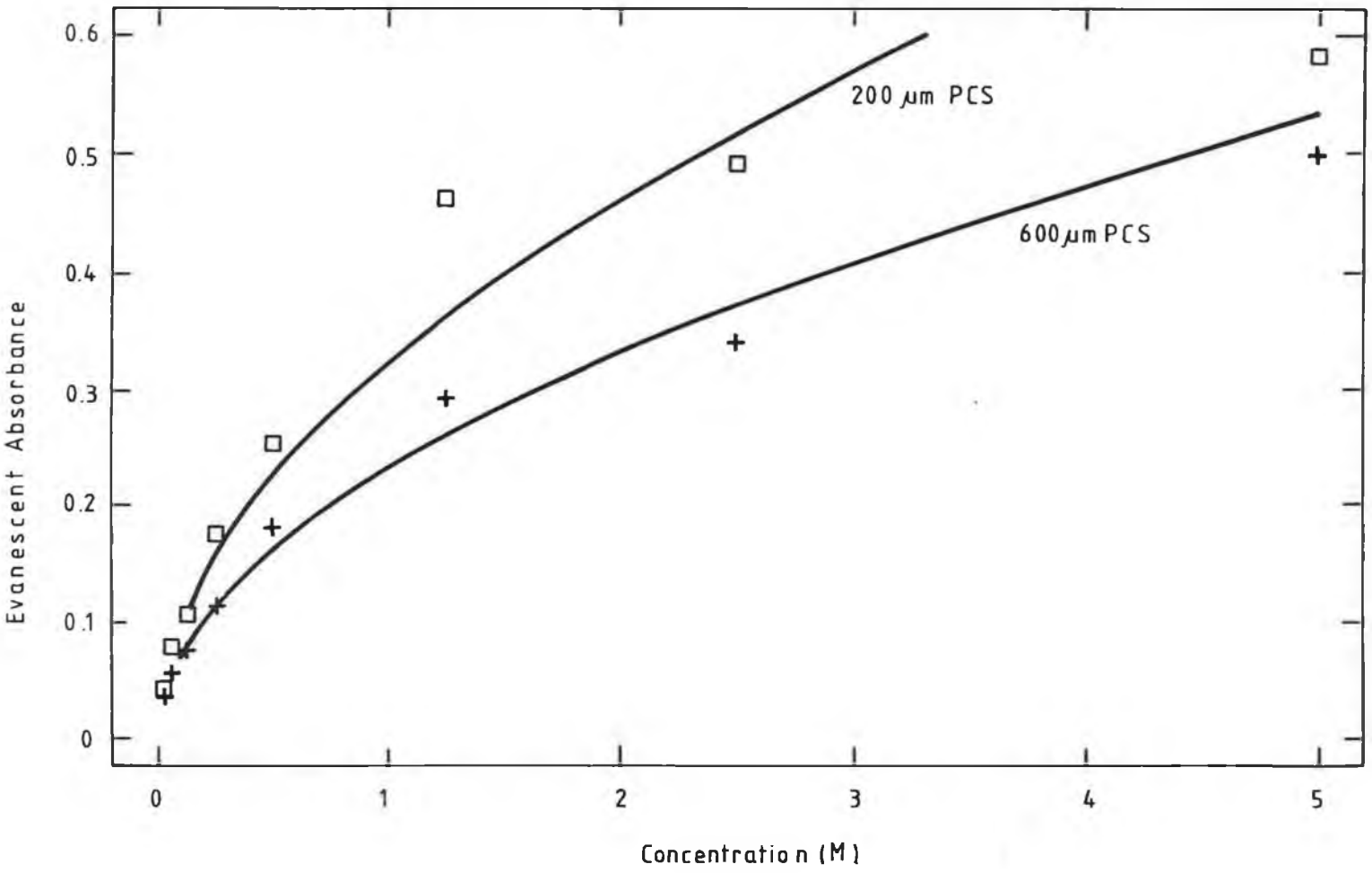

Fig. 35 : Evanescent Absorbance as a Function of Concentration for 200μm and 600μm PCS Unclad Fibre.
The Interaction Lengths were 22cm and 20.5cm, Respectively and the Absorber was Methylene Blue

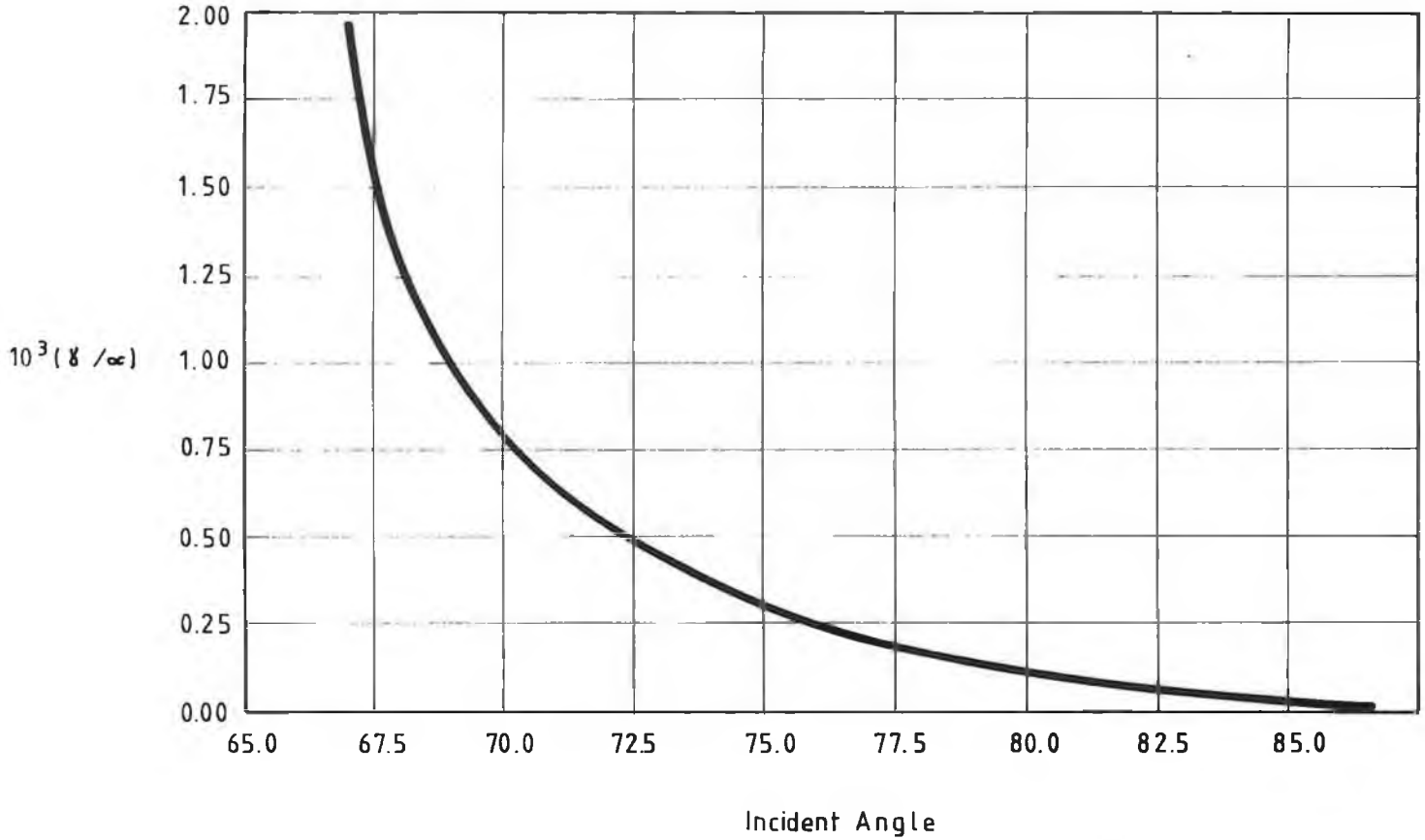

Fig. 36 : Ratio of Evanescent Absorption and Bulk Absorption Coefficient for 600 µm PCS Fibre in Methylene Blue as a Function of Incident Angle θ

maximum absorbance will occur at $\ominus = 70^{\circ}$ at which value γ/α is predicted to be approximately 8×10^{-4} (see Fig. 36). This yields (via equation 19) a theoretical evanescent absorbance for 1×10^{-6}M Methylene Blue of 1×10^{-3}. The experimental value of 0.2 is observed in figure 35. Thus an enhanced absorption which is non linear with concentration is observed.

A ln-ln plot of evanescent absorbance vs concentration is shown in figure 37 for the two fibre diameters used. A linear relationship is obtained in each case. Slopes of 0.52 and 0.519 were measured indicating an approximate square root dependence. A least-square fit analysis of this square root dependence yielded the correlation coefficients shown below;

Fibre Diameter (μm)	Coefficient of Determination	Coefficient of Correlation
200	0.925	0.962
600	0.989	0.994

This square root dependence on concentration is in contrast to the expected linear dependence given by equation (19) in chapter 2. In addition, it is in conflict with the predictions of both Snyder and Love (36) for a lossy cladding, and Stewart et al (47) for an evanescent wave chemical sensor. In both cases absorbance is predicted to increase linearly with concentration.

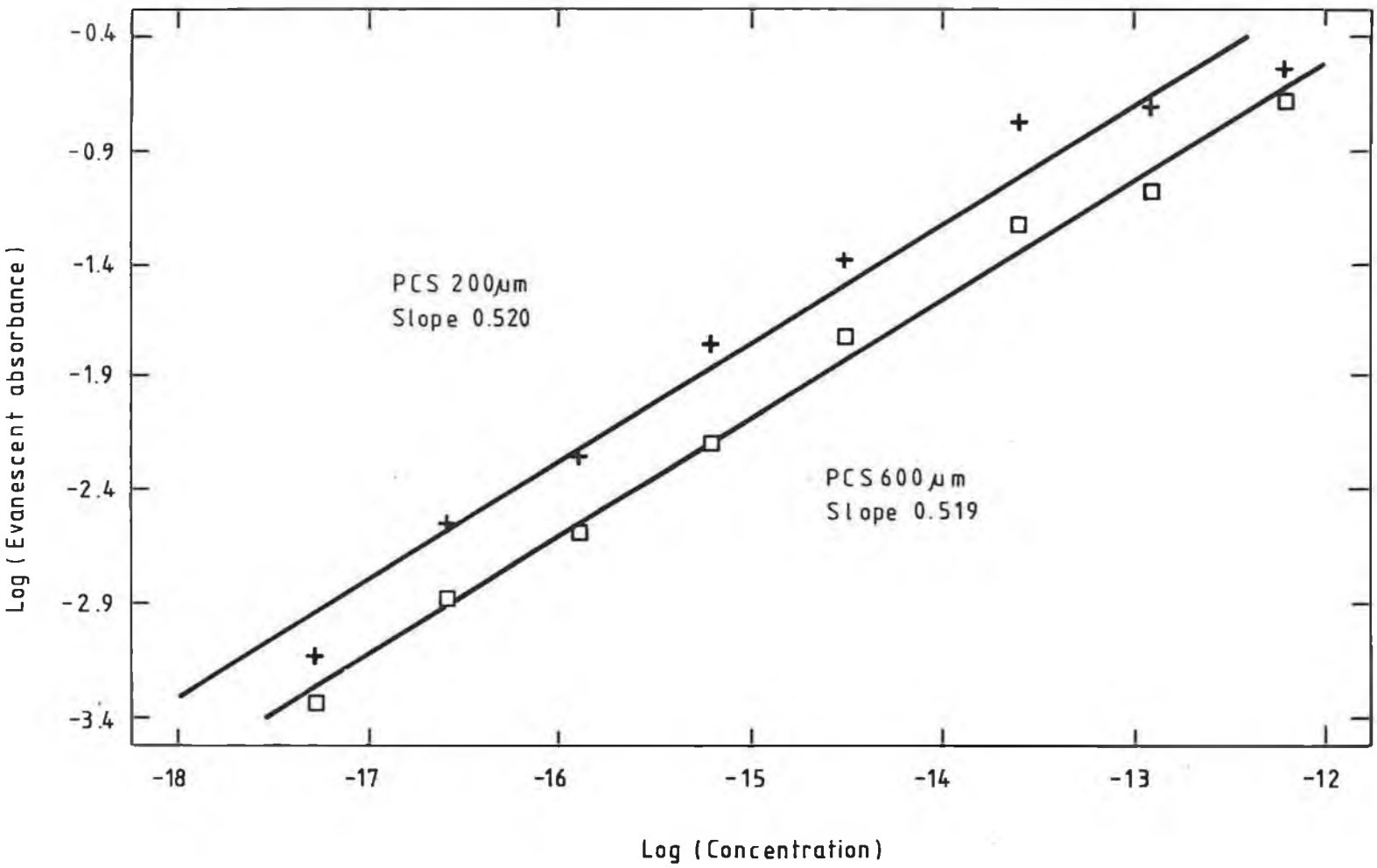

Fig.37 : ln (Absorbance) *vs* ln (Concentration) for Evanescent Absorption on 200µm and 600 µm PCS Fibre

However, the non linear dependence of absorbance on concentration has been observed for attenuated total reflection by other workers.

Using 200μm PCS fibre and Oxazine 4 perchlorate dye as the absorbing species, DeGrandpre and Burgess (15) measured absorbances for both clad and unclad fibre. The cladding was permeable to the non polar solvents used. In the case of the clad fibre a linear dependence of absorbance on concentration was observed. In the case of the unclad fibre, however, non linearity was reported. Data extracted from their work is shown in figure 38. The linear relationship between (evanescent absorbance)^2 and bulk absorbance is evident from this graph. This is equivalent to a square root dependence of evanescent absorbance on concentration for an absorbing material obeying Beer-Lambert law. Schnitzer et al (48) reported a parabolic dependence of evanescent absorbance on fluid concentration using 900μm core Silver Halide fibre operating at λ = 5.8μm.

4.2.3 Evanescent Absorbance dependence on V-Number.

Although the evanescent absorbance values for the 200μm fibre are greater at all concentrations than those obtained with the 600μm fibre, the enhancement factor is less than the threefold increase predicted by the 1/V dependence of equations (16) and (19). This may be due to the smaller mask diameter used with the 200μm fibre. This gives rise to

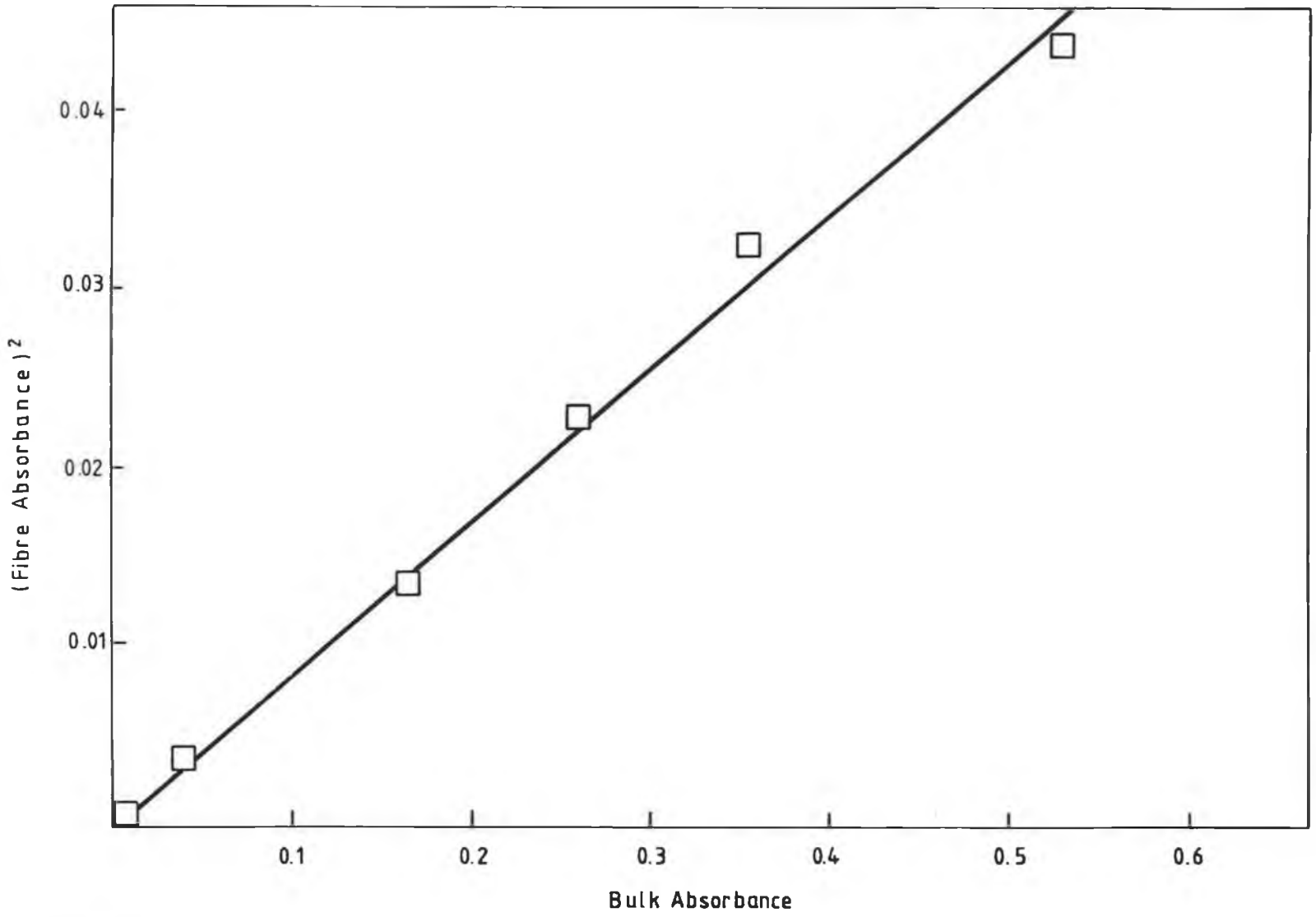

Fig. 38 : (Evanescent Absorbance)² *vs* Bulk Absorbance for Oxazine Perchlorate on Unclad 200 μm PCS Fibre. Data of De Grandpre and Burgess(15)

a different range of launching angles $\ominus$ and therefore a different modal propagation in the sensor. The modal propagation state of the sensor determines the fractional power flow, r, in the cladding. It was necessary to decrease the mask inner diameter in order to have sufficient optical throughput in the sensor. The larger absorbance for the smaller V-number fibre is however consistent with the general theory of sections 2.3.3 and 2.4.

4.3 Analysis.

The enhanced absorbance and parabolic dependence on concentration is consistent with adsorption of the ionic dye molecules on the polar surface of the fused silica core. The high density of OH ions on the glass is expected to give an enhanced concentration of dye molecules at the surface. These ions will tend to reduce the electric field experienced by other ions in solution.

This electrostatic shielding was treated by Debye and Hückel (49) as a modified Coulomb potential

$$\frac{\exp\ (-r/\lambda_D)}{r} \qquad (24)$$

where the shielding length λ_D is given by

$$\lambda_D = \sqrt{\frac{kT\varepsilon}{e^2 n_e}} \qquad (25)$$

where n_e is the ion density

ε is the electrical permittivity

k is Boltzmann's constant

T is the temperature in Kelvin

e is the electronic charge

For the concentration range (3×10^{-8} to 5×10^{-6} M) used here, the value 0f λ_D varies from 12% to 1% of the analytical wavelength (664 nm) and is substantially less than the penetration depth of the evanescent field in the solution.

Although the Debye - Hückel theory was derived to determine how far an electric field penetrates within a plasma in three dimensions, it is shown in appendix H that the same functional solution is obtained using cylindrical polar coordinates. The only difference is a numerical constant in equation (25), which does not affect the ion density n_e.

Application of the above model to this case requires the fibre to be considered as the electrode with the ion cloud as the large ionic dye molecules in thermal equilibrium about it. Because of thermal agitation, the ions cannot remain exactly static at the fibre; instead, they form a restless cloud in the vicinity of the fibre. Only inside the ion cloud does the fibre shield the ion solution; outside the cloud, the absorbing dye is unaffected. The thickness of the cloud is called the shielding distance, or the Debye distance and depends on the temperature of the dye in the vicinity of the fibre.

There is general agreement that the Debye - Hückel theory gives the correct description of the ion-ion interactions at the limit of extremely weak solutions (49). Because the shielding length depends on the square root of the ion density, it is observed in electrochemistry (50) that derivative functions of the Gibbs Energy such as partial molar volume exhibit a square root dependence on concentration for low concentrations ($< 1 \times 10^{-3}$M). A cube root dependence, based on a disordered lattice model is predicted to occur for concentrations of 0.1M - 4M, which is a substantially higher range than that used in this work.

Freundlich (51) expressed the adsorption dependence on concentration in the form of an empirical power law isotherm

$$X = Kc^{1/n} \qquad (26)$$

where X is the quantity of solute adsorbed, c is the concentration of the equilibrium solution and K is a constant. n is a parameter with a value greater than unity. A value of n = 2 is consistent with our observations.

Two groups (42,52) have observed a linear relationship between evanescent absorbance and fluid concentration. Villaruel et al (42) used Methylene Blue in water on 100μm diameter core silica fibre tapered to 30μm minimum diameter on a 37mm length. Their absorbance value was linear with concentration with γ/α value of 0.015. The maximum value of

the cladding power ratio (r) at the neck of the taper is calculated to be approximately 0.02. Thus no adsorption is indicated. This may be due to passivation of the surface by the etchant used in tapering. Paul and Kychaoff (52) used Rhodamine 6G dye in nonpolar organic solvents. Their data is consistent with the total mode analysis of section 2.4 with no enhanced absorption due to dye adsorption.

4.4 Summary.

Enhanced absorbance was observed in evanescent absorption of Methylene Blue on unclad silica multimode optical fibre. The absorbance was found to scale as the square root of dye concentration, i.e. the dye does not obey a Beer-Lambert law for evanescent absorption when the solvent used is water and the fibre is of silica. This non linearity can be explained by ionic shielding known as the Debye-Hückel effect.

The measured linear dependence of evanescent absorbance with unclad sensing length is consistent with the predicted functional forms of equations (18) and (19).

The relationship between evanescent absorbance and V-number showed an enhancement factor which was less than the threefold increase predicted by the 1/V dependence of equations (18) and (19).

CONCLUSION.

Evanescent wave absorption spectroscopy using multimode optical fibres has been demonstrated. It is shown that a length of silica fibre with an unclad central length may be used as an ATR absorbance probe for aqueous solutions which absorb visible radiation. A theoretical model followed by experimental verification was used to evaluate 600 μm PCS and 200 μm PCS fibre probes.

The launching of tunnelling modes which reach the sensing region at angles close to the critical angle significantly enhance the sensitivity of the technique. Measured evanescent absorbances using Methlene Blue are significantly greater, however, than values predicted by standard evanescent wave models. In addition, the observed dependence of evanescent absorbance on concentration deviates considerably from the predicted Beer-Lambert type linear relationship. Both of these effects have been attributed to surface adsorption due to electrostatic interactions between the polar silica surface and the ionic solution. The observed square root dependence of evanescent absorbance on concentration is consistent with the Debye-Hückel model for ion-ion interactions.

The measured linear relationship between evanescent absorbance and unclad sensing length is consistent with the predictions of the theoretical model.

Because of the irreversible nature of the adsorption process, the potential for evanescent wave spectroscopy on fused silica fibre is severly limited for ionic solutions. The effect may be exploited, however, in disposable probes to give increased sensitivity due to the enhanced surface concentrations. Adsorption may be minimized by treatment of the silica surface with a thin film of a hydrophobic material such as dichlorodimethylsilane (DDS). Such a film, of thickness of several nanometres, would not significantly attenuate the evanescent intensity available for absorption.

REFERENCES

1. J. Tyndall, "On Some Phenomena Connected with the Motion of Liquids", Proc. Roy. Instn.1, 446 (1854).
2. J.L. Baird, Brit. Patent 285,738 (1927).
3. C.W. Hansell, US Patent 1,751,584 (1930).
4. A.C.S Van Heel, "A New Method of Transporting Optical Images without Aberrations", Nature 173, 39 (1954).
5. C.K. Kao and G.A. Hockham, "Dielectric Fibre Surface Waveguides for Optical Frequencies", Proc. IEE, 113, 1151 (1966).
6. K.F. Hale, "Optical Fibre Sensors for Inspection Monitoring", Phys. Technol. Vol 15, (1984).
7. B.E. Jones "Optical Fibre Sensors and Systems for Industry", J. Phys. E Sci. Instrum., Vol. 18, 770, (1985).
8. T.G. Giallorenzi, J.A. Bucaro, A. Dandridge, G.H. Siegel, S.C.Rashleigh and R.G. Priest "Optical Fibre Sensor Technology", IEEE J. Quantum Electronics Vol. 18, 626 (1982).
9 T.H Maugh II, "Remote Spectrometry with Fiber Optics", Science 218, 875 (1982).
10 S.A. Borman, "Optrodes", Anal. Chem. 53, 1616A (1981).
11 A.C. Eckbreth, "Remote Detection of CARS Employing Fiber Optic Guides", Appl. Opt. 18, 3215 (1979).

12 K. Newby, W.M. Reichert, J.D. Andrade, and R.E. Benner, "Remote Spectroscopic Sensing of Chemical Adsorption using a single Multimode Optical Fiber", Appl. Opt., Vol.23, No. 11, (1984).

13 E. Hardy, D. J. David, N. S. Kapany and F.C. Unterleitner, "Coated Optical Guides for Spectrophotometry of Chemical reactions", Nature 257, 666 (1975).

14 D.W. Lubbers and N. Opitz, "The PCO_2-/PO_2 - Optode: A New Probe for Measurement of PCO_2 - PO_2 in fluids and Gases", Z. Naturforsch, 30 C, 532 (1975).

15 M.D. DeGrandpre and L.W. Burgess, "All - Fiber Spectroscopic Probe Based on Evanescent Wave Sensing Mechanism", SPIE Proc., Vol.0990, O/E Fibers Boston, (1988).

16 K. Chan, H. Ito, and H. Inaba,"An Optical-Fiber based Gas Sensor for Remote Absorption Measurement of low-level CH_4 Gas in the Near-Infrared Region", J. Lightwave Technol. LT-2(3), 234 (1984).

17 K. Chan, H. Ito, and H. Inaba, " Optical-Fibre Remote Sensing of Low-Level Propane Gas using a 1.68 μm InGaAs Light Emitting Diode", Opt. Lasers Eng. Vol.6, 2, 119 (1985).

18 H. Inaba, T. Kobayasi, M. Hirama, and M. Hanya,"Optical-Fiber Network System for Air-Pollution over a wide area by an Optical Absorption Method", Electron Lett. 15, 749 (1979).

19 T. Kobayasi, M. Hirama, and H. Inaba, "Remote Monitoring of NO_2 molecules by Differential Absorption using Optical Fiber link." Appl. Opt. 20, 3279 (1981).

20 K. Chan, H. Ito, and H. Inaba, "Optical Remote Monitoring of CH_4 Gas using Low-Loss Optical Fibre Link and InGaAsP Light Emitting Diode in 1.33 μm Region", Appl. Phys. Lett. Vol. 43, 7, 634 (1983).

21 S. Simhony and A. Katzir, "Remote Monitoring of Ammonia using a CO_2 Laser and Infrared Fibers", Appl. Phys. Lett. 47 (12), 1241 (1985).

22 G.J Muller, "Spectroscopy with the Evanescent Wave in the Visible Region of the Spectrum", Multichannel Image Detectors, edited by J. Talmi (American Chemical Society, New York), 241. (1979)

23 D.R. Battiste, S.E. Fry. T. White, M.W. Scoggins, and T.B.McWilliams, "Determination of Ethanol in Gasohol by Infrared Spectrometry", Anal. Chem. 53, 7, 1096 (1981).

24 S. Simhony, E.M. Kosower, and A. Katzir, "Novel Attenuated Total Internal Reflectance Spectroscopic cell using Infrared Fibers for Aqueous Solutions", Appl. Phys. Lett. 49 (5), 253 (1986).

25 H. Tanaka, T. Ueki, and H. Tai, "Fibre Optic Evanescent Wave Gas Spectroscopy", Optical Fibre Communication Conference, San Diego, CA ,USA (1985).

26 E.Hecht and A. Zajac, "Optics", Addison-Wesley World Student Series Edition (1974).

27 J. Fahrenfort,"Attenuated Total Reflection: a New Principle for the production of useful Infrared Relection Spectra of Organic Compounds", Spectrochim. Acta 17, 698 (1961).

28 N.J. Harrick, "Optical Spectrum of the Semi-Conductor Surface States from Frustrated Total Internal Reflections" Phys. Rev. 125 (4), 1165 (1962).

29 N.J. Harrick, "Internal Reflection Spectroscopy" New York, (1967).

30 C.K. Carniglia, L. Mandel, and K.H. Drexhage, "Absorption and Emission of Evanescent Photons", J. Opt. Soc.America, Vol. 62, 4, (1972).

31 R.M. Sutherland, C. Dähne, J.F. Place, and A.R. Ringrose, "Optical Detection of antibody-antigen reactions at a glass liquid interface", Clin. Chem. 30, 1533 (1984).

32 D. Marcuse, "Theory of Dielectric Optical Waveguides", Academic Press, New York, 1974.

33 A.W. Snyder and D.J. Mitchell, "Leaky Rays on Circular Optical Fibers", J. Opt. Soc. Amer., 64, 599 (1974).

34 H.G. Unger, "Planar Optical Waveguides and Fibres", Clarendon, Oxford, (1977).

35 J.D. Love, C. Winkler, R. Sammut, and K. Barrell, "Leaky Modes and Rays on Multimode Step-Index Waveguides", Electron. Lett., 14, 489 (1978).

36 A.W. Snyder and J.D. Love, "Optical Waveguide Theory", Chapman and Hall, London, New York, (1983).

37 S.E. Miller and A.G. Chynoweth , "Optical Fiber Telecommunications", Academic Press, New York, (1979).

38 D. Gloge, "Weakly Guiding Fibers", Appl. Opt. 10, 2252 (1971).

39 H. Tai, H. Tanaka, and T. Yoshino, "Fiber-Optic Evanescent Wave Methane Gas Sensor Using Optical Absorption for the 3.392-micron line of a He-Ne Laser", Opt. Lett. 12 (6), 437 (1987).

40 A.W. Snyder, D.J. Mitchell,"Leaky Rays on Circular Optical Fibers", J. Opt. Soc. Amer., 64(5), 599 (1974).

41 V. Ruddy, B.D. MacCraith, and J.A. Murphy, "Evanescent Wave Absorption Spectroscopy using Multimode Fibers", J. Appl. Phys., 67 (10) 1990.

42 C.A. Villaruel, D.D. Dominguez and A. Dandridge, "Evanescent Wave Fibre Optic Chemical Sensor", SPIE, Vol. 798, 225, Fiber Optic Sensors II, (1987).

43 PTR Optics Corporation, Optical Components Catalogue, USA.

44 TSL Group PLC, Optical Fibres , England.

45 K.E. Newby, A Remote Interfacial Chemical sensor using a Single Multimode Optical Fibre ,Thesis, University of Utah, USA, (1984).

46 V. Ruddy, "An Effective Attenuation Coefficient for Evanescent Wave Spectroscopy using Multimode Fiber", Fiber & Integrated Optics, Vol. 9, (1990).

47 G. Stewart, J. Norris, D. Clark, M. Tribble, I. Andonovic, and B. Culshaw, "Chemical Sensing by Evanescent Field Absorption: the Sensitivity of Optical Waveguides", SPIE. Vol. 0990, Boston (1988).

48 I. Schnitzer, A. Katzir, U. Schiessl, W. Riedel, and M. Tacke, "Fibre-Optic-based Evanescent Field Infrared Spectroscopy using Tunable Diode Lasers", SPIE, Vol. 1048, Los Angeles, (1989).

49 J.D. Jackson, "Classical Electrodynamics", Wiley & Sons, New York, (1962).

50 Y. Marcus, "Introduction to Liquid State Chemistry", Wiley & Sons, New York, (1977).

51 D.J. Shaw, "Introduction to Colloid and Surface Chemistry", Butterworths, London, (1986).

52 P.H. Paul and G. Kychakoff, "Fiber-Optic Evanescent Field Absorption Sensor", Appl. Phys. Lett., 51(1), 12, (1987).

53 R.M. Gagliardi and S. Karp, "Optical Communications", Wiley, New York (1976).

APPENDIX A

Internal Reflection Spectroscopy

Although geometric optics provides the condition for total internal reflection to occur, it offers no explanation of the phenomenon or any information about the energy distribution at reflection. To gain further insight into this phenomenon, the results of electromagnetic theory must be applied to the case. The following discussion is partially based on the treatment outlined by Hecht and Zajac (26).

Suppose that the incident monochromatic light wave is plane polarized so that it has the form

$$E_i = E_{oi} \exp [i(\tilde{k}_i.r - \omega_i t)] \qquad (A.1)$$

The reflected and transmitted waves can be written as

$$E_r = E_{ot} \exp [i(\tilde{k}_t.r - \omega_t t)] \qquad (A.2)$$

$$E_t = E_{ot} \exp [i(\tilde{k}_t.r - \omega_t t)] \qquad (A.3)$$

For TE modes, where the electric field vector is parallel to the boundary interface, it is shown by Hecht and Zajac (26) that the amplitude of the reflected wave, E_{or}, relative to the incident ray, E_{oi}, is given by the Fresnel amplitude reflection formulae

$$\frac{E_{or}}{E_{oi}} = \frac{\cos\Theta_i - (n_t/n_i) \cos\Theta_t}{\cos\Theta_i + (n_t/n_{i)} \cos\Theta_t} \qquad (A.4)$$

By manipulating Snell's law

$$n_i \sin\theta_i = n_t \sin\theta_t \qquad (A.5)$$

it can be shown that

$$\cos\theta = [1 - (n_i/n_t)^2 \sin^2\theta_i]^{1/2} \qquad (A.6)$$

Thus, replacing θ_t with θ_i gives

$$\frac{E_{or}}{E_{oi}} = \frac{\cos\theta_i - \frac{n_t}{n_i}[1 - (n_i/n_t)^2 \sin^2\theta_i]^{1/2}}{\cos\theta_i + \frac{n_t}{n_i}[1 - (n_i/n_t)^2 \sin^2\theta_i]^{1/2}} \qquad (A.7)$$

For $\theta_i > \theta_c$, it is possible for the terms within the square root to produce negative values.

Therefore, equation (A.5) becomes

$$\cos\theta_t = - [1 - (n_i/n_t)^2 \sin^2\theta_i]^{1/2} \qquad (A.8)$$

i.e. when total internal reflection occurs, equation (A.5) becomes

$$\frac{E_{or}}{E_{oi}} = \frac{\cos\theta_i + [\sin^2\theta_i - (n_t/n_i)^2]^{1/2}}{\cos\theta_i + [\sin^2\theta_i - (n_t/n_i)^2]^{1/2}} \qquad (A.9)$$

Because the numerator is the complex conjugate of the denominator the moduli of both are equal, i.e.

$$|E_{or}| = |E_{oi}| \qquad (A.10)$$

Since $E_{oi} = E_{or}$ all the energy in the wave is reflected which implies that $E_{ot} = 0$ (for $\theta_i = \theta_r$). Therefore, although the transmitted wave does exist, it cannot, on the average, carry energy across the boundary. It is shown by Hecht and Zajac that the incident and reflected waves do not have a phase difference of π and therefore destructive

interference cannot occur.

In order to satisfy the boundary conditions, there must be a disturbance in the second medium and we will therefore examine the transmitted wave function.

The wave function for the transmitted electric field is

$$E_t = E_{ot} \exp i\,(\tilde{k}_i.r - \omega t) \qquad (A.3)$$

From the propagation vectors of figure A.1, we have

$$k_t.\tilde{r} = k_{tx}\,\tilde{x} + k_{ty}\,\tilde{y} \qquad (A.11)$$

But $k_{tx} = k_t \sin\theta_t$ and $k_{ty} = k_t \cos\theta_t$

Using Snell's law (equation A.5), we have

$$k_{ty} = \pm\, ik_t\,[1 - (\sin\theta_i^2 / n_{ti}^2)]^{1/2} \qquad (A.12)$$

where $n_{ti} = n_t/n_i$.

But since $\sin\theta_i > n_{ti}$ for total internal reflection

$$k_{ty} = \pm i\,k_t\,[(\sin^2\theta_i / n_{ti}^2) - 1]^{1/2} = \pm\, i\,\delta \qquad (A.13)$$

Also,

$$k_{tx} = k_t \sin\theta_t = k_t \frac{\sin\theta_i}{n_{ti}} \qquad (A.14)$$

Therefore,

$$E_t = E_{ot} \exp_i\,(k_{tx}\,x + k_{ty}\,y - \omega t) \qquad (A.15)$$

$$= E_{ot} \exp_i\,(i\delta y) \exp(k_t \frac{\sin\theta_i}{n_{ti}}\,x - \omega t)$$

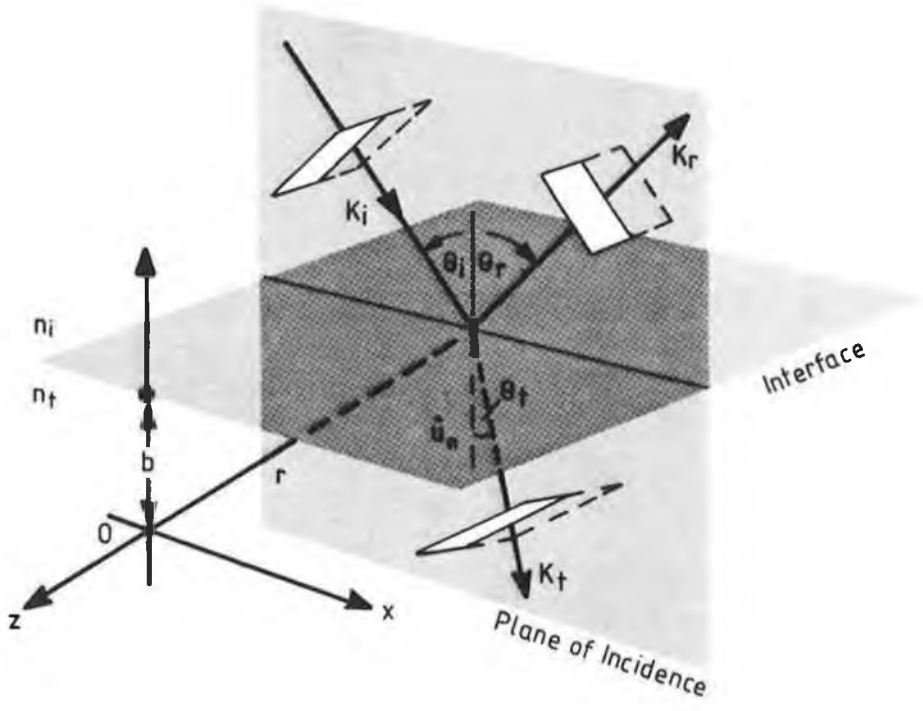

Fig. A1 : Plane Waves Incident on the Boundary between Two Homogeneous, Isotropic, Lossless Dielectric Media (26)

$$E_t = E_{ot}\, e^{-\delta y}\, e^{-i\,[k_t\,(\sin\theta_i/n_{ti})x\,-\,\omega t]} \qquad \text{(A.16)}$$

i.e. the disturbance in the less dense medium is therefore periodic in x but exponentially decaying in z. This is the evanescent wave.

In the denser medium a stationary wave pattern is set up owing to constructive interference between the incident and reflected beams and in the less dense medium the amplitude falls exponentially, although the amplitudes are equal at the interface.

The spatial rate of decay of the field in the second medium is determined by the attenuation constant δ.

From equation (13)

$$\delta = k_t\,[(\sin^2\theta_i/\, n_{ti}^2) - 1]^{1/2}$$

$$= \frac{2\pi}{\lambda_o}\,(n_i^2\,\sin^2\theta_i \;- n_t^2)^{1/2}$$

$$= \frac{2\pi n_i}{\lambda_o}\,(\sin^2\theta_i - n_{ti}^2)^{1/2}$$

The penetration depth d_p is defined as $1/\delta$,

so we have

$$d_p = \frac{\lambda_o}{2\pi n_i(\sin^2\theta_i - n_{ti}^2)^{1/2}} \qquad \text{(A.17)}$$

APPENDIX B

Total Number of Guided Modes

The V-number can be related to the number of modes M in a multimode fibre when the total number of modes M is large. An approximate relationship for step-index fibres can be derived from ray theory. A ray incident on the end of a fibre will be accepted by the fibre if it lies within an angle Θ defined by the numerical aperture (NA) as given by equation (B.1)

$$NA = \sin\Theta = (n_1^2 - n_2^2)^{1/2} \qquad (B.1)$$

For practical numerical apertures $\sin\Theta \cong \Theta$. The solid acceptance angle for the fibre is therefore

$$\Omega = \pi\Theta^2 = \pi(n_1^2 - n_2^2) \qquad (B.2)$$

For electromagnetic radiation of wavelength λ emanating from a laser or a waveguide the number of modes per unit solid angle is given by $2A / \lambda^2$, where A is the area the mode is entering or leaving (50). The area A in this case is the core cross section πa^2. The factor two comes from the fact that the plane wave can have two polarization orientations. The total numberof modes M entering the fibre is given by

$$M \cong \frac{2A}{\lambda^2}\Omega = \frac{2\pi^2 a^2}{\lambda^2}(n_1^2 - n_2^2) = \frac{V^2}{2} \qquad (B.3)$$

APPENDIX C

Evanescent Wave Spectroscopy using Multimode Optical Fibres.

The power loss due to an absorbing cladding cannot be described directly by geometric optics, because this loss occurs beyond the ray path and is, therefore, a wave effect, dependent on the wavelength of light in the core. In the limit of classical geometric optics, $\lambda = 0$, the fields are zero beyond the ray path.

For the values of λ greater than zero for light, the evanescent fields lose some of their power to the absorbing cladding. This in turns leads to a loss of power from the ray path.

The following analysis is based upon the expression of Snyder and Love (36)

$$\gamma = NT \qquad (C.1)$$

where γ is the evanescent absorption coefficient, N is the number of reflections per unit length and T is the Fresnel transmission coefficient at the interface of a lossless core and a lossy cladding. The refractive index of the latter is given by $n_2 - ik$, where

$$\alpha = 4\pi k/\lambda \qquad (C.2)$$

is the bulk absorption coefficient of the cladding material at an analytical wavelength. The approach adopted by Snyder and Love (36) was modified by Ruddy (46) to cater for non weakly guiding modes which occur when the cladding

refractive index (in this case a water based liquid) of refractive index of approximately 1.335 is not close to the core index of 1.457 for silica glass.

The number of reflections N is a function of the length L, the thickness of the waveguide T, and angle of incidence Θ

$$N = L/T.\ \cot\Theta \qquad (C.3)$$

The above equation assumes there are no skew rays.

The Fresnel transmission coefficient is given by (26)

$$T = \frac{4\ \sin\Theta_z\ (\sin^2\Theta_z - \sin^2\Theta_c)^{1/2}}{(\sin\Theta_z + \{\sin^2\Theta_z - \sin^2\Theta_c\}^{1/2})^2} \qquad (C.4)$$

In the case where the refractive index of the cladding is complex

$$n_{cl} = n^r_{cl} - in^i_{cl}$$

then equation (C.4) becomes

$$T = 4\ \sin\Theta_z \frac{\mathrm{Re}\ [(n^2_{cl} / n^2_{co}) - \cos^2\Theta_z]^{1/2}}{|\sin\Theta_z + \{\ (n^2_{cl} / n^2_{co}) - \cos^2\Theta_z\}^{1/2}|^2} \qquad (C.5)$$

If we write

$$n_{cl} = n^r_{cl} - in^i_{cl}$$

then $$n^2_{cl} = \left[n^r_{cl}\right]^2 - \left[n^i_{cl}\right]^2 + 2i\ n^r_{cl}\ n^i_{cl}$$

and because n_{cl}^{i} is very small, we can ignore $n_{cl}^{i\,2}$, so that

$$n_{cl}^{2} = [n_{cl}^{r}]^{2} + 2i\, n_{cl}^{r}\, n_{cl}^{i} \qquad (C.6)$$

If z is a complex number = $r\, e^{i\Theta}$ then

$$z^{1/2} = \sqrt{r}\; e^{i\Theta/2}$$

so that $\quad \text{Re}\; z^{1/2} = r^{1/2} \cos\Theta/2.$

Since $\quad \sin^{2}\Theta_{c} = 1 - \dfrac{n_{cl}^{2}}{n_{co}^{2}}$

then $\quad \dfrac{n_{cl}^{2}}{n_{co}^{2}} = 1 - \sin^{2}\Theta_{c} = \cos^{2}\Theta_{c} \qquad (C.7)$

Using Θ_{z} as illustrated in figure 10

equation (C.7) becomes

$$\sqrt{(n_{cl}^{2}/n_{co}^{2}) - \cos^{2}\Theta_{z}} = \sqrt{\cos\Theta_{c}^{2} - \cos\Theta_{z}^{2}} \qquad (C.8)$$

Because $\Theta_{c} > \Theta_{z}$

$\cos^{2}\Theta_{c} - \cos^{2}\Theta_{z}$ is negative and so the

$$\text{Re}\sqrt{(n_{cl}^{2}/n_{co}^{2}) - \cos^{2}\Theta_{z}} = r^{1/2} \sin\Theta/2$$

$$= \sqrt{\cos^{2}\Theta_{z} - \cos^{2}\Theta_{c}}\; [\sin \tfrac{\tan^{-1}\beta}{2}]$$

$$\text{where } \tan\beta = 2\, \frac{(n_{cl}^{r}\, n_{cl}^{i}) \,/\, n_{co}^{2}}{(n_{cl}^{2}/n_{co}^{2}) - \cos^{2}\Theta_{z}}$$

Because n_{cl}^{i} is so small, β is small

therefore $\tan\beta \cong \beta \cong \sin\beta$ implies that

$$\text{Re}\sqrt{(n_{cl}^2/n_{co}^2) - \cos^2\theta_z} = \frac{n^r_{cl} n^i_{cl}}{\cos^2\theta_z - \cos^2\theta_c}\sqrt{\cos^2\theta_z - \cos^2\theta_c}$$

therefore,

$$T = \frac{4 \sin\theta_z \left[\dfrac{n^r_{cl}\ n^i_{cl}}{n^2_{co}\sqrt{\cos^2\theta_z - \cos^2\theta_c}}\right]}{\left|\sin^2\theta_z + (\cos^2\theta_c - \cos^2\theta_z)^{1/2}\right|^2} \qquad (C.9)$$

$$= \frac{4 \sin\theta_z \left[\dfrac{n^r_{cl}\ n^i_{cl}}{n^2_{co}\sqrt{\cos^2\theta_z - \cos^2\theta_c}}\right]}{\left[\sin\theta_z + i(\cos^2\theta_z - \cos^2\theta_c)^{1/2}\right]^2}$$

$$= \frac{4 \sin\theta_z\ n^r_{cl}\ n^i_{cl}}{n^2_{co}\sqrt{\cos^2\theta_z - \cos^2\theta_c}\ (\sin^2\theta_z + \cos^2\theta_z - \cos^2\theta_c)}$$

$$= \frac{4 \sin\theta_z\ n^r_{cl}\ n^i_{cl}}{n^2_{co}\ \sin^2\theta_c\sqrt{\cos^2\theta_z - \cos^2\theta_c}} \qquad (C.10)$$

substituting $n^2_{cl} = \frac{\alpha\lambda}{4\pi}$

we get

$$\boxed{T = \frac{\alpha\lambda\ n_{cl}}{\pi\ n^2_{co}\ \sin^2\theta_c}\ \frac{\sin\theta_z}{\sqrt{\cos^2\theta_z - \cos^2\theta_c}}} \qquad (C.11)$$

or using equation (C.1) $\gamma = NT = \frac{\tan\Theta_z}{2a} T$

where a is the core radius.

$$\gamma = \frac{\alpha\lambda}{2\pi a} \frac{n_{cl}}{n_{co}^2} \frac{\sin\Theta_z \tan\Theta_z}{\sin^2\Theta_c \sqrt{\cos^2\Theta_z - \cos^2\Theta_c}}$$

If we use Harrick's (29) expression for the penetration depth

$$d_p = \frac{\lambda}{n_{co}} \frac{}{2\pi \sqrt{\cos^2\Theta_z - \cos^2\Theta_c}}$$

we get

$$\boxed{\gamma = \frac{\alpha}{a} \left[\frac{n_{cl}}{n_{co}}\right] \frac{d_p}{\sin^2\Theta_c} \sin\Theta_z \tan\Theta_z} \qquad (C.12)$$

for any $\Theta_z < \Theta_c$.

Because the penetration depth rises rapidly near the critical angle, γ will increase dramatically, accordingly.

In the small angle approximation

$$\sin\Theta_z \cong \Theta_z$$

$$\sin\Theta_c \cong \Theta_c$$

so that equation (C.12) reduces to

$$\gamma = \frac{\alpha}{a} \frac{n_{cl}}{n_{co}} \frac{}{\Theta_c^2} \frac{\lambda}{n_{co}} \frac{\Theta_z^2}{\sqrt{\Theta_c^2 - \Theta_z^2}} \qquad (C.13)$$

$$= \frac{\alpha}{a} \frac{n_{cl}}{n_{co}^2} \frac{\lambda}{2\pi} \frac{(\Theta_z/\Theta_c)}{\Theta_c \sqrt{1 - \Theta_z^2/\Theta_c^2}}$$

If $n_{cl} \cong n_{co}$, then

$$\gamma \cong \frac{\alpha}{n_{co}\, ak\, \Theta_c} \quad \frac{(\Theta_z/\Theta_c)^2}{\sqrt{1 - \Theta_z^2/\Theta_c^2}}$$

where $k=2\pi/\lambda$.

$$\boxed{\gamma = \frac{\alpha}{V} \left[\frac{\Theta_z}{\Theta_c}\right]^2 \frac{1}{\sqrt{1 - \Theta_z^2/\Theta_c^2}}} \qquad (C.14)$$

which is the final expression derived by Snyder and Love (equation 6-21, page 127)

$$\gamma = \frac{\alpha}{V} \left[\frac{\Theta_z}{\Theta_c}\right] \frac{1}{\sqrt{1 - (\Theta_z^2/\Theta_c^2)}}$$

This result is accurate for bound rays, with the exception of those few rays whose directions are close to $\Theta_z = \Theta_c$.
In the case of a silica core in contact with an aqueous solution the weakly guiding approximation is no longer valid; i.e. $n_{cl} < n_{co}$. Removing this condition and allowing all values of $\Theta_z < \Theta_c$, Ruddy (46) shows that the transmission coefficient becomes

$$\boxed{T = \frac{\alpha\lambda\, n_{cl}}{\pi\, (n_{co}^2 - n_{cl}^2)} \frac{\cos\Theta}{\sqrt{\sin^2\Theta - (n_{cl}/n_{co})^2}}} \qquad (C.15)$$

and the attenuation coefficient $\gamma(\Theta)$ of that ray

$$\gamma(\Theta) = \frac{\alpha\lambda\ n_{cl}\ f(\Theta)}{2\pi a\ (n_{co}^2 - n_{cl}^2)} \qquad \text{(C.16)}$$

$$\text{where } f(\Theta) = \frac{\cos^2\Theta}{\sin\Theta}\sqrt{\sin^2\Theta - (n_{cl}^2/n_{co}^2)}$$

Using equations (C.15) and (C.16), the final expression relating the evanescent absorption coefficient $\gamma(\Theta)$ and bulk absorption coefficient α is

$$\boxed{\frac{\gamma}{\alpha} = \frac{\lambda\ n_{cl}\ \cos^2\Theta}{2\pi a\ \sin\Theta\ (n_{co}^2 - n_{cl}^2)\ \sqrt{\sin^2\Theta - (n_{cl}^2/n_{co}^2)}}} \qquad \text{(C.17)}$$

APPENDIX D

Specification of the Monochromator.

f number.....3.9

Focal length.....74mm

Grating.....1800g/mm,holographic

Resolution (600μm slits).....4.3nm

Wavelength Accuracy.....± 0.2%

Spectral Range.....300 - 800nm

APPENDIX E

Specification of PCS Optical Fibre.

PCS fibre consists of:

silica core

silicone resin optical cladding

ETFE protective coating

Characteristics		PCS 200	PCS 600
Core diameter	μm	200 ± 8	600 ± 24
Cladding diameter	μm	380 ± 30	750 ± 60
Coating diameter	μm	600 ± 48	1060 ± 85
Numerical aperture		0.4	0.4

APPENDIX F

Electronic Circuit Diagrams.

This appendix contains the circuit diagrams of the power supply, analog/digital converter and digital to analog converter. Their operation is as described in section 3.5.1.

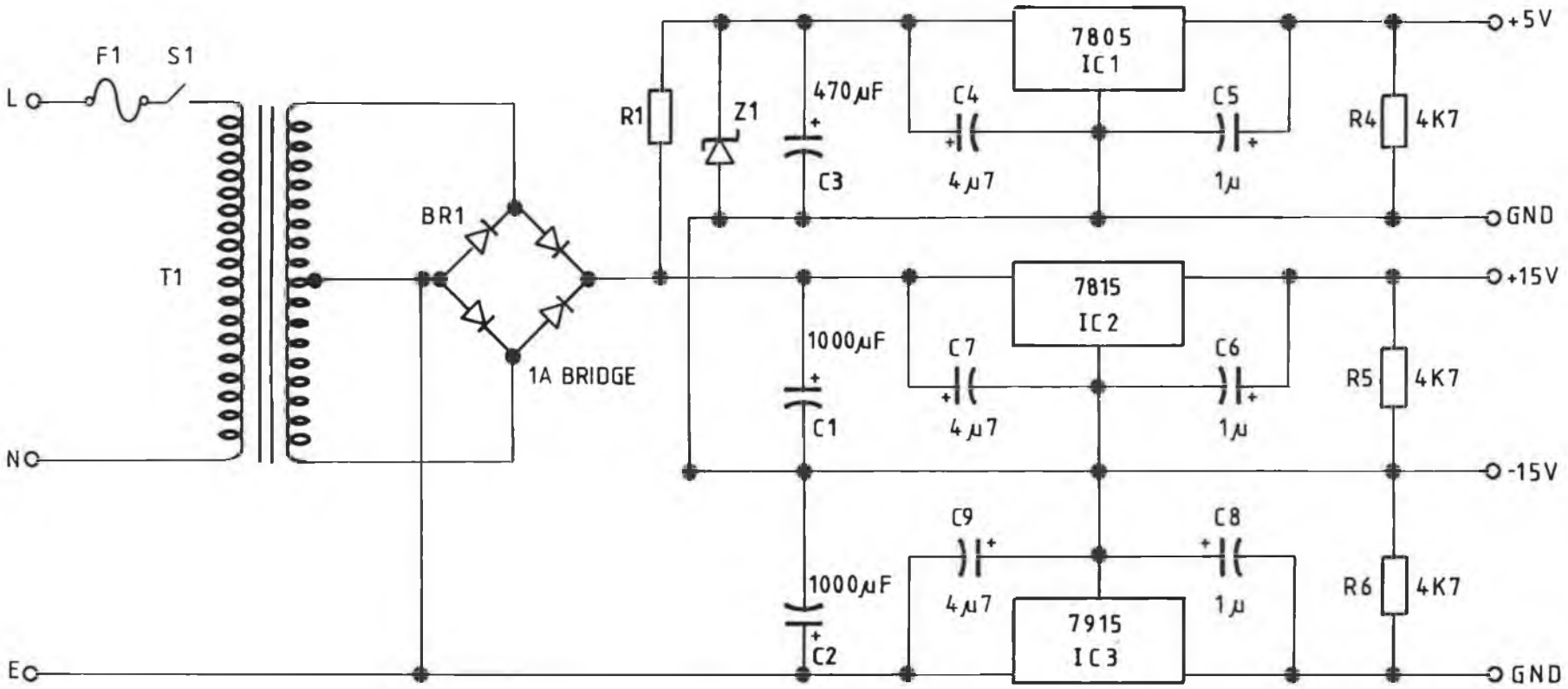

Fig. F1 : Power Supply Unit

F2

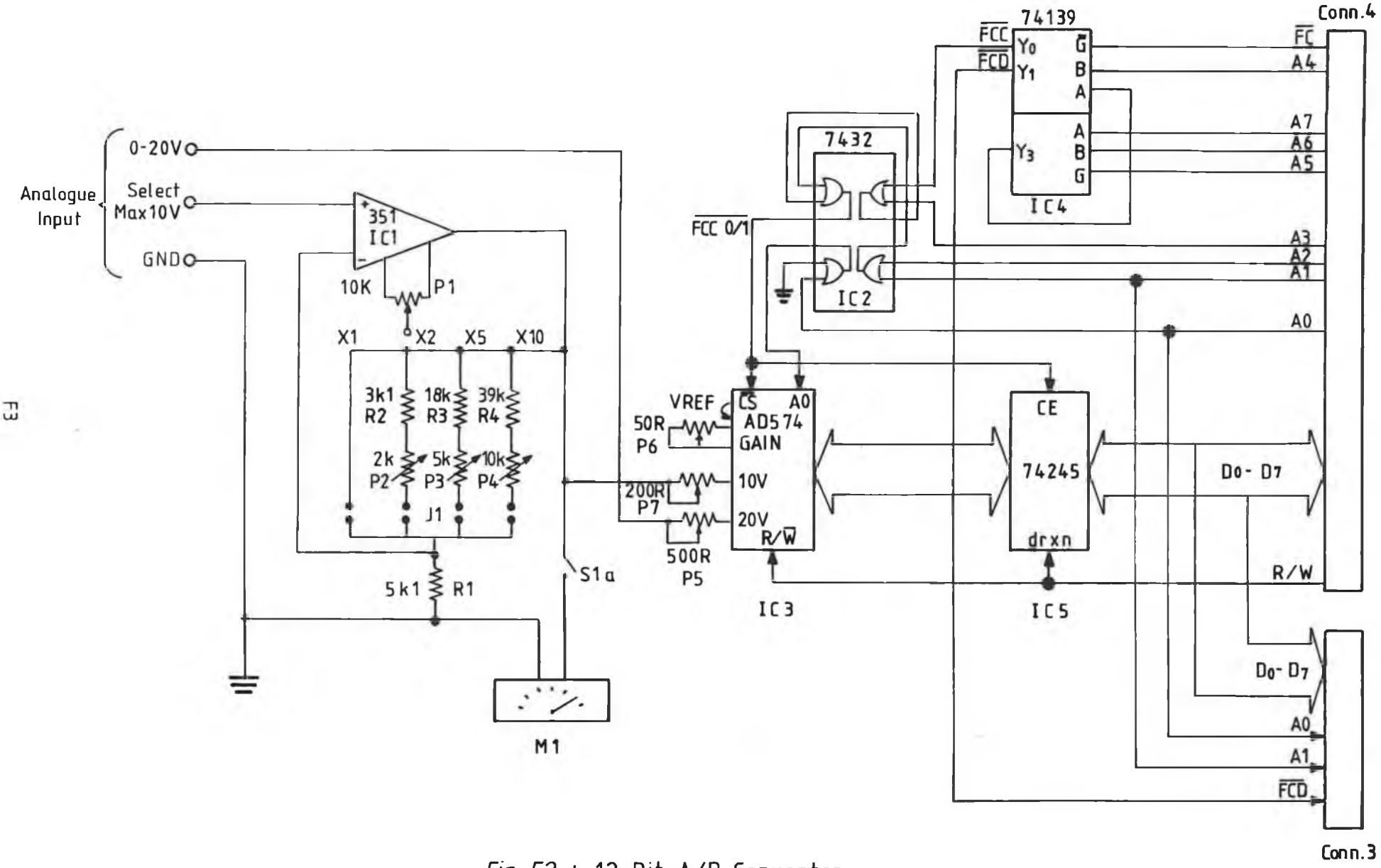

Fig. F2 : 12 Bit A/D Convertor

Analogue
Out
741
IC2
10K
P1

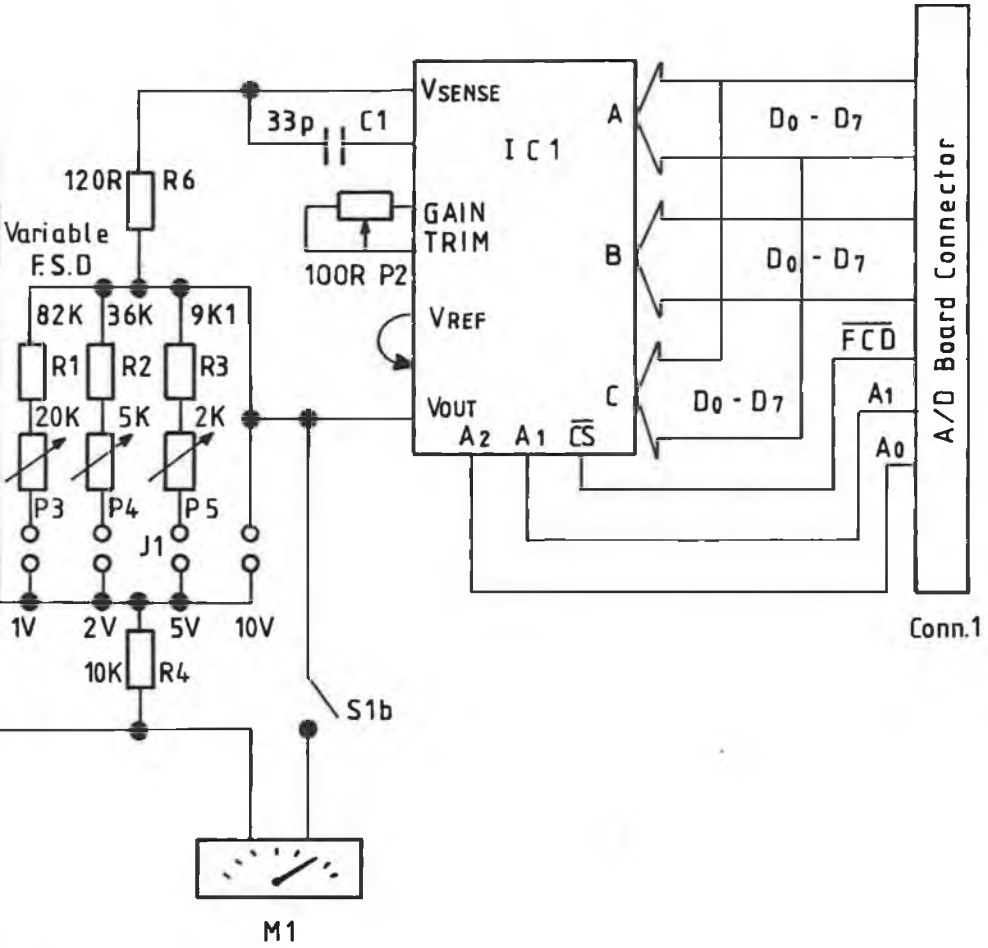

Fig. F3 : 12 Bit DAC

APPENDIX G

Software Programs.

The following pages contain all the software written for this project in BASIC. The structure of the programs are explained in section 3.5.2.

```
 10 REM ******************************
 20 REM **                            **
 30 REM ** PROGRAM TO CONTROL THE     **
 40 REM **        MINICHROM           **
 50 REM **        MODEL Ø2            **
 60 REM **                            **
 70 REM ******************************
 80 MODE4
 90 DIM Y(1000)
100 VDU15
110 YMAX=0:F=0
120 PRINT:PRINT
130 PROCMENU
140 END
150 DEF PROCMENU
160 CLS
170 PRINT"SELECT FUNCTION:-"
180 PRINT:PRINT
190 PRINT TAB(12) "SET PARAMETERS    1"
200 PRINT TAB(12) "SET WAVELENGTH    2"
210 PRINT TAB(12) "SINGLE SCAN       3"
220 PRINT TAB(12) "MANUAL SCAN       4"
230 PRINT TAB(12) "SAVE DATA ON FILE 5"
240 INPUT "SELECT OPTION";d
250 IF d=1 GOTO 410
260 IF d=2 GOTO 810
270 IF d=3 GOTO 1190
280 IF d=4 GOTO 1430
290 IF d=5 GOTO 2020
300 IF d<>1 GOTO 130
310 REM ****************************
320 REM *                          *
330 REM * THE FOLLOWING PROGRAM    *
340 REM * INTERFACES WITH THE CB1  *
350 REM * CONTROLLER AND CHANGES ANY*
360 REM * OF THE PARAMETERS        *
370 REM*                          *
380 REM ****************************
390 VDU3
400  MODE3
410 PRINT:PRINT
420PRINT "GO TO ZERO ORDER:TYPE G1"
430 PRINT:PRINT
440 PRINT "DO YOU WANT TO CHANGE:"
450 PRINT:PRINT
460 PRINT TAB(22) "DIVIDING FACTOR D"
470 PRINT:PRINT
480 PRINT TAB(22) "INITIAL VELOCITY I"
490 *FX7,7
500 REM RECEIVE BAUD RATE
510 *FX8,7
520 REM TRANSMIT BAUD RATE
530 *FX229,1
```

```
540 OSBYTE=&FFF4
550 REM OSBYTE CALL
560:
570 L%=0
580 FOR I1=1 TO 1000
590 A%=138:X%=2:
600 REM RS423 O/P BUFFER
610 *FX2,2
620 IF ADVAL(-1)>0 Y%=GET:CALL OSBYTE
630 IF ADVAL(-3)>0 Y%=GET:CALL OSBYTE
640 *FX2,1
650 REM GET CHAR FROM KBRD,ENABLE RX
660 IF ADVAL(-2)>0 CHAR%=GET:
670 VDU CHAR%:L%=L%+1:
680 IF CHAR% =13 VDU10:L%=0
690 REM CHECKS NO. OF CHARS IN KBRD
700 REM CHECKS NO. OF CHARS IN RS423
710 IF L%=60 VDU10:VDU13:L%=0
720 REM MOVE CURSOR TO NEW LINE
730 NEXT
740 :
750 *FX2,2
760 *FX229,0
770 REM ESCAPE ENABLE
780 *FX3,4
790 Z=0
800 PROCMENU
810 CLS
820 REM**************************
830 REM*                        *
840 REM* THE FOLLOWING SETS THE*
850 REM* MONOCHROMATOR TO A    *
860 REM* SPECIFIED WAVELENGTH  *
870 REM*                        *
880 REM**************************
890 PRINT:PRINT
900 INPUT "Wavelength position (nm)",W
910 REM W<=6400 SETS THE MAXIMUM
920 REM SCAN   TO 800nm
930 W=W*8:IF W>=6400 THEN 900
940 IF W < F THEN 1020
950 A=Z/8:PRINT A
960 B%=(W-F)
970 F=W
980 *FX3,3
990 VDU2
1000 PRINT "+";STR¤(B%)
1010 GOTO 1070
1020 REM
1030 PRINTF:B%=ABS(W-F)
1040 *FX3,3
1050 VDU2
1060 PRINT"-";STR¤(B%)
1070 *FX3,4
```

```
1080 VDU3
1090 F=W
1100 GOTO120
1110 REM************************
1120 REM*                      *
1130 REM*THE NEXT ROUTINE MAKES*
1140 REM*THE MONOCHROMATOR SCAN*
1150 REM*BETWEEN TWO SPECIFIED *
1160 REM*WAVELENGTHS           *
1170 REM*                      *
1180 REM************************
1190 INPUT"Starting wavelength (nm)",S
1200 INPUT"Finishing wavelength (nm)",F
1210 F=F*8
1220 INPUT" Incremental rate "Inc
1230 P%=F-S:IF P%>=6400 THEN GOTO 1190
1240 IF P%<0 THEN GOTO 1190
1250 INPUT" Entrance slit (um)"S1
1260 INPUT" EXIT slit (um)"S2
1270 INPUT" PMT slit (um)"S3
1280 INPUT"Send to ADC or Chart A/C",a$
1290  IF a$="C" THEN PROCCHART
1300 CLS
1310 X=0
1320 P1=(F-S)/(Inc*8)
1330 FOR i=1 TO P1
1340 *FX3,3
1350 PRINT "+";STR$(P%/P1)
1360 *FX3,4
1370  PROCDATA
1380 FOR L1=1 TO 100:NEXT
1390 *FX21,1
1400 NEXT i
1410 *FX3,4
1420 PROCSAVE:PROCDRAW:PROCMENU
1430 REM MANUAL SCAN
1440 REM************************
1450 REM*                      *
1460 REM*THE NEXT SEGMENT ALLOWS*
1470 REM*MANUAL SCAN           *
1480 REM*                      *
1490 REM************************
1500 PRINT"To scan forward press"CHR$(93)
1510 PRINT"To scan backward press"CHR$(91)
1520 PRINT:"Press Q to finish"
1530 *FX4,1
1540 Q$=GET$
1550 IF Q$=CHR$(&89) THEN PROCFORWARD
1560 IF Q$=CHR$(&88) THEN PROCBACK
1570 IF Q$="Q" THEN PROCFINISH
1580 DEF PROCFORWARD
1590 V%=10
1600 *FX3,1
1610 PRINT "+";STR$(V%)
```

```
1620 *FX3,4
1630 GOTO 1540
1640 ENDPROC
1650 DEF PROCBACK
1660 P%=10
1670 *FX3,1
1680 PRINT "-";STR$(P%)
1690 *FX3,4
1700 GOTO 1540
1710 ENDPROC
1720 DEF PROCFINISH
1730 *FX4,0
1740 *FX3,4
1750 *FX21,0
1760 GOTO 120
1770 ENDPROC
1780 DEF PROCCHART
1790 *FX3,1
1800 PRINT "+";STR$(P%)
1810 *FX3,4
1820 PROCMENU
1830 ENDPROC
1840 VDU3
1850 CLOSE#0:A=&FCC0
1860 REM ***   Data points stored   ***
1870 REM ***       in array Y(D).    ***
1880 REM ********************************
1890 DEF PROCDATA
1900 a=0
1910 *FX3,4
1920 FOR I=1 TO 60
1930 A=&FCC0
1940 A?0=0:Y=((A?0)*16)+((A?1)DIV16)
1950 a=a+Y
1960 NEXT
1970 Y(i)=(a/60)
1980 MOVE X,Y(i)/2
1990 DRAW X,Y(i)/2:X=X+1200/P1
2000 ENDPROC
2010 REM ********************
2020 DEF PROCSAVE
2030 S=S/8:F=F/8:
2040 PRINT:PRINT
2050 PRINT TAB(15)"INSERT DATA DISK"
2060 INPUT"Name of file"B$:Y=OPENOUT(B$
2070 FOR D=1 TO P1
2080 PRINT#Y,Y(D) :NEXT:CLOSE#0
2090 FOR i=1 TO P1
2100 IF Y(i)>YMAX THEN YMAX=Y(i)
2110 NEXT
2120 DEF PROCDRAW
2130 CLS
2140 X=50
2150 FOR I1=1 TO P1
```

```
2160 MOVE X,Y(I1)*900/YMAX+50
2170 DRAW X,Y(I1)*900/YMAX+50
2180 X=X+1100/P1
2190 NEXT
2200 VDU5
2210 MOVE 50,50:DRAW 1200,50
2220 DRAW 1200,1000:DRAW 50,1000:
2230 DRAW 50,50
2240 FOR I2=1 TO 4
2250 MOVE 50,237.5*I2:PRINT"-"
2260 NEXT
2270 MOVE 200,950:
2280 PRINT"Intensity vs Wavelength (nm) "
2290 REM F=1600:S=800
2300 B=(F-S)/(800)
2310 FOR I2=0 TO B
2320 MOVE 37+1150/((B))*I2,60:PRINT"ö"
2330 NEXT
2340 é%=&10
2350 FOR I2=0 TO 2
2360 MOVE -420+(1150/((B)))*I2*(B/2),30
2370 PRINT S+I2*(F-S)/(B)*(B/2)
2380 NEXT
2390 VDU4
2400 PRINT TAB(3,5)"REPEAT SCAN Y/N"
2410 INPUT G$:IF G$="Y" GOTO 2430
2420 GOTO 120
2430 B%=(F-S)*8
2440 *FX3,3
2450 VDU2
2460 PRINT"-";STR$(B%)
2470 *FX3,4
2480 VDU3
2490 PRINT"PRESS ANY KEY TO REPEAT SCAN"
2500 K=GET
2510 F=F*B:S=S*8
2520 GOTO 1300
2530 END
```

```
 10 REM ******************************
 20 REM **                            **
 30 REM ** THIS PROGRAM CORRECTS      **
 40 REM ** SPECTRA BY DIVIDING  THE   **
 50 REM ** RECORDED SPECTRA BY        **
 60 REM ** THE SYSTEM RESPONSE.       **
 70 REM ** A HARDCOPY IS OBTAINED     **
 80 REM ** ON A RIKADINKI PLOTTER.    **
 90 REM **                            **
100 REM ******************************
110 VDU14
120 CLOSE#0
130 é%=131850
140 *.
150 PRINT:PRINT
160 PROCSUBTRACT
170 PROCSAVE
180 CLOSE#0
190 END
200 DEF PROCSUBTRACT
210
220 INPUT"NAME OF FILE " ,B$
230 L=OPENIN(B$)
240 K=OPENIN"SYSF9"
250 P1=300
260 XMAX=0
270 DIM Y1(P1),X1(P1),X(P1)
280 CLS
290 FOR I=1 TO P1
300
310 INPUT#K,Y1(I):INPUT#L,X1(I)
320
330
340 REM MOVE X,Y1(I):DRAW X,Y1(I)
350 REM MOVE X,X1(I):DRAW X,X1(I)
360 REM X=X+1200/P1
370 NEXT
380 X1=0
390 CLS
400
410 VDU29,0;50;
420  FOR I=10 TO P1
430 X(I)=X1(I)/Y1(I)
440 NEXT
450 FOR I =10 TO P1
460 IF X(I)>XMAX THEN XMAX=X(I)
470 NEXT
480 FOR I=10 TO  P1
490 X(I)=X(I)/XMAX
500 NEXT
510 FOR I=10 TO P1
520 MOVE X1,X(I)* 500:DRAW X1,X(I)*500
530 X1=X1+1200/P1
```

```
540 NEXT
550 ENDPROC
560 DEF PROCSAVE
570 PRINT:PRINT
580 PRINT:PRINT
590 INPUT"NAME OF FILE"B¤:Y=OPENOUT(B¤)
600 FOR D=10  TO P1
610 PRINT #Y,X(D):NEXT:CLOSE#0:
620 PRINT"PRESS P FOR A PLOT"
630 PRINT"PRESS C TO DIVIDE ANOTHER SPECTRUM"
640 B¤=GET¤ :IF B¤="P" GOTO 660
650 IF B¤="C" THEN GOTO 200 ELSE 2330
660 REM RIKADENKI PLOTTER PROGRAM
670 *DRIVE0
680 VDU15
690 *.
700 PRINTCHR¤(130)"NAME OF FILE":INPUTB¤
710 PRINTCHR¤(130)"ADDITIONAL INFO":INPUT A¤
720 L=OPENIN(B¤)
730 INPUT"Start ",Start
740 INPUT"End ",End
750 V=Start
760 U=End
770 N=End -Start
780 DX=N-1
790 X=0 :Start=Start-(V-1):End=End-V
800 VDU29,0;500;
810 FOR I=Start TO End
820 INPUT#L,A
830 X(I)=A
840 X(I)=-1*LOG(X(I))
850 MOVE X,X(I)*3:DRAW X,X(I)*3
860 X=X+1200/(End-Start+1)
870 NEXT I
880 INPUT "TYPE IN TITLE";NAME¤
890 PRINT:PRINT
900 INPUT"Do you want a specific wavelength range"
910 IF GET¤="Y" THEN PROCSPEC
920 REM PLOTTER PROGRAM BEGINS HERE
930 E%=10
940 PRINT:PRINT
950 PRINT "PRESS R FOR RIKI COPY"
960 PRINT"PRESS L FOR LINE PROFILE ONLY"
970 B¤= GET¤ :IF B¤ = "R" GOTO 990
980 IF B¤="L" THEN GOTO 1040 ELSE GOTO 1090
990 PROCWINDOW
1000 PROCGRAD
1010 PROCTITLE
1020 PRINT "PRESS J FOR LINE THRU POINTS"
1030 B¤ = GET¤ :IF B¤ = "J" THEN GOTO 1040 ELSE GOTO 1050
1040 PROCLINE
1050 PRINT "PRESS B FOR BOX"
1060 B¤=GET¤:
1070 IF B¤="B" THEN GOTO 1080 ELSE GOTO 1090
```

```
1080 PROCBOX
1090 END
1100 REM PROCEDURES BEGIN HERE
1110 DEF PROCWINDOW
1120 VDU2
1130 PRINT "S4"
1140 PRINT "M400,200"
1150 PRINT "D2300,200"
1160 PRINT "D2300,1600"
1170 PRINT "D400,1600"
1180 PRINT "D400,200"
1190 FOR I = 1 TO 4
1200 L =(200+(350*I))-20
1210 REM 20 TO BRING TO CENTRE OF GRAD
1220 K =0.25*I
1230 PRINT  "M120,"L""
1240 PRINT "Q0P"K""
1250 NEXT I
1260 A=V
1270 B=((U-V)/4)+V
1280 C=((U-V)/2)+V
1290 D=((U-V)*3/4)+V
1300 R=U
1310 PRINT "M200,130"
1320 PRINT "P"A""
1330 PRINT "M675,130"
1340 PRINT "P"B""
1350 PRINT "M1150,130"
1360 PRINT "P"C""
1370 PRINT "M1625,130"
1380 PRINT "P"D""
1390 PRINT "M2100,130"
1400 PRINT "P"R""
1410 PRINT "H"
1420 VDU3
1430 ENDPROC
1440 REM ********************
1450 DEF PROCPOINT
1460 VDU2
1470 FOR I = 1 TO N
1480 L = INT(1900*(I-1)/DX+400.5)
1490 K = INT(1400*(Y(i))+200.5)
1500 PRINT "M"L","K""
1510 PRINT "N3"
1520 NEXT I
1530 VDU3
1540 ENDPROC
1550 REM*********************
1560 DEF PROCTITLE
1570 VDU2
1580 PRINT "M1000,5S4,5"
1590 PRINT "Q0PW A V E L E N G T H   (nm)"
1600 PRINT"M1557,45S1,2"
1610 PRINT"Q0P0"
```

```
1620 PRINT "M1888,175S5"
1630 PRINT "M1600,1100S4,5"
1640 PRINT "P"+NAME$
1650 PRINT"M1600,1000S4,5"
1660 PRINT "M1600,900S4,5"
1670 PRINT "P"+A$
1680 PRINT"M180,650S4,5"
1690 PRINT"Q1PABSORBANCE (Arb)"
1700 PRINT "S3"
1710 PRINT "H"
1720 VDU3
1730 ENDPROC
1740 REM ******************
1750 DEF PROCLINE
1760 VDU2
1770 PRINT "M400,200"
1780 FOR I = 1 TO N
1790 L = INT(1900*(I-1)/DX+400.5)
1800 K = INT(1400*(X(I))+200.5)
1810 PRINT "D"L","K""
1820 NEXT I
1830 PRINT "H"
1840 VDU3
1850 ENDPROC
1860 REM ******************
1870 DEF PROCBOX
1880 VDU2
1890 PRINT "M0,0"
1900 PRINT "D2500,0"
1910 PRINT "D2500,1800"
1920 PRINT "D0,1800"
1930 PRINT "D0,0"
1940 PRINT "H"
1950 VDU3
1960 ENDPROC
1970 REM******************
1980 REM******************
1990 PROCSPEC
2000 PRINT:PRINT
2010 CLS
2020 INPUT "Wavelength range",Start,End
2030 X=0:Start=Start-5400:End=End-5400
2040 FOR i=Start TO End
2050 MOVE X,Y(i)/2
2060 DRAW X,Y(i)/2
2070 X=X+1200/(End-Start)
2080 NEXT
2090 ENDPROC
2100 REM******************
2110 DEF PROCGRAD
2120 VDU2
2130 PRINT"M400,200"
2140 PRINT"D400,190"
2150 PRINT"M875,200"
2160 PRINT"D875,190"
2170 PRINT"M1350,200"
```

```
2180 PRINT"D1350,190"
2190 PRINT"M1825,200"
2200 PRINT"D1825,190"
2210 PRINT"M2300,200"
2220 PRINT"D2300,190"
2230 PRINT"M400,550"
2240 PRINT"D390,550"
2250 PRINT"M400,900"
2260 PRINT"D390,900"
2270 PRINT"M400,1250"
2280 PRINT"D390,1250"
2290 PRINT"M400,1600"
2300 PRINT"D390,1600"
2310 PRINT"H"
2320 VDU3
2330 ENDPROC
```

```
 10 REM ******************************
 20 REM **                            **
 30 REM ** PROGRAM TO SMOOTH AND     **
 40 REM ** DISPLAY STORED SPECTRA     **
 50 REM **                            **
 60 REM ******************************
 70 CLS
 80 *DRIVE2
 90 *.
100 PRINT::INPUT"ENTER FILENAME  :";FILE$
110 PRINT:INPUT"NEW FILENAME:"; J$
120 DIM A(2002)
130 Y=OPENIN(FILE$)
140 FOR I=1 TO 400
150 INPUT#Y,A(I)
160 NEXT I
170 VDU7
180 MODE4
190 PROCDRAW
200 PROCPLOT
210 PROCSMOOTH
220 CLS
230 PROCDRAW
240 PROCPLOT
250 CLOSE#0
260 PROCDRAW
270 PROCINTERVAL
280 PROCENPLOT
290 *DRIVE2
300 END
310 DEF PROCENPLOT
320 PLOT 69,((I*.6)+22),100+((A(I)*.5)*0.8)
330 ENDPROC
340 DEF PROCDRAW
350 MOVE 25,100:DRAW 1225,100:
360 DRAW 1225,900:DRAW 25,900:DRAW 25,100
370 FOR I=1 TO 5
380 PLOT 69,(I*200)+25,100
390 DRAW (I*200)+25,80
400 NEXTI
410 ENDPROC
420 DEF PROCINTERVAL
430 PRINT:PRINT"DO YOU WANT TO EXAMINE ANY"
440 INPUT"   PARTICULAR REGION (Y/N)";A$
450 IF A$<>"Y" ENDPROC
460 PRINT:INPUT"ENTER REGION START WAVELENGTH";X
470 PRINT:INPUT"ENTER REGION FINISH WAVELENGTH";Y
480 J=X:K=Y
490 N=INT(Y-X)
500 S=1200/N:P=1
510 CLS:PROCDRAW
520 FOR I=J TO K
530 PLOT 69,25+(P*S),100+(A(I)*0.5)
```

```
530 PLOT 69,25+(P*S),100+(A(I)*0.5)
540 P=P+1
550 NEXT I
560 ENDPROC
570 DEF PROCSMOOTH
580 PRINT:"3 PT. RUNNING AVERAGE UNDER WAY"
590 *DRIVE2
600 Y=OPENOUT J¤
610 FOR I=1 TO 400
620 Y1=((A(I-1)+(2*A(I))+A(I+1))/4)
630 PRINT#Y,Y1
640 NEXT I
650 CLOSE#0
660 Y=OPENIN J¤
670 FOR I=1 TO 400
```

```
 10 REM ******************************
 20 REM **                            **
 30 REM ** THIS PROGRAM CALCULATES **
 40 REM ** CONCENTRATION OF         **
 50 REM ** ABSORBED LIQUID          **
 60 REM **                            **
 70 REM ******************************
 80 P1=790
 90 DIM Y1(P1),X1(P1)
100 INPUT"NAME OF FILE ",B$
110 INPUT"ABSORPTION CONSTANT ",e
120 INPUT"CELL LENGTH",b
130 L=OPENIN(B$)
140 P1=400
150 FOR I=1 TO P1
160 INPUT#L,Y1(I)
170 NEXT
180 B=0
190 FOR I=1 TO P1
200 B=B+Y1(I)
210 NEXTI
220 A=400-B
230 c=A/(e*b)
240 PRINT "CONCENTRATION C= ",c
250 END
```

```
 10 REM ********************************
 20 REM **                              **
 30 REM ** RIKADENKI PLOTTER PROGRAM**
 40 REM **                              **
 50 REM ********************************
 60 REM RIKADENKI PLOTTER PROGRAM
 70 CLOSE#0
 80 DIM Y(2005)
 90 *DRIVE0
100 MODE7:VDU15
110 i=0
120 absmax=0
130 *.
140 PRINTCHR¤(130)"NAME OF FILE":INPUTB¤
150 L=OPENIN(B¤)
160 INPUT"Start",Start
170 INPUT"End ",End
180 V=Start
190 U=End
200 N=End -Start
210 DX=N-1
220 X=0 :Start=Start-(V-1):End=End-V
230 MODE4
240 VDU29,0;500;
250 FOR I=Start TO End
260 INPUT#L,A
270 Y(I)=A
280 Y(I)=-1*LOG(Y(I))
290 MOVE X,Y(I)*3:DRAW X,Y(I)*3
300 X=X+1200/(End-Start+1)
310 NEXT I
320 IF i = 0 THEN 330 ELSE 520
330 FOR I= Start TO End
340 IF Y(I)> absmax THEN absmax =Y(I)
350 i=1
360 NEXT I
370 INPUT "TYPE IN TITLE";NAME¤
380 PRINT:PRINT
390 INPUT"Do you want a specific wavelength range"
400 IF GET¤="Y" THEN PROCSPEC
410 REM PLOTTER PROGRAM BEGINS HERE
420 é%=10
430 PRINT:PRINT
440 PRINT"PRESS R FOR RIKI COPY"
450 PRINT"PRESS L FOR LINE PROFILE ONLY"
460 B¤= GET¤ :IF B¤ = "R" GOTO 490
470 IF B¤="L" THEN GOTO 550 ELSE GOTO 600
480 é%=131850
490 PROCWINDOW
500 PROCGRAD
510 PROCTITLE
520 PRINT "PRESS J FOR LINE THRU POINTS"
530 B¤ = GET¤
```

```
540 IF B¤ = "J" THEN GOTO 550 ELSE GOTO 560
550 PROCLINE
560 PRINT "PRESS B FOR BOX"
570 B¤=GET¤ :
580 IF B¤="B" THEN GOTO 590 ELSE GOTO 600
590 PROCBOX
600 GOTO 130
610 REM PROCEDURES BEGIN HERE
620 DEF PROCWINDOW
630 REM
640 VDU2
650 PRINT "S4"
660 PRINT "M400,200"
670 PRINT "D2300,200"
680 PRINT "D2300,1600"
690 PRINT "D400,1600"
700 PRINT "D400,200"
710 FOR I = 1 TO 4
720 L =INT((200+(350*I))-20)
730 REM 20 TO BRING TO CENTRE OF GRAD
740 K =0.25*I*absmax
750 PRINT  "M120,"L""
760 É%=131850
770 PRINT "Q0P"K""
780 É%=&10
790 NEXT I
800 A=V
810 B=((U-V)/4)+V
820 C=((U-V)/2)+V
830 D=((U-V)*3/4)+V
840 R=U
850 PRINT "M50,130"
860 PRINT "P"A""
870 PRINT "M525,130"
880 PRINT "P"B""
890 PRINT "M1000,130"
900 PRINT "P"C""
910 PRINT "M1475,130"
920 PRINT "P"D""
930 PRINT "M1950,130"
940 PRINT "P"R""
950 PRINT "H"
960 VDU3
970 ENDPROC
980 REM
990 DEF PROCPOINT
1000 VDU2
1010 FOR I = 1 TO N
1020 L = INT(1900*(I-1)/DX+400.5)
1030 K = INT(1400*(Y(i))/absmax+200.5)
1040 PRINT "M"L","K""
1050 PRINT "N3"
1060 NEXT I
1070 VDU3
```

```
1080 ENDPROC
1090 **********************
1100 DEF PROCTITLE
1110 VDU2
1120 PRINT "M1000,5S4,5"
1130 PRINT "Q0PW A V E L E N G T H   (nm)"
1140 PRINT"M1557,45S1,2"
1150 PRINT"Q0P0"
1160 PRINT "M1888,175S5"
1170 PRINT "M1600,1100S4,5"
1180 PRINT "P"+NAME¤
1190 PRINT"M1600,1000S4,5"
1200 PRINT "M1600,900S4,5"
1210 PRINT"M180,650S4,5"
1220 PRINT"Q1PABSORBANCE (Arb)"
1230 PRINT "S3"
1240 PRINT "H"
1250 VDU3
1260 ENDPROC
1270 REM
1280 DEF PROCLINE
1290 VDU2
1300 PRINT "M400,200"
1310 FOR I = 1 TO N
1320 L = INT(1900*(I-1)/DX+400.5)
1330 K = INT(1400*(Y(I))/absmax+200.5)
1340 PRINT "D"L","K""
1350 NEXT I
1360 PRINT "H"
1370 VDU3
1380 ENDPROC
1390 REM
1400 DEF PROCBOX
1410 VDU2
1420 PRINT "M0,0"
1430 PRINT "D2500,0"
1440 PRINT "D2500,1800"
1450 PRINT "D0,1800"
1460 PRINT "D0,0"
1470 PRINT "H"
1480 VDU3
1490 ENDPROC
1500 REM
1510 REM
1520 PROCSPEC
1530 PRINT:PRINT
1540 CLS
1550 INPUT "Wavelength range",Start,End
1560 X=0:Start=Start-5400:End=End-5400
1570 FOR i=Start TO End
1580 MOVE X,Y(i)/2
1590 DRAW X,Y(i)/2
1600 X=X+1200/(End-Start)
1610 NEXT
```

```
1620 ENDPROC
1630 **********************
1640 DEF PROCGRAD
1650 VDU2
1660 PRINT"M400,200"
1670 PRINT"D400,190"
1680 PRINT"M875,200"
1690 PRINT"D875,190"
1700 PRINT"M1350,200"
1710 PRINT"D1350,190"
1720 PRINT"M1825,200"
1730 PRINT"D1825,190"
1740 PRINT"M2300,200"
1750 PRINT"D2300,190"
1760 PRINT"M400,550"
1770 PRINT"D390,550"
1780 PRINT"M400,900"
1790 PRINT"D390,900"
1800 PRINT"M400,1250"
1810 PRINT"D390,1250"
1820 PRINT"M400,1600"
1830 PRINT"D390,1600"
1840 PRINT"H"
1850 VDU3
1860 ENDPROC
```

APPENDIX H

The Debye-Hückel Limiting Law in 3-D.

There is general agreement that the Debye-Hückel theory gives the correct description of the ion-ion interactions at the limit of extremely dilute solutions (49). The main features of the theory are a consideration of the solvent as a dielectric medium having an electrical permittivity ε, and of the ions as point charges $z_i e$, capable of approaching each other to a distance of closest approach *a* (which may be interpreted as the mean diameter of the ions). The main approximation in the theory is that the electrostatic potential energy V of an ion **i** at a distance **r** from an ion **j** is equal to the potential of mean force between the ions.

The spatial distribution of charges in thermal equilibrium in an electrostatic potential V is given by

$$n(r) = n_o \exp^{-eV/kT} \qquad (H.1)$$

where k is Boltzmann's constant.

If a test charge z_e is placed at the origin, then the charge density is

$$\rho = \rho_{ions} + \rho_{electron} \qquad (H.2)$$
$$= z_i n_{io} e - n_{eo} e \exp(eV/kT).$$

But for overall neutrality

$$z_i n_{io} = n_{eo}.$$

Therefore,

$$\rho = n_{eo}\, e\, \{1 - \exp(eV/kT)\}$$

$$= n_{eo} e\, \{1-[1-(eV/kT) + (eV/kT)^2\ 1/2! + ...]\}$$

$$= n_{eo}\, \frac{e^2 V}{kT} \qquad \text{(H.3)}$$

But $\nabla^2 V = \rho/\varepsilon$, Poissons equation.

In 3D, $$\nabla_r^2 = \frac{1}{r^2}\ \frac{\partial}{\partial r}\ \left|\ r^2\ \frac{\partial V}{\partial r}\ \right| \qquad \text{(H.4)}$$

therefore,

$$\frac{1}{r^2}\ \frac{\partial}{\partial r}\ \left[\ r^2\ \frac{\partial V}{\partial r}\ \right] = -\ \frac{n_{eo}\ e^2}{kT}\ V$$

$$= V/\ \lambda_D^2$$

or $$\frac{\partial^2 V}{\partial r^2} + \frac{2}{r}\ \frac{\partial V}{\partial r} = -\ \frac{V}{\lambda_D^2}\ . \qquad \text{(H.5)}$$

This has the general solution

$$V(r) = \frac{1}{r}\ \{\ A\ e^{-r/\lambda_D} + B\ e^{r/\lambda_D}\ \} \qquad \text{(H.6)}$$

With $V(r) \rightarrow 0$ ar $r \rightarrow$, B must be zero.

Therefore,

$$V(r) = \frac{A}{r}\ e^{-r/\lambda_D} \qquad \text{(H.7)}$$

which is the screened Coulomb potential.

In cylindrical polar coordinates

$$\nabla_r^2 = \frac{1}{r}\frac{\partial}{\partial r}\left[r\,\frac{\partial V}{\partial r}\right]$$

$$= \frac{\partial^2 V}{\partial r^2} + \frac{1}{r}\,\frac{\partial V}{\partial r}$$

Therefore,

$$\frac{\partial^2 V}{\partial r^2} + \frac{1}{r}\,\frac{\partial V}{\partial r} = -\frac{V}{\lambda_D^2} \qquad \text{(H.8)}$$

Now equations (H.5) and (H.8) have the same functional form so they will have the same form of solution. Because of the differing multiplicative constant on the $\partial V/\partial r$ term, a slightly modified λ_D will arise. It will only introduce numerical constant in λ_D and not effect the n_e^2 dependence.